

**Modelling human development and disease with in vitro pluripotent stem cell  
derived intestinal tissue and cells**

Andrew Taehun Song

Department of Anatomy and Cell biology, School of Biomedical sciences, Faculty of  
Medicine and Health Sciences, McGill University, Montreal

July 2023

A thesis submitted to McGill University in partial fulfillment of the requirements of the  
degree of Doctor of Philosophy in Cell Biology

© Andrew Taehun Song, 2023

## Table of contents

<b>Abstract (en)</b> .....	5
<b>Resume (fr)</b> .....	7
<b>Acknowledgements</b> .....	9
<b>Contribution to original knowledge</b> .....	10
<b>Contribution of authors</b> .....	11
<b>List of figures and tables</b> .....	12
<b>List of abbreviations</b> .....	13
<b>Introduction</b> .....	16
<b>Chapter 1</b> .....	16
<b>Rationale</b> .....	16
<b>Objectives</b> .....	16
<b>Chapter 2</b> .....	16
<b>Rationale</b> .....	16
<b>Objectives</b> .....	17
<b>Literature review</b> .....	18
<b>Relevance: Chapter 1</b> .....	18
<b>Intestine</b> .....	18
<b>Macrophages</b> .....	20
<b>Intestinal Macrophages</b> .....	23
<b>Lesser-known functions of macrophages</b> .....	25
<b>Models used to study macrophages</b> .....	27
<b>Intestinal organoids</b> .....	28
<b>Relevance: Chapter 2</b> .....	30
<b>CAID syndrome</b> .....	30
<b>SGO1</b> .....	31
<b>Enteric nervous system</b> .....	32
<b>Human intestinal organoid with enteric nervous system</b> .....	34
<b>Chapter 1: Developmental role of macrophages modelled in human pluripotent stem cell derived intestinal tissue</b> .....	36
<b>Research findings (Chapter 1)</b> .....	36
<b>Derivation of human intestinal organoids with macrophages (HIO/Mac)</b> .....	36
<b>Cellular composition of the intestinal organoid resembles fetal intestine</b> .....	37

Macrophage recruitment and retention by the organoid.....	39
Enteric neurons do not affect resident macrophage establishment.....	40
Macrophages migrate to the wound site upon injury.....	42
Macrophages localize to intestinal micro-anatomical niches in xenograft-matured organoids .....	43
Organoid macrophages acquire transcriptomic profile alike fetal intestinal macrophages.....	46
Macrophages regulate intestinal organoid growth .....	51
Macrophages attenuate mesenchymal cell glycolysis in developing intestinal organoids .....	55
Oncostatin M (OSM) reduces glycolytic gene expression in mesenchymal cells .....	59
Methodology (Chapter 1) .....	62
<b>Chapter 2: Modelling Chronic Atrial and Intestinal Dysrhythmia in patient iPSC-derived human intestinal organoid and cells. ....</b>	<b>75</b>
<b>Research findings (Chapter 2).....</b>	<b>75</b>
<b>Patient enteric neurons have disorganized morphology and lack surrounding interstitial cells of cajal.....</b>	<b>75</b>
<b>Patient iPSC-derived organoids show erratic contractile pattern .....</b>	<b>76</b>
<b>Organoids with patient iPSC-derived VNCCs have more erratic contractile pattern... ..</b>	<b>78</b>
<b>Patient iPSC-derived VNCCs are normal in size, proliferation, and migration.....</b>	<b>80</b>
<b>Patient iPSC-derived VNCCs overexpress <i>PLXNA3</i> .....</b>	<b>82</b>
Methodology (Chapter 2) .....	85
<b>Comprehensive discussion.....</b>	<b>87</b>
<b>Relevance: Chapter 1 .....</b>	<b>87</b>
<b>Derivation of human intestinal organoids with macrophages (HIO/Mac) .....</b>	<b>87</b>
<b>Cellular composition of the intestinal organoid resembles fetal intestine.....</b>	<b>88</b>
<b>Macrophage recruitment and retention by the organoid.....</b>	<b>89</b>
<b>Enteric neurons do not affect resident macrophage establishment.....</b>	<b>89</b>
<b>Macrophages migrate to the wound site upon injury.....</b>	<b>90</b>
<b>Macrophages localize to intestinal micro-anatomical niches in xenograft-matured organoids .....</b>	<b>90</b>
<b>Organoid macrophages acquire transcriptomic profile alike fetal intestinal macrophages.....</b>	<b>91</b>
<b>Macrophages regulate intestinal organoid growth .....</b>	<b>92</b>

<b>Macrophages attenuate mesenchymal cell glycolysis in developing intestinal organoids .....</b>	<b>93</b>
<b>Oncostatin M (OSM) reduces glycolytic gene expression in mesenchymal cells .....</b>	<b>93</b>
<b>Limitations of the study .....</b>	<b>94</b>
<b>Relevance: Chapter 2 .....</b>	<b>94</b>
<b>    Patient enteric neurons have disorganized morphology and lack surrounding interstitial cells of cajal (ICC) .....</b>	<b>94</b>
<b>    Patient iPSC-derived organoids show erratic contractile pattern .....</b>	<b>95</b>
<b>    Organoids with patient iPSC-derived VNCCs have more erratic contractile pattern...</b>	<b>95</b>
<b>    Patient iPSC-derived VNCCs are normal in size, proliferation, and migration .....</b>	<b>96</b>
<b>    Patient iPSC-derived VNCCs overexpress <i>PLXNA3</i> .....</b>	<b>96</b>
<b>    Limitations of the study .....</b>	<b>97</b>
<b>Overview .....</b>	<b>98</b>
<b>Final conclusion and summary .....</b>	<b>99</b>
<b>    Relevance Chapter 1 .....</b>	<b>99</b>
<b>    Relevance: Chapter 2 .....</b>	<b>100</b>
<b>Appendices .....</b>	<b>102</b>
<b>    Supplementary figures (Chapter 1) .....</b>	<b>102</b>
<b>    Supplementary figures (Chapter 2) .....</b>	<b>117</b>
<b>Bibliography .....</b>	<b>119</b>

## **Abstract (en)**

Macrophages populate the embryo early in gestation but their role in the developmental process remains largely unknown. In particular, specification and function of macrophages in intestinal development remain little explored. Pluripotent stem cell (PSC)-derived intestinal tissue, known as human intestinal organoid (HIO), mimics a developing human intestine and can be a useful model to study intestinal macrophages in development. To study this event in human developmental context, we derived and combined HIO and macrophages from PSCs. Macrophages migrated into the organoid, proliferated, and occupied the emerging micro-anatomical niches of epithelial crypts and ganglia. They also acquired a transcriptomic profile similar to fetal intestinal macrophages and displayed tissue macrophage behaviors, such as recruitment to tissue injury. Using this model, we show that macrophages reduce glycolysis in mesenchymal cells and limit tissue growth without affecting tissue architecture, in contrast to the pro-growth effect of enteric neurons. In short, we engineered an intestinal tissue model populated with macrophages, and we suggest that resident macrophages contribute to regulation of metabolism and growth of the developing intestine.

HIO can also be a powerful tool to understand human disorder. Chronic Atrial and Intestinal Dysrhythmia (CAID) is a rare genetic disorder that results in a progressive dysfunction of cardiac and intestinal contraction. There is no effective treatment for the intestinal dysfunction, or chronic intestinal pseudo-obstruction (CIPO). CAID syndrome is caused by a mutation in the gene *SGO1* which regulates the unloading of cohesin complex from the chromatids and centrosome during cell division. Mutation in another cohesin complex protein *RAD21* also causes CIPO and disrupts neuronal gene

expression. Both RAD21 and SGO1 are expressed in enteric neuronal ganglia; thus, we suspect CIPO in CAID to be neuropathological in origin. To model the disease, we utilized patient-derived induced pluripotent stem cells (iPSC) to derive human intestinal organoids (HIO) and vagal neural crest cell (VNCC) and combined to engineer HIO with enteric nervous system (HIO/ENS), as previously described. Isometric force measurement of patient organoids showed erratic contractile patterns. Furthermore, a genotype hybrid of HIO/ENS derived from patient or control iPSCs indicate a neuropathological origin of the erratic contractile pattern. Patient VNCC also showed dysregulation of *PLXNA3* expression, a gene involved in neuronal development. In conclusion, our patient-derived organoid and cellular model indicate neuropathological origin of intestinal dysfunction seen in CAID syndrome.

## **Resume (fr)**

Les macrophages peuplent l'embryon au début de la gestation, mais leur rôle dans le processus de développement reste largement inconnu. En particulier, la spécification et la fonction des macrophages dans le développement intestinal restent peu explorées. Le tissu intestinal dérivé de cellules souches pluripotentes (PSC), connu sous le nom d'organoïde intestinal humain (HIO), imite un intestin humain en développement et peut être un modèle utile pour étudier les macrophages intestinaux en développement. Pour étudier cet événement dans le contexte du développement humain, nous avons dérivé et combiné les HIO et les macrophages des PSC. Les macrophages ont migré dans l'organoïde, proliféré et occupé les niches micro-anatomiques émergentes des cryptes épithéliales et des ganglions. Ils ont également acquis un profil transcriptomique similaire aux macrophages intestinaux fœtaux et ont affiché des comportements de macrophages tissulaires, tels que le recrutement de lésions tissulaires. En utilisant ce modèle, nous montrons que les macrophages réduisent la glycolyse dans les cellules mésenchymateuses et limitent la croissance tissulaire sans affecter l'architecture tissulaire, contrairement à l'effet pro-croissance des neurones entériques. En bref, nous avons conçu un modèle de tissu intestinal peuplé de macrophages, et nous suggérons que les macrophages résidents contribuent à la régulation du métabolisme et à la croissance de l'intestin en développement.

HIO peut également être un outil puissant pour comprendre le désordre humain. La dysrythmie auriculaire et intestinale chronique (CAID) est une maladie génétique rare qui se traduit par un dysfonctionnement progressif de la contraction cardiaque et intestinale. Il n'existe pas de traitement efficace pour le dysfonctionnement intestinal ou la pseudo-

obstruction intestinale chronique (CIPO). Le syndrome CAID est causé par une mutation du gène *SGO1* qui régule la décharge du complexe cohésine des chromatides et du centrosome lors de la division cellulaire. La mutation dans une autre protéine complexe de cohésine *RAD21* provoque également le CIPO et perturbe l'expression des gènes neuronaux. *RAD21* et *SGO1* sont tous deux exprimés dans les ganglions neuronaux entériques; ainsi, nous suspectons CIPO dans CAID d'être d'origine neuropathologique. Pour modéliser la maladie, nous avons utilisé des cellules souches pluripotentes induites dérivées de patients (iPSC) pour dériver des organoïdes intestinaux humains (HIO) et des cellules de crête neurale vagale (VNCC) et combinés pour concevoir HIO avec le système nerveux entérique (HIO/ENS), comme précédemment décrit. La mesure de la force isométrique des organoïdes des patients a montré des schémas contractiles erratiques. De plus, un hybride de génotype de HIO / ENS dérivé de iPSC de patients ou de contrôle indique une origine neuropathologique du schéma contractile erratique. Les VNCC des patients ont également montré une dérégulation de l'expression de *PLXNA3*, un gène impliqué dans le développement neuronal. En conclusion, notre modèle organoïde et cellulaire dérivé des patients indiquent l'origine neuropathologique du dysfonctionnement intestinal observé dans le syndrome CAID.

## **Acknowledgements**

I would like to take this chance to express my gratitude to those directly involved.

First, I thank my supervisor Gregor Andelfinger for sharing my enthusiasm, mentorship, and his unyielding support. I thank my co-supervisor Craig Mandato for his support throughout the PhD. I thank the PhD committee members: Elaine Davis, Chris Rocheleau, Alex Gregorieff, and Luke Healy for the discussion and input. I would also like to recognize and thank the following individuals and organizations. CHUSJ core facilities: Reprogramming of cells and gene editing, Basma Benabdallah; Cytometry, Ines Boufaied; Imaging by microscopy, Elke Kuster. Sabine Herblot from Michel Duval lab provided the human dendritic cell. Sylvain Chemtob lab offered the use of isometric force measurement apparatus. Fonds de Recherche du Québec Nature et Technologies for the for the doctoral scholarship.

## **Contribution to original knowledge**

Chapter 1: We demonstrate an efficient and reliable method to populate human intestinal organoids with resident macrophages (HIO/Mac). These HIO/Mac were characterized with histology, single-cell transcriptomic, and functionally, which showed similarity between the HIO/Mac to the *in vivo* counterpart. In functional studies, we showed supporting evidence for previous studies on mice, which showed enteric neural cell-independent establishment of embryonic macrophages and embryonic macrophage recruitment to injury site. Finally, our studies suggest novel functions of embryonic intestinal macrophages on regulating glycolytic metabolism and organ growth.

Chapter 2: By using patient iPSC-derived human intestinal organoid with enteric nervous system (HIO/ENS) we find evidence that CAID syndrome is a result of aberration in vagal neural crest cells. Specifically, we find erratic contractile pattern in organoids with patient iPSC-derived ENS and transcriptomic analysis of the enteric nervous system precursors (vagal neural crest cells) and patient iPSCs show dysregulation of neurodevelopmental gene in both cell types. Together, the results suggest that *SGO1* mutation in patients cause developmental predisposition to aberration in neural lineage.

## **Contribution of authors**

Chapter 1:

*Andrew T. Song, Renata H. M. Sindeaux, Yuanyi Li, Hicham Affia, Tapan Agnihotri, Severine Leclerc, Patrick Piet van Vliet, Mathieu Colas, Jean-Victor Guimond, Natasha Patey, Jean-Sebastien Joyal, Elie Haddad, Luis Barreiro, Gregor Andelfinger*

R.S., A.S., and S.L. derived the macrophages. Y.L. performed surgical procedures in mice. S.L. and P.V. prepared the libraries for scRNAseq. A.S., H.A. performed bioinformatics analyses. T.A. performed the glycolytic stress test. M.C. and A.S. performed image analyses. J.G. and N.P. collected the fetal tissues. A.S. conducted the other experiments, designed the experiments, and wrote this thesis. G.A. supervised all aspects of the study and provided funding.

Chapter 2:

*Andrew T. Song, Lara Feulner, Severine Leclerc, Gregor Andelfinger*

S.L. and A.S. performed histology on patient samples. L.F. analyzed bulk RNA sequencing data. A.S. conducted the other experiments, designed the experiments, and wrote this thesis. G.A. supervised all aspects of the study and provided funding.

## **List of figures and tables**

*\*Actual figures and tables are embedded within the 'Research findings' in the relevant location or in the 'Appendices'.*

### **Figures (Chapter 1)**

Figure1. Derivation of human intestinal organoid with macrophages (HIO/Mac).

Figure2. Cellular composition of human intestinal organoid (HIO) with macrophages and enteric neurons.

Figure3. Macrophages localize to intestinal micro-anatomical niches in xenograft-matured intestinal organoid.

Figure4. Intestinal organoid macrophages acquire transcriptomic profile alike fetal intestinal macrophages.

Figure5. Macrophages reduce the growth of intestinal organoid without affecting tissue architecture.

Figure6. Macrophages attenuate mesenchymal cell glycolysis in developing intestinal organoids.

Figure7. Oncostatin M (OSM) reduces glycolytic gene expression in mesenchymal cells.

### **Figures (Chapter2)**

Figure1. Patient enteric neurons have disorganized morphology and lack surrounding interstitial cells of cajal (ICC).

Figure2. Patient iPSC-derived organoids show erratic contractile pattern.

Figure3. Organoids with patient iPSC-derived VNCCs have more erratic contractile pattern.

Figure4. Patient iPSC-derived VNCCs are normal in size, proliferation, and migration.

Figure5. Patient iPSC-derived VNCCs overexpress PLXNA3.

### **Supplementary figures (Chapter 1)**

FigureS1. Macrophages in early embryonic mouse intestine, fetal intestine, and human intestinal organoid (HIO), related to Figure1 & 2 & 4.

FigureS2. Migration and retention of macrophages in the organoid, related to Figure1 & 2.

FigureS3. Characterization of grafted organoids, related to Figure3.

FigureS4. scRNAseq analyses of fetal intestine and organoid macrophages, related to Figure4.

FigureS5. Efficiency of macrophage removal using magnetic microbead, related to Methods & Figure6.

FigureS6. Characterization of hiPSC-derived human intestinal organoid, vagal neural crest, and macrophage, related to Methods.

Table S1. Related to Figure2, 7, and S6.

### **Supplementary figures (Chapter 2)**

Supplementary Figure1. Some organoids lack enteric neurons and erratic contractile pattern does not correlate. Related to Figure2 and 3.

### **List of abbreviations**

\*Full phrases and their abbreviations also recur throughout the thesis for convenience.

2-DG (2-Deoxy-D-glucose)

APC (Antigen-presenting cells)

AV (Atrioventricular)

BF (Bright field)

CS (Carnegie stage)

CPI (Chemotactic precision index)

CAID (Chronic atrial and intestinal dysrhythmia)

CIPO (Chronic intestinal pseudo-obstruction)

DC (Dendritic cell)

hiPSC<sup>eGFP</sup> (eGFP-tagged hiPSC)

EDM-base (Endoderm differentiation media base)

eGFP (enhanced green fluorescent protein)

ENS (Enteric nervous system)

EMP (Erythromyeloid progenitors)

E.coli (Escherichia coli)

ECAR (Extracellular acidification rate)

GI (Gastro-intestinal)

HES (Hematoxylin-eosin-saffron)

HIO/ENS or HE (HIO with enteric nervous system)

HIO/ENS/Mac or HEM (HIO/Mac with ENS)

Mac<sup>eGFP</sup> (hiPSC<sup>eGFP</sup>-derived macrophages)

hiPSC (Human induced pluripotent stem cells)

HIO (Human intestinal organoid)

HIO/Mac (Human intestinal organoid with macrophages)

NSG (non-obese diabetic/Prkdc<sup>SCID</sup>/Il2rg<sup>null</sup>)

iPSC (Induced pluripotent stem cells)

ICC (Interstitial cells of cajal)

IBM (intestinal basal media)  
ISC (Intestinal stem cell)  
IFM (Isometric force measurement)  
Mac (Macrophages)  
MMC (Migrating motor complex)  
NIM (Neural induction media)  
OSM (Oncostatin M)  
PBMC (Peripheral blood mononuclear cell)  
PSC (Pluripotent stem cell)  
IPAN (Primary afferent neurons)  
qPCR (Quantitative PCR)  
scRNAseq (Single-cell RNA-sequencing)  
TAD (Topologically associated domain)  
TMS (Trichrome Masson)  
UMAP (Uniform Manifold Approximation and Projection)  
VNCC (Vagal neural crest cell)  
Y27 (Y27632)

## **Introduction**

### **Chapter 1**

#### **Rationale**

Macrophages occupy the embryo early on but their role in the developmental process remains largely unknown. In particular, specification and function of macrophages in intestinal development remain unexplored. Understanding how macrophages initially specify into intestinal macrophages and how they behave during the development may give insight into the nature of their dualistic roles in intestinal disease progression and recovery.

#### **Objectives**

- 1) Recapitulate the migration of macrophages into intestine with pluripotent stem cell-derived macrophages and human intestinal organoid (HIO).
- 2) Characterize the macrophage populated human intestinal organoid (HIO/Mac).
- 3) Compare organoids with or without macrophages to see if there are macrophage-specific effects.

### **Chapter 2**

#### **Rationale**

Chronic Atrial and Intestinal Dysrhythmia (CAID) is a rare genetic disorder that results in a progressive dysfunction of cardiac and intestinal contraction<sup>1</sup>. Cardiac arrhythmia can be managed with a pacemaker; however, no effective treatment or medical procedure can manage the debilitating intestinal dysfunction or chronic intestinal pseudo-obstruction

(CIPO). Thus, the end goal is to understand the pathomechanism in order to develop a treatment. Furthermore, it is an opportunity to study CIPO and intestinal pseudo obstruction in general, taking advantage of the fact that a singular genetic mutation is causing the illness. Mouse models with the patient's homozygous *SGO1* mutation or knockout were embryonic lethal and conditional knock out in adult did not display CAID phenotypes. Patient iPSC-derived human intestinal organoids (HIO) and cells, thus, presents as an alternative to a traditional model to understand CAID syndrome in a human biological context. Previous studies showed genetic insults on a protein-coding gene in the same protein complex as *SGO1* also cause CIPO and dysregulation in neurogenesis. Thus, we tested if CAID syndrome is neuropathic in origin.

### **Objectives**

- 1) Derive patient iPSC-derived human intestinal organoid with enteric nervous system and assess their motility.
- 2) If the patient organoids display intestinal motility phenotype, generate genetic hybrids of HIO and ENS from patient vs. control iPSC lines.
- 3) Assess patient iPSC-derived neural crest cells against controls.

## **Literature review**

### **Relevance: Chapter 1**

#### **Intestine**

Gastro-intestinal (GI) tract is a muscular tube that moves the ingested food through its tract with the primary objective to absorb the contents for bodily use and expel the waste. Along the tract, it sequentially digests the contents to absorbable units with the physical force of the contraction and digestive enzymes derived from the pancreas. The lumen of the GI tract is, thus, contiguous with the outside world and is constantly in contact with foreign material and microorganisms against which it must defend itself.

Intestinal epithelial barrier is the first line of defense. Tightly inter-bound epithelial cells provide a cellular barrier against invasion by microorganisms. Intestinal epithelial cells additionally produce mucous, water trapped in a mesh of hydrophilic protein, which contains anti-microbial proteins and is controlled in pH, optimized for defense. Behind this epithelial barrier are specialized immune cells such as macrophages, T cells, B cells, mast cells, which provides a second line of defense. Specialized epithelial cells called Microfold cells pass on luminal content to specialized immune cells called antigen-presenting cells (APC) to sample the current immunological state of the intestine. Antigen-presenting cells, such as macrophages and dendritic cells also extend their cellular projections to phagocytose the contents of the lumen directly. The APCs then interact with other immune cells to mount an additional defense mechanism as required. Due to constant exposure to the microbiome within the tract, intestinal immune cells must stay vigilant and at the same time do not mount an unnecessary degree of immune response, which can damage the organ<sup>2,3</sup>. Though almost unperceivable to us, GI tract is constantly

undergoing a motion to mix, digest, and move the contents caudally. This motion is also thought to keep the more permanent microorganisms in the gut in the caudal segments of the tract<sup>4</sup>.

The contractile motion of the intestine is referred to as peristalsis and the force is generated by densely packed contiguous array of smooth muscle cells. There are two major configurations of smooth muscle within the intestine: circular and longitudinal. As the name suggests, the two array of muscle tissues squeeze and push, respectively, the content of the lumen caudally. The muscle contraction is initiated by specialized network of cells called interstitial cells of cajal. The initiation of contraction is further regulated by the intestine's intrinsic neuronal network, called the enteric nervous system, with additional feedback from the central nervous system by extrinsic neurons<sup>4,5</sup>.

Intestine is developmentally constructed from all three-germ layers, each playing an indispensable role in the organ's function. Shortly after gastrulation, endoderm begins to fold on to itself and forms the gut tube forming the intestinal epithelium. Mesoderm-derived mesenchymal cells surround the tube and differentiates into smooth muscle layers, subepithelial myofibroblasts, and fibroblasts. Ectoderm-derived neural crest cells then migrate from the neural tube into the developing intestine. Macrophages, first formed in the yolk sac, also migrate into the intestine as the first immune cell and homeostatic regulator. Each cell type relies on chemical and physical cues from the others to form the vilified intestinal structure in adult<sup>6,7</sup>. The development of the corrugated epithelial structure referred to as the villi, for example, is dependent on the differentiation of mesoderm into smooth muscle. The smooth muscle physically restricts the circumference

of the epithelium layer, which folds to form the villi under the force generated from its own proliferation<sup>8</sup>.

## **Macrophages**

Macrophages are innate immune cells with high phagocytic capacity and amoeba-like behaviors. They are ubiquitous throughout the body and show variations in morphology and behavior depending on the spatial niche they reside in. In recent years, much advancement in our understanding of macrophages has been made in their ontology and non-immunological functions.

Initially thought to derive exclusively from the bone marrow, macrophages are now known to first arise at early embryonic development from the yolk sac and spread throughout the embryo. Embryonic macrophages first arise from hemogenic endothelium in the yolk sac blood vessel. Erythromyeloid progenitors (EMP) gives rise to primitive nucleated erythroblasts and myeloid cells: macrophages, and megakaryocytes. These yolk sac macrophages spread throughout the embryo. These EMPs seed the fetal liver, where macrophage and erythroblast production makes a transition from yolk sac to the fetal liver<sup>9</sup>. Subsequently, definitive hematopoietic stem cells (HSC) form at the aorta-gonad-mesonephros and seed the fetal liver giving rise to all other hematopoietic lineages including monocytes/macrophages. In the later stage of development and after birth, HSCs seeded in the bone marrow takes over the hematopoietic production from the fetal liver. In summary, macrophages are one of the first three blood cells to form in the embryonic development, and the major production site transitions from yolk sac to fetal liver to bone marrow<sup>10</sup>. Macrophages seeded throughout the embryo establish local proliferation and become self-maintaining. Additional production at the bone marrow

supplies local demand when required and systemic demands throughout the organism's life<sup>10,11</sup>.

As the early embryonic production alludes to, macrophages are an evolutionarily ancient cell type, which can also be found in invertebrate like starfish. Older vertebrates such as fruit flies do not have traditional adaptive immune cell as mammals (T cells and B cells) and relies on phagocytes (or macrophages) for cellular immunity. Thus, perhaps unsurprising in retrospect, function of these ubiquitously distributed phagocytes is not limited to innate immunity.

Macrophages play diverse roles that are either assistive or crucial to tissue homeostasis, varying greatly from tissue to tissue. Cardiac macrophages support normal electrophysiological conduction at the atrioventricular (AV) node of the heart. They are electrochemically linked with the node via gap junction protein connexin 43 (*GJA1*) and maintains the resting membrane to be more positive. Macrophage-specific conditional deletion of connexin 43 results in delayed AV node conduction<sup>12,13</sup>. Osteoclasts are fused-multinucleated macrophages, which remodel bone extracellular matrix along with osteoblasts. Macrophages also maintain epithelial stem cell homeostasis in multiple organs, regulate neuronal function, and regulate insulin resistance and thermogenesis in white and brown adipose tissue. Phagocytic capacity is also re-purposed in various occasions, such as removal of nuclei from erythroblast in the bone marrow to iron recycling in the spleen and liver. The range of tissue-specific function of macrophages is vast<sup>14–18</sup>.

Homeostatic regulatory function of macrophages is also crucial in wound healing. Following a tissue injury, macrophages adopt a pro-inflammatory state (M1) in order to

recruit additional immune cells via inflammatory cytokines and mount a more active phagocytic response for defense and debris clearing. As the infection and/or tissue damage clears, macrophages adopt an alternative fate to promote regeneration (M2) and produce growth factors to promote angiogenesis and cell proliferation, promote extracellular matrix formation, and suppress further inflammation<sup>19</sup>. Similarly, macrophages are also indispensable for regeneration in species such as axolotl, which has higher regenerative capacity than humans. Macrophages display M1 and M2 fate simultaneously during limb regeneration after amputation, and fails regenerate when these macrophages are ablated<sup>20</sup>. Recruitment of macrophages in embryonic and fetal wound healing was also previously noted<sup>21,22</sup>.

Macrophages can be recruited by a diverse array of chemokine signals to the site of inflammation. The most prominent cytokine involved in inflammation is CCL2 (MCP1). Monocytes in circulation express the receptor CCR2, and are recruited in a CCL2-dependent manner<sup>23</sup>. CCL7 is also an alternate ligand to the receptor CCR2<sup>24</sup>. CCR1, CCR4, CCR5 also bind to CCL3 and CCL5 and are involved in recruiting the macrophages, and have been shown to recruit macrophages to the site of renal and neuro-inflammation<sup>25,26</sup>. CX3CR1-CX3CL1 is involved in recruiting macrophages to the inflammatory site such as atherosclerosis, but also shown to be involved in macrophage recruitment to the embryo proper during the development. CX3CR1 knock out mice embryos have significantly reduced number of tissue-resident macrophages, but not deficient. This indicates that macrophage recruitment during the development is multifactorial is not entirely dependent on CX3CR1-CX3CL1 signaling<sup>27-29</sup>. CSF1R-CSF1 is also involved in macrophage recruitment during the development and induces

chemotactic response from macrophages in vitro. CSF1 is also a crucial to macrophage survival, proliferation, and differentiation factor<sup>30–32</sup>. However, what signaling or how infiltrating macrophages localize to each sub-anatomical niche (e.g. neuron vs. vascular) is little addressed. It is also worth noting here that categorizing cytokines often involved with inflammation as “inflammatory” may be an oversimplification. For example, though CCL2 is upregulated in injury and infection it is expressed in virtually all tissues at a base level and is crucial for monocyte recruitment in the steady-state in adult intestine<sup>23,33</sup>.

Gross effect of macrophages on organ development is also striking<sup>31</sup>. Ablation of macrophages in *Csf1r* knockout mice show defects in musculoskeletal development, likely due to lack of osteoclasts. The overall body weight is also lower. Organs such as kidney show reduced medullary area but relative increase in the cortex, suggesting developmental defect when combined with previous observation on macrophage’s effect on kidney development<sup>34</sup>. Serum glucose is also lower, and liver accumulates lipid droplets when macrophages are ablated. Peyer’s patches in the intestines are reduced; however, no other gross anatomical defects or epithelial differentiation anomaly seem to be observable in this knock out model. Re-introduction of macrophages seems to rescue the musculoskeletal and hepatic defects.

### **Intestinal Macrophages**

Understanding of intestinal macrophages has also expanded significantly in recent years. Adult intestinal macrophages are constantly replenished by bone-marrow-derived monocytes from circulation<sup>23</sup>. This fast turnover, however, seems to apply mostly for macrophages in the mucosa performing immune functions. Many other subtypes of macrophages undergo local proliferation, not unlike macrophages in other organs. More

surprisingly, a small percentage of these locally self-maintaining population was shown to be embryonic in origin<sup>35</sup>. This embryonic population establishes as early as E9.5 (E, days after post-coitus) in mice foregut<sup>36</sup>.

Intestine harbors a range of macrophage subtypes in distinct spatial niches. Within the villi, they phagocytose contents of the lumen through the epithelium either directly through inter-epithelial cellular projections or indirectly via Microfold cells which relay pre-processed antigen to the other side of the epithelial barrier<sup>37-39</sup>. Additionally, mucosa-villi residing macrophages have reduced pro-inflammatory response to inflammatory stimuli but maintain their phagocytic capacity, making intestinal macrophages a prime subtype to study for their involvement in inflammatory diseases<sup>3</sup>. A long-standing perception was that intestinal macrophages are entirely derived from circulating monocytes and only short-lived. This observation remains supported for a large majority of intestinal macrophages; however, recent findings suggest that certain subtypes in specific spatial niches are self-maintaining and furthermore a small portion derives from embryonic macrophages<sup>35</sup>. In further detail regarding these self-maintaining populations, crypt-associated macrophages regulate epithelial stemness, differentiation, and regeneration. Macrophages seems to produce Wnt4 and Rspo1 to exert this effect. Furthermore, reduced proportion of proliferating crypt cells, Paneth cells, and Microfold cells has been observed in macrophage ablation experiments in adult mice<sup>40-42</sup>. External innervation and enteric nervous system collaborate with adjacent macrophages to regulate immune response and peristalsis. Enteric neurons provide CSF1, a crucial macrophage survival and differentiation cue, and macrophages in turn produce BMP2 for enteric neurons which modulates peristalsis. Furthermore, sympathetic innervation signal the status of distal

infection to intestinal macrophages via beta-2-adrenergic receptor signaling<sup>35,43,44</sup>. In regulating peristalsis, macrophages also detect thermal, mechanical, and chemical changes in the environment via TRPV4 surface protein and directly regulates smooth muscle motility via prostaglandin E2<sup>45</sup>. Intestinal macrophages also associate closely with the blood vessels and their ablation disrupts intestinal vasculature<sup>35</sup>. Though many functional subtypes of intestinal macrophages have been defined in adult organisms, why macrophages populate the organ so early on in the embryonic development remains unaddressed.

### **Lesser-known functions of macrophages**

Developmental roles of macrophages are generally less understood than their functions in cellular immunity and niche-specific homeostasis. Evidence in mice and ex-vivo studies thus far suggest that they are indispensable for proper development of certain tissues. Specifically, comparison of macrophage ablation at adulthood versus the transgenic mice that constitutively lacks macrophages showed less severe phenotypes in ablation at adulthood in certain organs, suggesting that their presence during prenatal development has more impact on the organs than their presence in adulthood<sup>46</sup>. At an embryonic stage, they have been shown to regulate the growth of kidney and ureteric bud branching, the development of pancreatic islet, and formation of coronary plexus and lymphatic vessel in developing heart<sup>34,47-50</sup>. During post-natal development, they seem to be required for proper mammary epithelial remodelling, vascular remodelling in the eye, and brain development<sup>51-55</sup>. In the central nervous system development, macrophages actively phagocytose neuronal synapses to prune neuronal network, where ablation of macrophages resulted in morphological disfigurement of the brain, electrophysiological

dysregulation of the neurons, and behavioral studies show impairment of olfactory capacity<sup>54,55</sup>. Enteric nervous system has as many neurons as the spinal cord. Unsurprisingly, a recent report shows that a similar process regulate post-natal development of the enteric nervous system. Depletion of macrophages in postnatal mice disrupts synaptic pruning of enteric neurons and results in abnormal intestinal transit. Tgf-beta produced by the enteric neuron seems to regulate the differentiation of macrophages to the neuron-associated phenotype which regulates the peristalsis<sup>56,57</sup>. Macrophages' role in embryonic and perinatal stage has been shown to be essential in the proper development of the organism; however, data on their involvement in early development is disproportionately lacking, in part due to lack of tools to study such early events.

Macrophages also regulate the metabolism of peripheral cells. They have been shown to regulate insulin-dependent glucose metabolism of adipocytes. Pparg is required to attain macrophages that regulate glucose homeostasis and macrophage-specific knock out of Pparg result in glucose intolerance, insulin resistance, and diet-induced obesity. This metabolic regulatory role is in contrast with infiltrating macrophages that are pro-inflammatory in state, since ablation of these macrophages reduced insulin sensitivity in mice. These two results also emphasizes the magnitude of macrophage specification has on its regulatory function<sup>16,58</sup>. Furthermore, macrophages regulate thermogenesis in brown adipose tissue. Cold environment triggered Il4-dependent macrophage specification which increased energy expenditure of the mice. The Il4 dependent macrophages seems to be triggering thermogenesis by producing catecholamines<sup>17</sup>.

Oncostatin M (OSM) is a multifunctional growth factor that binds to the receptors OSMR and LIFR. OSM is highly expressed in macrophages and T cells<sup>59</sup>. *Osmr* knock out in

mice causes adipose tissue inflammation and insulin resistance. Treatment of the mice with Osm increased insulin sensitivity indicating its role in suppression of the development of insulin resistance<sup>60</sup>. Further studies show that lack of Osm-signaling worsens high-fat diet induced metabolic disorder in mice<sup>61,62</sup>. A more recent study demonstrates elevated OSM expression in patients with obesity and hyperglycemia<sup>63</sup>. The role of macrophages and T cells has been suggested but no direct association with metabolic regulation of adipocytes has been demonstrated. Not unlike the Pparg-mediated macrophages and thermogenic regulation of macrophages, macrophage-OSM may play a role in regulating glucose metabolism. Finally, it raises a question if macrophage's regulation of metabolism is also present in other tissues or developmental stages.

This metabolic regulatory mechanism by macrophages seems to be abused by cancer cells to promote tumor growth. Tumor-associated macrophages stimulate Pgc1 pathway in glycolysis of cancer cells via secretion of Il6. PGK1 activation also correlates with prognosis of human cancer, such as glioblastoma<sup>64</sup>. Macrophages are enriched in majority of solid tumor. Considering tumor itself does not generate *de novo* mechanisms, but rather abuse existing macrophage capacity, understanding macrophage functionality may have direct relevance to clinical translation.

### **Models used to study macrophages**

Ever since Ilya Mechnikov first defined the mobile-phagocytic cells in the transparent starfish larvae, many models were used to build the current understanding of macrophages, each with strengths and weaknesses. Zebrafish is an excellent vertebrate model that can produce a high number of offspring. Furthermore, its external development along with nearly transparent embryo provides high *in vivo* optical accessibility. Its gross

anatomical structures, however, differ much from that of human. Mouse has a short life cycle and is anatomically and genetically closer to human. Transgenic mouse models such as tamoxifen inducible CSF1R or CX3CR1-fluorescent protein lineage tracing and Fas-induced or diphtheria toxin receptor-mediated cell ablation models have facilitated pivotal discoveries in recent years<sup>65–67</sup>. Gene-specific models such as above, however, show variable efficacy in ablation towards specific macrophage subtypes and between different organs, largely due to macrophage heterogeneity<sup>68</sup>. Human cell culture such as immortalized cell lines THP-1 and U937 along with blood monocyte-macrophage culture has also been a useful tool to study fundamental cell biology; however, they are limited in their capacity to model cell state in native tissue environments<sup>69</sup>. Now, advancements in pluripotent stem cell culture and its directed differentiation, enables us to generate cell types and tissue-like multicellular constructs to model human biology *in vitro*. Versatility in manipulation and complexity of the tissue-like constructs, also known as organoids, should be particularly useful to model early human development where access to human samples is difficult or implausible.

### **Intestinal organoids**

A miniature version of a human intestine that is smaller than a pea can be grown in a dish. There are two major categories of intestinal organoids: epithelial organoid or multi-cell type organoid, though the terminology used in the field often does not make the distinction. Epithelial organoid, also referred to as ‘epithelioid’, consists only of epithelial cells. Intestinal stem cell (ISC), maintained by growth factors in the media, proliferate and create three-dimensional villi-crypt-like structures. They can be derived from ISCs isolated from intestinal biopsies or from differentiation of PSC<sup>70,71</sup>. Multi-cell type intestinal

organoid, also referred to as human intestinal organoid (HIO), is generated from PSC or iPSC by recapitulating the embryonic development. HIO contains both the endodermal lineage that gives rise to the epithelial cells and mesodermal lineage that gives rise to mesenchymal progenitors. Compared to epithelioid, HIO can model more complex intestinal environment due to the mesenchymal progenitors and different cell types that derives from it, which interacts with the epithelium. Additionally, grafting HIO onto immunodeficient mouse matures the organoid further and recapitulates histological complexity comparable to that of late fetal stage and undergoes spontaneous peristaltic-like contractions<sup>72-74</sup>. HIO in itself, however, does not contain all the progenitor lineages to develop into a complete intestine, if one were to define an organ as an isolated unit. Two major lineages that are missing are: neural crest cells that becomes the enteric nervous system and immune cells. Vagal neural crest co-culture with HIO has been shown to give rise to enteric ganglia and glial network within the organoid<sup>75</sup>. With immune cells, a recent report attempted to incorporate macrophages with 'gut organoid', which does not utilize directed differentiation approach. The resulting tissue lacked convincing histological architecture of an intestine, and impact of macrophages on organoid and vice versa were little explored. Furthermore, the context of intestinal development and implication of macrophages were not explored<sup>76</sup>.

The method to generate PSC-derived macrophage, which resembles yolk-sac derived embryonic macrophages was described previously<sup>77,78</sup>. Thus, in Chapter1, I first aimed to use established directed differentiation method to derive HIO and the PSC-derived macrophages in order to recapitulate the early migration of macrophages into the embryonic intestine.

## Relevance: Chapter 2

### CAID syndrome

Our lab has previously identified a rare genetic mutation in *SGO1* (K23E) that results in a progressive dysfunction of cardiac and intestinal contraction called chronic atrial and intestinal dysrhythmia (CAID). The disease was first identified in 16 patients French Canadians and 1 Swede with common genetic heritage with founders originating from Europe. The patients have sick sinus syndrome, a cardiac arrhythmia originating from the sinus node, and chronic intestinal pseudo-obstruction (CIPO), a blockage of the intestinal transit without mechanical obstruction. Patient fibroblasts showed accelerated cell cycling, increased senescence, and heightened sensitivity to TGF-beta activation and increased response. *SGO1* is involved in correct chromosome segregation during mitosis and meiosis. Chromosomal pair showed a defective centromeric cohesion, but without signs of aneuploidy. *Sgo1* was expressed in the developing heart of zebrafish. Morpholino knockdown of *Sgo1* in the developing zebrafish resulted in bradycardia<sup>1</sup>.

Though the arrhythmia of the heart can be addressed with a cardiac pacemaker, there is no effective treatment for CIPO. Clinically, CIPO is generally considered to be caused by two pathological origins: myopathic and neuropathic. Patient biopsies showed thinning and fibrosis of the smooth muscle layer. Furthermore, enteric ganglia were mislocalized. Manometry, a measurement of the propulsive force throughout the tract, showed inconclusive diagnosis on the pathological origin. Median age of diagnosis is 15 years old, but the onset of symptoms seems to be much earlier with the earliest diagnosis at 4 years of age. CIPO in itself can also be caused by mutations in other genes (*RAD21*, *SOX10*, *TYMP*, *POLG*, *FLNA*, *L1CAM* and *ACTG2*) where mechanisms may vary but

affected cell types are either smooth muscle or enteric neural cells<sup>79,80</sup>. For instance, SOX10 is involved in neural crest, which gives to the enteric nervous system, development and causes neuropathic CIPO<sup>81</sup>.

## **SGO1**

The patients are homozygous for a recessive point mutation in *SGO1*, resulting in a Lysine-to-Glutamic acid change at the highly conserved amino acid 23 (A>G, K23E). *SGO1* is part of the cohesion complex, which plays a major role in correct cell division. *SGO1* regulates the unloading of the cohesin complex from the chromatids during cell division<sup>1,82,83</sup>. Cohesin complex is a triangular loop-like structure made up of four core units regulated by several proteins. The core unit is comprised of the two arms (SMC1A, SMC3), the third arm (RAD21), and attachments to the third arm (STAG1/2). During mitosis and meiosis, cohesin complexes are distributed between the sister chromatids, holding them together with its loop. ESPL1 (Separase) acts to cleave the complex to separate the chromatids. *SGO1* prevents this cleavage until the metaphase is complete by recruiting the phosphatase protein PP2A to the cohesin complex. Similarly, this mechanism is also applied at the centrosome to ensure centriole pair separation occurs at the correct moment<sup>84</sup>. In this context, it is intriguing to note that *SGO1*-K23E mutation does not seem to confer increased susceptibility to cancer or noticeable effect on adult stem cell population such as intestinal stem cell (epithelium) in CAID patients<sup>1,85</sup>. Beyond cell division, the cohesion complex modulates three-dimensional genomic structure at topologically associated domain (TAD). They maintain the chromatin loop structures at TADs by wrapping the genomic DNA strand at the base of the loop via its interaction with the protein CTCF<sup>86</sup>. *Sgo1* in yeast, indeed, is involved in the organization of chromatin

structure during cell division in association with the cohesion complex. Unsurprisingly, knockout of *RAD21* shows chromatin loop dysregulation and gene expression changes in certain cell types, such as cortical neurons<sup>87</sup>. It is intriguing to note that *RAD21* mutation causes CIPO in humans and is expressed in enteric neuronal cells<sup>88–90</sup>. Our previous study also found SGO1 expression in enteric neuronal cells and retinal neurons in mouse<sup>91</sup>.

### **Enteric nervous system**

The enteric nervous system (ENS) is established by migrating neural crest from the vagal region of the neural tube<sup>5,92,93</sup>. The neural crest cell derivation relies on WNT signaling from the neural tube and the rest of the ectodermal structures<sup>94</sup>.

These vagal neural crest cells (VNCC) migrate into the proximal intestine and spread through out the tract early in the embryonic development. They subsequently proliferate and differentiate into enteric neurons and glial cells. Multiple neurons of different types are organized in a bundle called ganglion and connected to each other to form a vast neuronal network, which contains as many neurons as the spinal cord<sup>56,57</sup>. One of the genes that seems to be involved in ENS development is *PLXNA3*. *Plxna3* was previously identified in a transcriptomic analysis of developing zebrafish with *GFP* tagged *Phox2b* cells, a marker of enteric neural lineage, against non-neural cells<sup>95</sup>. *PLXNA3* also plays a role in neuronal guidance. During the development, gonadotropin-releasing hormone (GnRH) neurons migrate into the brain. This migration is guided by SEMA3A-NRP signaling pathway and *PLXNA* is a co-receptor for the receptor, NRP. Previous reports demonstrate that simultaneous loss of *Plxna1* and *Plxna3* results in olfactory and GnRH hypothalamic defects in mice. *Plxna1* and *Plxna3* were expressed in the migrating

neurons and olfactory ensheathing cells, glial cells that envelop olfactory axons<sup>96</sup>.

Additionally, missense variants of *SEMA3F* and *PLXNA3* cause defects in olfactory and hypogonadotropic hypogonadism in humans<sup>97</sup>.

Ganglia are located, at large, in between the two smooth muscle layers (myenteric) or the space below the epithelial domain (submucosa). ENS is involved in development of epithelial-barrier, detect mechanical and chemical changes, and contractile motion or peristalsis of the intestine, thus, integral to the organ's homeostasis and function<sup>4,5,92,93</sup>.

In detail, enteric glial cells produce s-nitroglutathione which reinforces epithelial barrier function by increasing cell-to-cell junction protein expression. Ablation of the enteric glia disrupted this barrier capacity and s-nitroglutathione treatment of patient biopsy samples showed an improvement of the barrier<sup>98</sup>. Intrinsic primary afferent neuron (IPAN), situated beneath the epithelium, also detects mechanical and chemical stimuli and relays this signal to the myenteric layer. Physical stimulation of the epithelium by a blow of nitrogen gas or cholera toxin activated the IPANs, which projects to the myenteric layer. Furthermore, physical stretching of the muscle preparation showed activation of afferent neurons within the muscular layer<sup>99,100</sup>.

The nature of the motility of the intestine is comparable to that of the heart. The electrical impulse that triggers the contraction is generated within the organ and regulated top-down by extrinsic neuronal input (e.g. sympathetic input). The initial electrical impulse is generated by interstitial cells of cajal (ICC), comparable to sinoatrial node in the heart, which forms a network directly on the smooth muscle<sup>101,102</sup>. ENS and ICC interact with each other and the smooth muscle directly to coordinate the contractile motion that propagates caudally. At large, peristalsis is regulated by three types of

myenteric neurons: excitatory and inhibitory motor neurons, interneurons, and IPANs. Motor neurons stimulate or inhibit smooth muscle contraction directly. Interneurons construct the neuronal circuitry. IPANs relay information from the lumen, such as mechanical stretch from food-intake, to the other myenteric neurons. In the absence of food intake, intestine undergoes an automatic motion referred to as migrating motor complex (MMC). In a clinical setting, MMC is observed by manometry in order to assess the status of the peristaltic capacity. MMC's is categorized into repetition of contractile patterns: quiescent to low activity (Phase I-II) and higher activity (phase III-IV).

### **Human intestinal organoid with enteric nervous system**

Previous report described human intestinal organoid model incorporated with enteric nervous system (HIO/ENS)<sup>75</sup>. HIO derivation begins by committing the pluripotent stem cells (PSC) to definitive endoderm and mesodermal cells by activation of nodal signaling pathway. The definitive endoderm and mesodermal cells are then committed to mid-hind gut identity by activation of FGF signaling and WNT activation. The resulting CDX2-positive mid-hindgut structures are then further cultured with a cocktail of growth factors promoting cell growth and epithelial expansion. As described, HIO derivation does not contain cell fate commitment to ectodermal lineage which gives rise to the neural tube and the migrating neural crest cells. The previous report adopted the neural crest differentiation from another established method, which commits PSC to ectodermal and neural tube formation<sup>103</sup>. The neural tube structure is then exposed to retinoic acid to modulate the anterior-posterior axis fate to be patterned into the vagal region. The vagal neural tube structure is then allowed to attach to a substrate and vagal neural crest-like cells are allowed to migrate and spread.

Since vagal neural crest cells (VNCC) actively migrate into and through the intestinal tract, the rationale was to co-culture the HIO and the VNCCs. Workman and colleagues demonstrate that the resulting HIO/ENS contained neuronal and glial cells, which differentiated from the incorporated VNCCs. Grafted HIO/ENS showed enteric ganglionic network, though immature, with glial cells distributed within the submucosa and in between the two muscle layers. These enteric ganglia were also enveloped with interstitial cells of cajal (ICC). Strikingly, the grafted organoids show spontaneous contraction reminiscent of the migrating motor complex, though the frequency of the contraction were higher than that of an adult. Recording of the motility of the grafted HIO/ENS with neuro-inhibitory compounds (tetrodotoxin) and stimulatory compound (dimethyl-phenyl-piperazinium) showed neuron-coupled motility.

*PHOX2B* mutation in humans causes Hirschsprung's disease where lack of enteric neurons results in a severe intestinal contractile dysfunction. Workman and colleagues showed that the HIO/ENS derived with *PHOX2B* mutant VNCCs also lacked enteric neuronal cells in the grafted organoids. These results indicated that the model can be useful to study the pathomechanism of CIPO in CAID syndrome.

In conclusion, mutation and knock out experiments in another cohesion complex protein *RAD21* suggest a neuropathic origin of CIPO. In order to test if *SGO1* mutation in CAID patients cause neuropathological CIPO, we utilized patient-derived induced pluripotent stem cells (iPSC) to model the disease. Human intestinal organoids (HIO) and vagal neural crest cells were derived with patient and control iPSC to create a HIO with functional enteric nervous system (HIO/ENS), as previously described, to understand the pathomechanism of CAID syndrome<sup>75</sup>.

## **Chapter 1: Developmental role of macrophages modelled in human pluripotent stem cell derived intestinal tissue**

### **Research findings (Chapter 1)**

#### **Derivation of human intestinal organoids with macrophages (HIO/Mac)**

Embryonic macrophages begin to migrate and populate the organism early in the development<sup>36,104</sup>. We postulated macrophages would migrate and populate the intestinal organoid most efficiently beyond a specific developmental time point; thus, inquired when intestinal macrophages are first observable. In mice, macrophages (AIF1<sup>+</sup>) were first observed in the mid-hindgut at E10.5, which approximately corresponds to 30 days post conception (day 30) in human development or Carnegie stage 13 (CS13)<sup>105</sup>(FigureS1A, Figure1A). In humans, we identified macrophages in a single-cell RNA-sequencing (scRNAseq) dataset of day 47 fetal proximal intestine, the earliest dataset reported to date<sup>106</sup> (Figure2B-D, FigureS1D). The results thus indicate that macrophages populate both the mouse and human intestine at an early embryonic stage. Based on these results, we estimated that the first macrophage occupation of the human intestine would start approximately at day 30.

HIOs and macrophages were derived from human induced pluripotent stem cells (hiPSC) based on previously described methods with minor modifications<sup>72,75,77</sup>. We used macrophage derivation which recapitulates early embryonic macrophage ontogeny<sup>78</sup>. Day 21-28 HIOs were used, which roughly corresponds to day 30 based on our previous estimation taking the inner cell mass formation (~7days since conception) into account. HIOs were co-cultured with the macrophages in a three-dimensional Matrigel droplet for 7 days, during which macrophages in the periphery migrated into HIOs (Figure1C-F,

FigureS1F). HIOs with macrophages (HIO/Mac) were then transferred into a new Matrigel droplet and cultured in the absence of peripheral macrophages for 7 days (Figure1B). As expected, CD14<sup>+</sup>/AIF1<sup>+</sup> macrophages were present in HIO/Mac but not in HIO (Figure1D, F). Furthermore, macrophages proliferated within the HIO alike embryonic tissue resident macrophages (FigureS1B,C). Similar to E15.5 mice, macrophages in the HIO either associated tightly with the epithelium or were found within the surrounding mesenchyme (FigureS1E).

### **Cellular composition of the intestinal organoid resembles fetal intestine**

We first examined the cellular composition of the organoid. In the intestine, neurons of the enteric nervous system (ENS) localize closely with macrophages and together regulate peristalsis and immune response<sup>35,43,44</sup>. To increase the complexity of HIO/Mac for following characterizations and experiments, we also derived HIO/Mac with ENS (HIO/ENS/Mac) by incorporating hiPSC-derived vagal neural crest cells, precursors to ENS<sup>75</sup> (Figure2A). We then performed scRNAseq on HIO/ENS/Mac to compare to the day 47 fetal intestine dataset. Presumptive cell identities were assigned to unsupervised clusters based on known gene markers (Figure2B-C). Like the fetal intestine, the organoid consisted of mesenchyme, epithelium, enteric neurons, glial-like progenitors, and macrophages. Unlike the fetal intestine, the organoid did not yet develop any distinct smooth muscle cells or endothelial cells. Expectedly, the organoid lacked lymphocytes, and erythroblasts (Figure1B,C). A more detailed look at the cellular proportions indicated, though the organoid was more abundant in mesenchymal cells, the ratio of epithelial-to-mesenchyme and glial/progenitor-to-enteric neuron were comparable to the fetal intestine, whereas the proportion of the neural cells and macrophages were lower than

the fetal intestine (Figure1D). Cell type identity were more directly compared between the fetal intestine and the organoid by merging the dataset and performing unsupervised clustering. Lymphocytes and erythroblasts were only present in the fetal intestine as expected, whereas smooth muscle-like cells and endothelial-like cells were identified in the organoid. This likely indicates the potential for mesenchymal cells to differentiate into smooth muscle cells and endothelium as previously demonstrated in grafted organoids and VEGF-treated HIOs, respectively<sup>74,107</sup>. Together, the results indicate that our organoid model consists of expected cell types found in an early embryonic intestine.

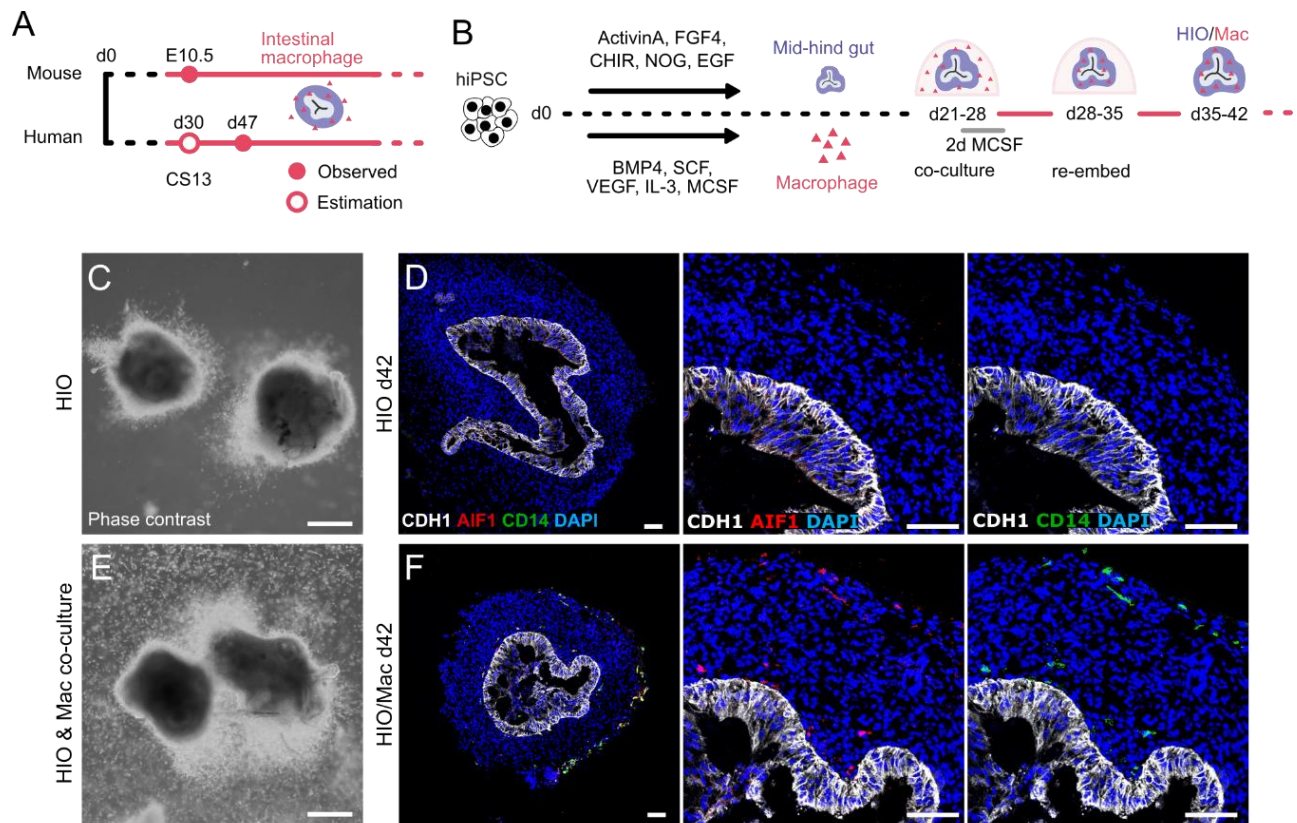


**Figure1. Derivation of human intestinal organoid with macrophages (HIO/Mac).**

(A) Timeline of macrophage habitation of mid-hindgut in mouse and human. d, days post conception; E, embryonic day; CS, Carnegie stage. See FigureS1.

(B) Overview of the derivation of HIO with macrophages (HIO/Mac). hiPSC, human induced pluripotent stem cell; CHIR, CHIR99021.

(C and E) Phase contrast image of day 28 HIO alone (c) or HIO in co-culture with hiPSC-derived macrophages (Mac). Arrowhead, HIO. Scale bars = 0.5mm (C and E).

(D and F) Immunofluorescence of HIO and HIO/Mac for markers of epithelium (CDH1), macrophage (AIF1, CD14), and nucleus (DAPI). Scale bars = 75 $\mu$ m (D and F).

### **Macrophage recruitment and retention by the organoid**

CSF1 (MCSF) is a crucial regulator of macrophage differentiation, survival, and proliferation, which is present in circulation and produced locally in tissues<sup>108,109</sup>. It is unclear which specific cell types produce CSF1 in the developing intestine. Since macrophages occupied deep within the organoid and proliferated, we suspected that HIO produced CSF1. Single cell datasets revealed that mesenchymal cells were the major cell type expressing *CSF1* in both the organoid and day 47 to 127 fetal intestines. *CSF1* was also expressed in lymphocytes (T and NK) and endothelial cells in the fetal intestines though these cells represented a much smaller proportion of *CSF1* expressing cells (FigureS2A). We have previously supplemented the media with 100ng/ml of MCSF; however, above results suggested that the macrophages may not constantly require external MCSF. To the point, we found that 20ng/ml MCSF during the first two days of the co-culture was sufficient to derive HIO/Mac and the addition of MCSF was not required for further culture (Figure1B). In conclusion, we identify mesenchymal cells as the major producer of CSF1 in the developing intestine, which is recapitulated in the organoid, and

find that this local production is sufficient to maintain the macrophage population in the organoid.

Next, we inquired if the recruitment and retention of the macrophages to the organoid could be due to abnormal level of inflammatory signaling. To this end, we looked at a curated list of ligands upregulated during inflammation that promotes macrophage recruitment. The ligand genes on the HIO cells (mesenchyme, epithelium, glial-progenitor, and enteric neuron) showed little to no mutual expression with corresponding receptor expression on macrophages. On the other hand, *CX3CR1-CX3CL1* and *CSF1-CSF1R*, which are known effectors of macrophage recruitment and/or survival during the development, showed high mutual expression (FigureS2B)<sup>27,30-32</sup>. Receptor expression levels were then validated with quantitative PCR (qPCR) on macrophages that were yet co-cultured with the HIO (FigureS2C). In conclusion, our data infer that the HIO does not rely on abnormal levels of inflammatory chemoattractant to recruit the macrophages.

### **Enteric neurons do not affect resident macrophage establishment**

A previous report suggests that enteric neurons are the main source of CSF1 in the muscularis of adult mouse intestines<sup>44</sup>. On the other hand, during the development, we observed little *CSF1* expression in enteric neurons of the organoid and day 47 to 127 fetal intestines (FigureS2A). To test directly if enteric neurons affect macrophage establishment in the developing intestinal organoid, we derived HIO combined with macrophages either with or without the vagal neural crest cells. Presence of enteric neurons within the HIO did not affect the number of macrophages in the HIO (Figure2F). This observation supports a previous report that the lack of enteric neurons in neonatal *Ret*<sup>-/-</sup> mice and children with Hirschsprung's disease does not affect the establishment of

intestinal macrophages<sup>36</sup>. In conclusion, our results support that enteric neurons do not affect the macrophage colonization in early developing intestine.

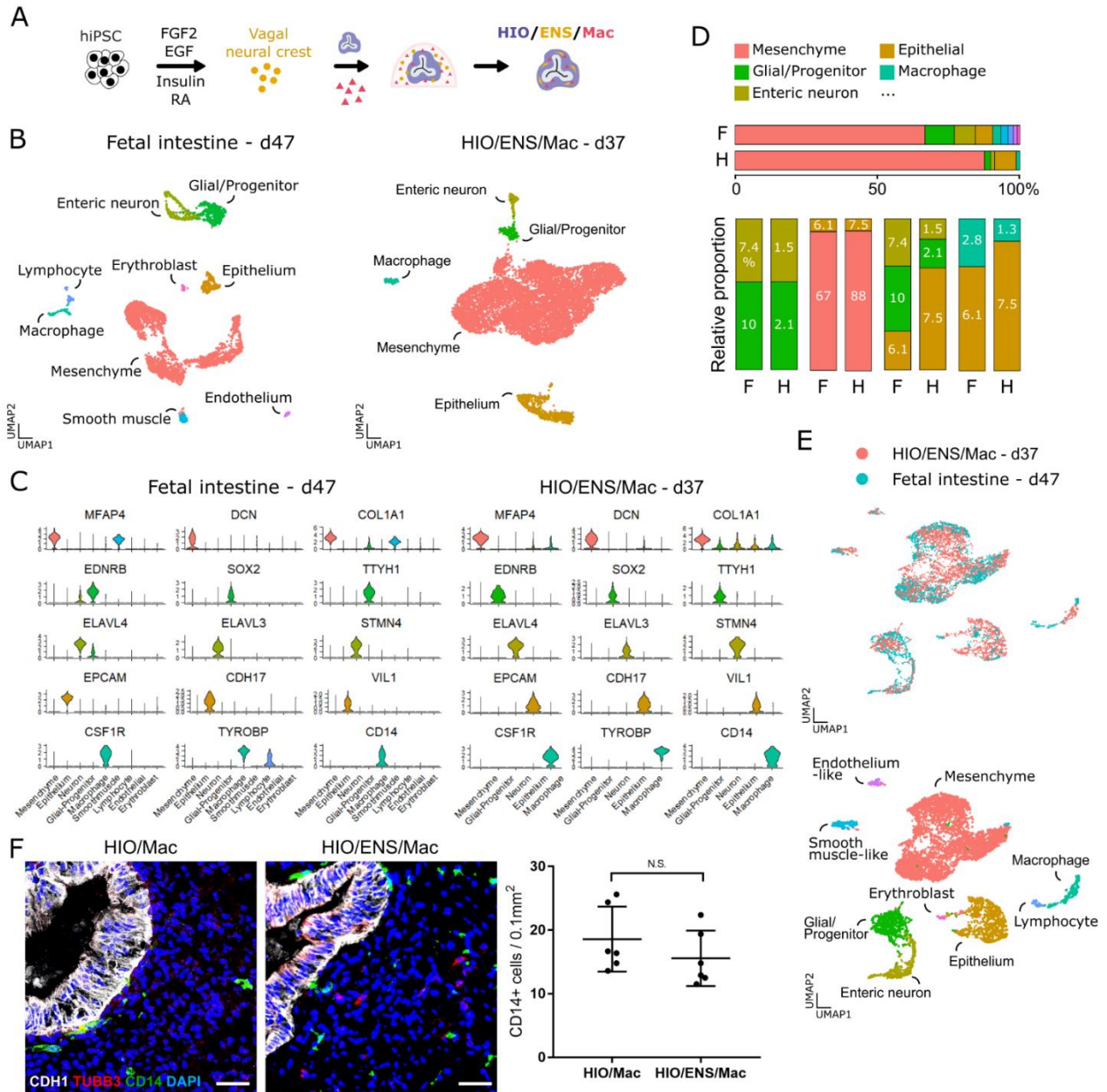


**Figure2. Cellular composition of human intestinal organoid (HIO) with macrophages and enteric neurons**

(A) Schematic of the derivation of HIO with enteric nervous system (ENS) and macrophages (HIO/ENS/Mac).

(B) Uniform Manifold Approximation and Projection (UMAP) plot of single-cell RNA sequencing (scRNAseq) of day 47 human fetal proximal intestine and day 37 HIO/ENS/Mac.

(C) Violin plot of a representative gene used to identify the cell type of each cluster in UMAP.

(D) Percent cell type composition and relative proportion of cell types in each dataset.

(E) UMAP plot of merged dataset of day 47 human fetal proximal intestine and day 37 HIO/ENS/Mac.

(F) Immunofluorescence of day 42 HIO co-cultured only with macrophage or with macrophage and vagal neural crest cells (ENS precursor). Epithelium (CDH1), Neuron (TUBB3), macrophage (CD14), nuclei (DAPI) and the quantification of macrophage numbers within the HIOs. CD14-positive cells within the DAPI-positive and CDH1-negative region. Each data point represents an organoid. Scale bar = 45 $\mu$ m.  $n = 6$  each. Mean & s.d.  $p = 0.2996$ . student's  $t$ -test.

### **Macrophages migrate to the wound site upon injury**

We wanted to test if macrophages in the organoid displayed behaviors of *in vivo* macrophages. One of characteristic behaviors of macrophages is their recruitment to tissue injury, also observable during embryonic development<sup>21,22</sup>. To test if organoid macrophages can migrate to the injury site, we derived macrophages from eGFP-tagged hiPSC (hiPSC<sup>eGFP</sup>) and tracked their movements within the organoid after a puncture

injury. Macrophages migrated towards the injury site during the 12 hours following the injury, whereas the movements of macrophages in the uninjured organoids were not concerted. Assessment of their relative distance to the injury and the chemotactic precision index, which quantifies directional movement, supported this observation (FigureS2D-F). In conclusion, we show that macrophages in the early-stage *in vitro* organoid display recruitment behavior upon injury, as observed in developing mice.

### **Macrophages localize to intestinal micro-anatomical niches in xenograft-matured organoids**

Macrophages localize to specific micro-anatomical niches within the intestine, such as villi, crypts, and enteric ganglia<sup>35,40,41,43,44,110</sup>. To test if macrophages in HIOs localize to these niches, we grafted HIO/ENS/Macs to immunodeficient *non-obese diabetic/Prkdc<sup>SCID</sup>/Il2rg<sup>null</sup>* (NSG) mice for 8-12 weeks to facilitate further development, forming more complex tissue structures<sup>74</sup> (Figure3A). Furthermore, macrophages were derived from hiPSC<sup>eGFP</sup> line to trace their origin. The grafted organoids maintained CDX2<sup>+</sup> intestinal epithelial identity and developed crypts, villi, smooth muscle, enteric ganglia, and glia<sup>111</sup>. More so, the eGFP<sup>+</sup> macrophages were observed in micro-anatomical niches of grafted organoids (Figure3B-D, FigureS3A).

In more detail, at the epithelium, macrophages positioned flat against the MKI67<sup>+</sup>CDH1<sup>+</sup> epithelial crypt cells and congregated within the villi, comparable to the distribution and morphology seen in day 119 human fetal intestinal macrophages and in mouse<sup>35</sup> (Figure3C). Intestinal monocytes/macrophages near the epithelium phagocytose luminal content, such as bacteria<sup>37-39</sup>. To test if macrophages in the organoid display such

transepithelial phagocytic activity, we injected Escherichia coli (E.coli) particles conjugated to pH-sensitive fluorescent dye into the lumen of grafted HIO/Mac<sup>eGFP</sup>. Confocal microscopy images showed that eGFP<sup>+</sup> macrophages near the epithelium internalized the particles, indicating transepithelial phagocytic activity (FigureS3D). In adult mice, intestinal macrophages were shown to regulate epithelial repair and intestinal stem cell niche<sup>40-42</sup>. In particular, macrophage ablation were shown to decrease the number of MKI67<sup>+</sup> (KI67), a common proliferation marker, crypt cells<sup>41</sup>. To test if macrophages affect the crypt during development, we grafted HIO/ENS and HIO/ENS/Mac for comparison. Intriguingly, the number of proliferative cells in the epithelium were lower without the macrophages (FigureS3E). We note here that GFP<sup>-</sup>/AIF1<sup>+</sup> macrophages were found in both HIO/ENS and HIO/ENS/Mac, indicating that macrophages from the NSG mice populated the grafted organoids (FigureS3C). Previous reports indicate that macrophages of NSG mice display a delay in maturation and defects in immune function, but is unclear if their homeostatic capacities are affected<sup>112-116</sup>. Regarding our grafted experiments, hiPSC-derived human macrophages seem to exert an effect post-grafting that NSG mouse macrophages does not. In conclusion, grafted organoids recapitulate macrophages localization in the intestinal mucosa and their transepithelial phagocytosis. Furthermore, hiPSC-derived macrophages increase the number of MKI67<sup>+</sup> crypt cells in the developing organoid, similar to the previous reports in adult mice.

At the enteric ganglia, organoid macrophages localized adjacent to the ELAVL4<sup>+</sup> TUBB3<sup>+</sup> neurons, resembling neuron-associated intestinal macrophages in day 119 human fetal intestine and adult mice<sup>35,44</sup>(Figure3D). Cell ablation studies in adult mice indicate that

macrophages regulate intestinal peristalsis<sup>35,44</sup>. Grafted organoids undergo spontaneous peristalsis-like contractions. To test if macrophages affect organoid peristalsis, we recorded the isometric force generated by whole grafted organoids with or without macrophages. However, we did not observe differences in motility between the two conditions (FigureS3F). In conclusion, macrophages in the organoid associated with enteric ganglia as observed in the fetal and adult mouse intestine, but this physical association may not affect peristalsis during the development.

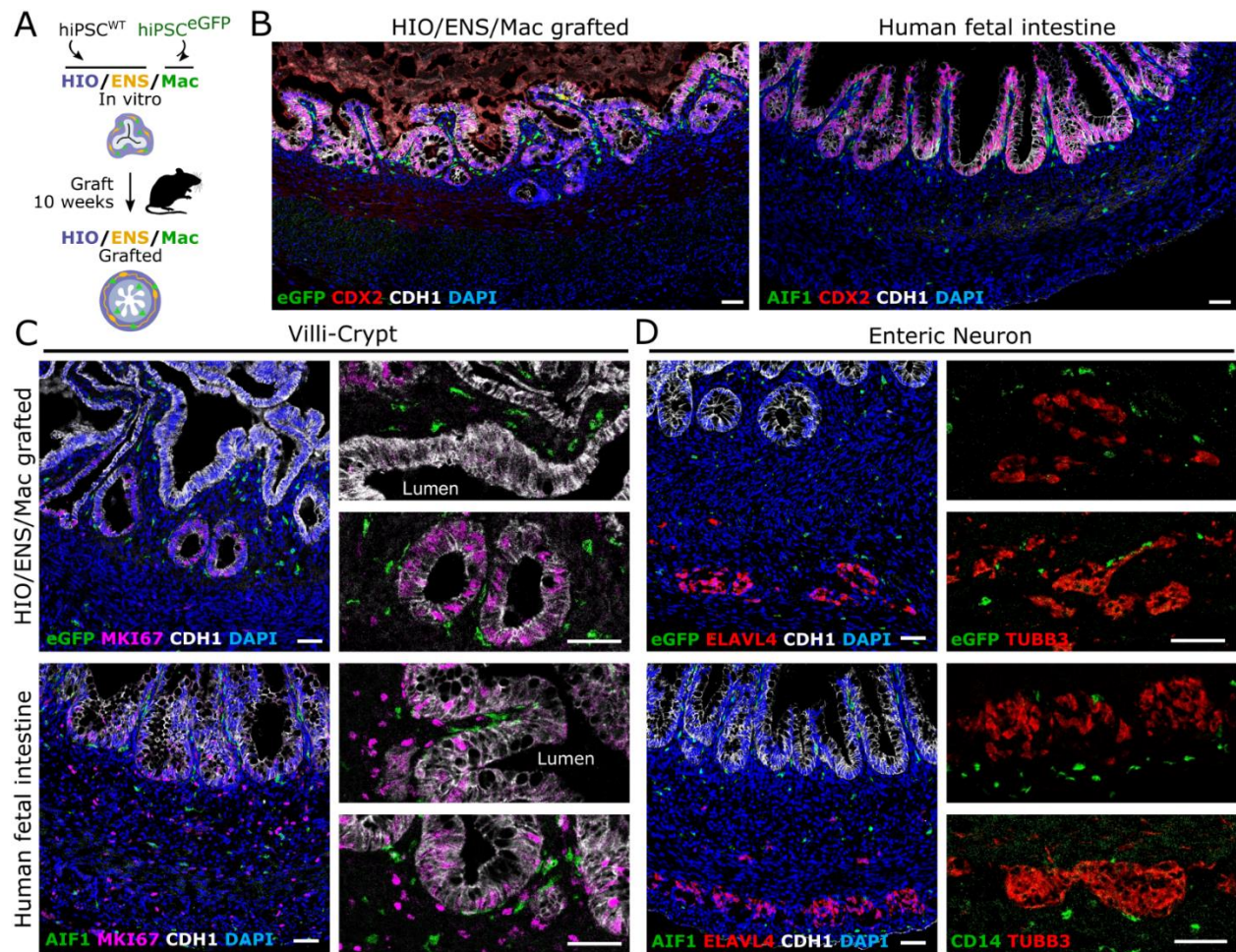


**Figure3. Macrophages localize to intestinal micro-anatomical niches in xenograft-matured intestinal organoid.**

(A) Strategy to track macrophages by deriving it from enhanced green fluorescent protein (eGFP) tagged hiPSC (hiPSC<sup>eGFP</sup>) and further differentiation and growth of the organoids by xenografting to the immunodeficient (NSG) mice.

(B and C) Representative immunofluorescence confocal microscopy images of day 112 grafted HIO/ENS/Mac and day 119 human fetal proximal intestine for intestinal epithelium specific identity (CDX2, CDH1) and macrophages (eGFP or AIF1).

(C) Localization of macrophages (eGFP or AIF1) within the villi (CDH1) and to crypts (MKI67, CDH1).

(D) Localization of macrophages with enteric ganglia (TUBB3, ELAVL4).

Nuclei (DAPI). Scale bars = 50µm.

## **Organoid macrophages acquire transcriptomic profile alike fetal intestinal macrophages**

Macrophages/monocytes migrate into each organ and further differentiate to fulfill the locale-specific function<sup>23,27,35</sup>. Similar to this *in vivo* observation, murine iPSC-derived embryonic-like macrophages were shown to take on a microglia-like transcriptomic profile when co-cultured with neurons<sup>117</sup>. We examined with scRNAseq if organoid macrophages differentiate in response to their tissue environment by comparing their transcriptional changes to that of human fetal intestinal macrophages and fetal distal lung macrophages as a reference<sup>106,118</sup>. Macrophage were isolated from day 80 and day 127 of the fetal proximal intestine and distal lung datasets, and for day 37 *in vitro* organoid and day 121 grafted HIO/ENS/Mac<sup>eGFP</sup> datasets. In detail, these macrophage clusters from the

unsupervised clustering of each dataset were further selected for *CSF1R* and *CD14* expressing cells (Figure4A, see Methods).

Unsupervised clustering of the datasets showed that earlier stage (day 80) fetal intestinal and lung macrophages were still similar to each other, though early stage (day 47) organoid macrophages were less alike. Furthermore, later stage day 127 fetal macrophages diverged away from each other, and day 121 organoid macrophages grouped closer to the later stage intestinal macrophages (Figure4B). Principal component analysis also showed that later stage organoid macrophages have diverged away from earlier stage macrophages to a similar dimension as the later stage fetal intestinal macrophages (Figure4C). To quantify this observation at large, we calculated the correlation of coefficient between the different macrophages. The correlation was higher between intestinal and organoid macrophages compared to lung and organoid macrophages (Figure4D).

To see what specific changes each macrophages undergo, we analyzed differentially expressed genes between the later and earlier time points of each macrophage. Each fetal macrophages showed distinct gene upregulation. Intestinal macrophages increased antigen presentation-related gene expressions (HSPs, HLAs, *TMEM176A*, *TMEM176B*), whereas distal lung macrophages upregulated genes that were previously known to regulate lung morphogenesis (*SCGB3A2*, *ADH1B*, *RARRES2*) and extracellular matrix protein enriched in the lung (*FBLN1*)<sup>119–124</sup> (Figure4E).

Differentially regulated profiles were then compared to that of organoid macrophages. Heatmap of top ten differentially expressed genes from intestinal and distal lung

macrophages demonstrated that organoid macrophages shared upregulated genes with intestinal but not with distal lung macrophages (Figure4F). Specifically, 33 out of 77 upregulated genes were shared between intestinal and organoid macrophages, with significant enrichment of 'Antigen processing and presentation' in intestinal and organoid macrophages (Figure4G-I, FigureS4A). Genes only upregulated in intestinal macrophages included additional HLA genes (FigureS4A,B). Comparisons of additional fetal intestinal datasets with varying developmental intervals showed similar signature where antigen-presentation genes are upregulated (FigureS4C). Downregulation profiles between intestinal and distal lung macrophages were less discernable (Figure4F,G). In conclusion, we find that macrophages in the organoid undergo similar tissue-specification as that of the fetal intestine at a transcriptional level.

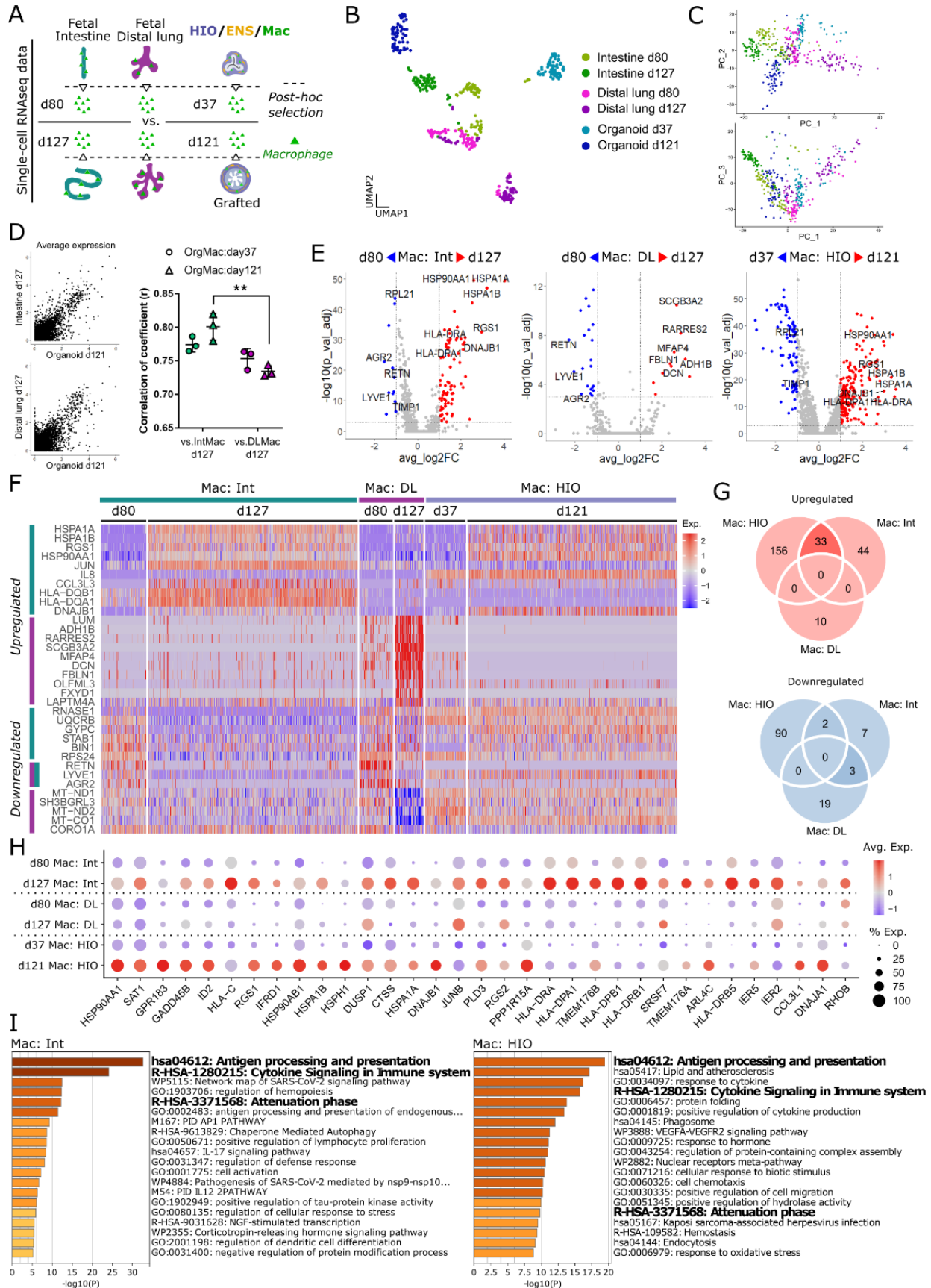


**Figure4. Intestinal organoid macrophages acquire transcriptomic profile alike fetal intestinal macrophages.**

(A) Overview of post hoc selection process for macrophages from organoid and fetal tissue scRNAseq datasets.

(B) UMAP plot of early and late stage fetal and organoid macrophages on the left and principal component analyses of the same on the right.

(C) Representative scatter plots of average gene expression between fetal and organoid macrophages. Pearson's correlation of coefficient ( $r$ ) of the average gene expression comparisons.  $P$ -value = 0.0082. Student's  $t$ -test performed on  $z$ -scores, calculated from  $r$  values using Fisher's transformation.

(D) Volcano plots of differentially expressed genes in the macrophages between late and early developmental time points. Threshold of discovery (dotted line),  $\log_2$ fold change  $> 1$ , adjusted  $p$ -value  $< 0.001$ , Wilcoxon rank sum test. Macrophage, Mac; Intestine, Int; Distal lung, DL.

(E) Heatmap of top ten upregulated and downregulated genes of the late vs. early fetal proximal intestine (b), and distal lung (c) in the order of fold change. Number of cells in 'Mac: HIO' were downsampled for visualization. Exp, scaled expression level.

(F) Venn diagram of the number of upregulated (f) and downregulated genes (g) from (b-d).

(G) Dot plot of the 33 commonly upregulated genes between intestinal and organoid macrophages (f). Avg. Exp., average expression; % Exp, percentage of cells expressing the gene.

*(H) Gene ontology annotation of intestinal (i) and organoid macrophages (j) generated with all the upregulated genes for each dataset.*

### **Macrophages regulate intestinal organoid growth**

Intriguingly, HIO/ENS engrafted for 10 weeks in the NSG mice were smaller when iPSC-derived macrophages were incorporated (Figure5A-C). Organoids used for the co-culture with macrophages were randomized during their derivation and their size shortly after the macrophage co-culture was still comparable (Figure5G). Histology did not show differences in tissue morphology between the two conditions in 10-week grafted organoids. We argued that if the macrophages induced a chronic pro-inflammatory effect, they can in turn cause abnormal fibrosis due to prolonged inflammatory state, and in turn stunt growth; however, we did not observe any signs of abnormal fibrosis or tissue architecture in histology (Figure5A,B). Additional organoids with macrophages that were grafted for 8 weeks and 12 weeks were also smaller compared to organoids without macrophages (Figure5C,E). Exponential fit of the organoid size as function of time indicated that the rate of growth was reduced when incorporated with macrophages (Figure5D).

Macrophages are professional phagocytes; thus, we next tested if the reduction in size of grafted organoids by the macrophages is due to the removal of apoptotic cells. Level of immunofluorescence signal for apoptotic cells, however, were comparable between the grafted organoids with or without macrophages (Figure5F). Thus, the size difference is not due to the removal or accumulation of apoptotic cells.

In the report that described the HIO/ENS derivation, bulk-RNA sequencing showed that organoids combined with ENS had higher EGF expression, though size difference was not noted<sup>75</sup>. Additionally, macrophages in the brain (microglia) were shown to phagocytose neuronal processes and required for proper brain development and morphology<sup>54,55</sup>. Thus, intestinal macrophages may suppress overt expansion of enteric neurons and in turn inhibit tissue overgrowth. We hypothesized that the reduced growth of organoids by macrophages is dependent on the presence of ENS. Comparison between grafted HIO and HIO/ENS showed that ENS did have positive growth effect; however, reduced organoid growth by macrophages was independent of ENS (Figure 5G,H). We conclude that ENS and macrophages regulate organoid growth in a positive and negative manner, respectively, and that neither of the effects are necessarily dependent on each other.

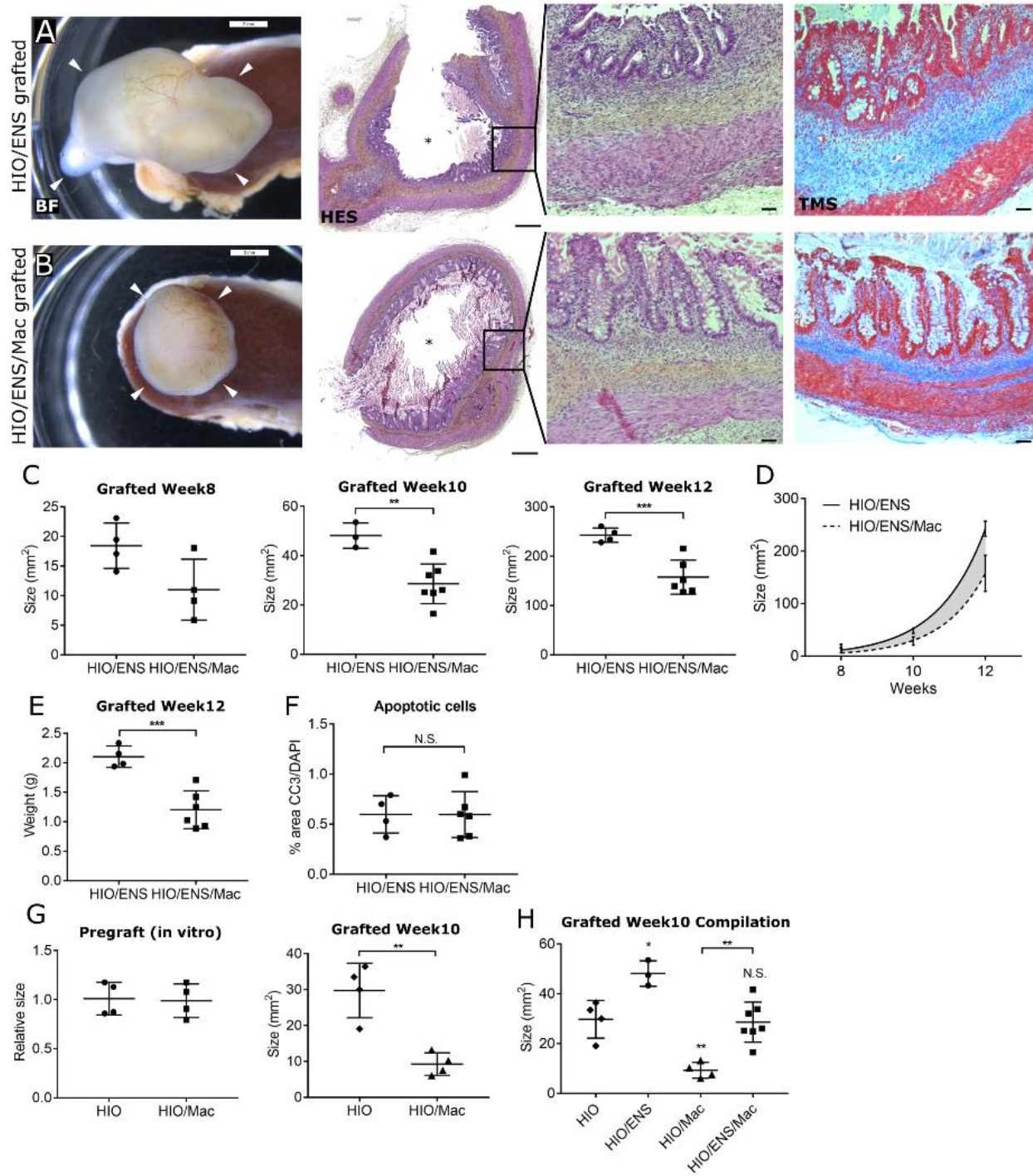


**Figure 5. Macrophages reduce the growth of intestinal organoid without affecting tissue architecture.**

*(A and B) Representative bright field (BF) images of week 10 grafted organoids still attached to the mouse kidney at the site of the engraftment, White arrowheads point to the organoid. Hematoxylin-eosin-saffron (HES) stained sections of the grafted organoids. Trichrome Masson (TMS) stained sections. Asterisks, lumen. Scale bar = 2mm (BF), 0.4mm (HES), 50 $\mu$ m (HES and TMS insets).*

*(C) Size measured by the area of the grafted organoids from bright field images, isolated at 8 weeks, 10 weeks, and 12 weeks after the engraftment. Week 8: HIO/ENS,  $n = 4$ , HIO/ENS/Mac,  $n = 4$ ,  $p = 0.0633$ ; Week 10: HIO/ENS,  $n = 3$ , HIO/ENS/Mac,  $n = 7$ ,  $p = 0.0034$ ; Week 12: HIO/ENS,  $n = 4$ , HIO/ENS/Mac,  $n = 6$ ,  $p = 0.0010$ . Welch's  $t$ -test.*

*(D) Exponential regression of the size of the grafted organoids over time from (C).  $p < 0.0001$ , two-way ANOVA*

*(E) Weight of 12-week grafted organoids from (C).  $p = 0.0005$ , Welch's  $t$ -test.*

*(F) Level of apoptosis in grafted organoids. Quantified by calculating the area of cleaved caspase 3 (CC3) divided by the area of nuclei (DAPI) in confocal microscopy images of immunofluorescence. HIO/ENS,  $n = 4$ , HIO/ENS/Mac,  $n = 6$ .  $p = 0.995$ , Welch's  $t$ -test.*

*(G) Relative size of HIO and HIO/Mac in vitro two weeks after the combination procedure and the size of the same organoids from after a 10-week engraftment. HIO,  $n = 4$ , HIO/Mac,  $n = 4$ .  $p = 0.8625$ ,  $p = 0.0075$ . Welch's  $t$ -test.*

*(H) Sizes of all 10-week grafted organoids combined with or without ENS precursors and/or macrophages.  $p < 0.0001$ , one way ANOVA; HIOvs.HIO/ENS,  $p = 0.0148$ , HIOvs.HIO/Mac,  $p = 0.0038$ , HIOvs.HIO/ENS/Mac,  $p = 0.9930$ , HIO/ENSvs.HIO/Mac,  $p$*

$< 0.0001$ , *HIO/ENS* vs. *HIO/ENS/Mac*,  $p = 0.0045$ , *HIO/Mac* vs. *HIO/ENS/Mac*,  $p = 0.002$ ,  
posthoc: Tuckey.

Each data point represents an organoid. Results from three independent experiments.

Batch one: Week 8 and Week 10 (C). Batch two: week 12 (C,E). Batch three: week 10

(G). All graphs are mean & s.d

### **Macrophages attenuate mesenchymal cell glycolysis in developing intestinal organoids**

To further investigate the roles of macrophages in early intestinal development, we performed scRNAseq on organoids with or without macrophages (two HIO/ENS pairs and one HIO pair) and looked at the transcriptomic differences between each cell type (Figure6A). Differentially expressed genes common in all three sample pairs were found in the mesenchyme and the epithelium (Figure6B). The most discernable gene ontology annotation among these results was the downregulation of glycolytic enzymes (*ENO1*, *LDHA*, *PFKP*, *PGK1*, and *TPI1*) in mesenchyme, suggesting a decrease in their glycolysis when macrophages are present (Figure6C,E). Macrophages were previously shown to regulate glucose uptake and metabolic response to cold in adipocytes<sup>16,17</sup>. They were also shown to upregulate glycolysis in cancer cells and promote tumor growth<sup>64</sup>. Mapping protein-protein association of the downregulated mesenchymal genes revealed a network of the aforementioned glycolytic genes as expected, but also their associations with *MIF* (Figure6D). *MIF* was previously shown to promote glucose uptake and glycolysis of muscle and cancer cells, and shown to be expressed in intestinal epithelium<sup>125–127</sup>. *MIF* was also downregulated in the organoid epithelium (Figure6E). In conclusion, organoid

macrophages reduced the expression of glycolytic genes of the organoid mesenchymal cells.

We used the metabolic-flux assay (Seahorse XF) to test whether macrophages downregulate glycolysis in HIO's mesenchymal cells as indicated by the scRNAseq result. Mesenchymal cells were dissected and isolated into single cell suspension from either HIO or HIO/Mac. Macrophages were removed from the cell suspension with anti-CD14-antibody mediated magnetic separation (FigureS5, see Methods). Extracellular acidification rate (ECAR) of the mesenchymal cells was measured to gauge their glycolytic activity (Figure6F). Non-glycolytic acidification in the glucose-depleted state showed comparable ECAR between the two conditions. Introduction of glucose induced an increase in ECAR in both conditions as expected; however, mesenchymal cells from HIO/Mac showed a smaller increase indicating a lower level of glycolysis. Subsequent inhibition of mitochondrial respiration with oligomycin, necessitating the cells to use glycolysis-driven ATP generation, showed that the glycolytic capacity was also lower in mesenchymal cells from HIO/Mac. Lastly, inhibition of glucose-uptake by 2-Deoxy-D-glucose (2-DG) decreased the ECAR again to a comparable level for both conditions, indicating the differences were due to the metabolism of glucose (Figure6G). Thus, metabolic flux assay supports our transcriptomic result that macrophages reduce the glycolysis of mesenchymal cells.

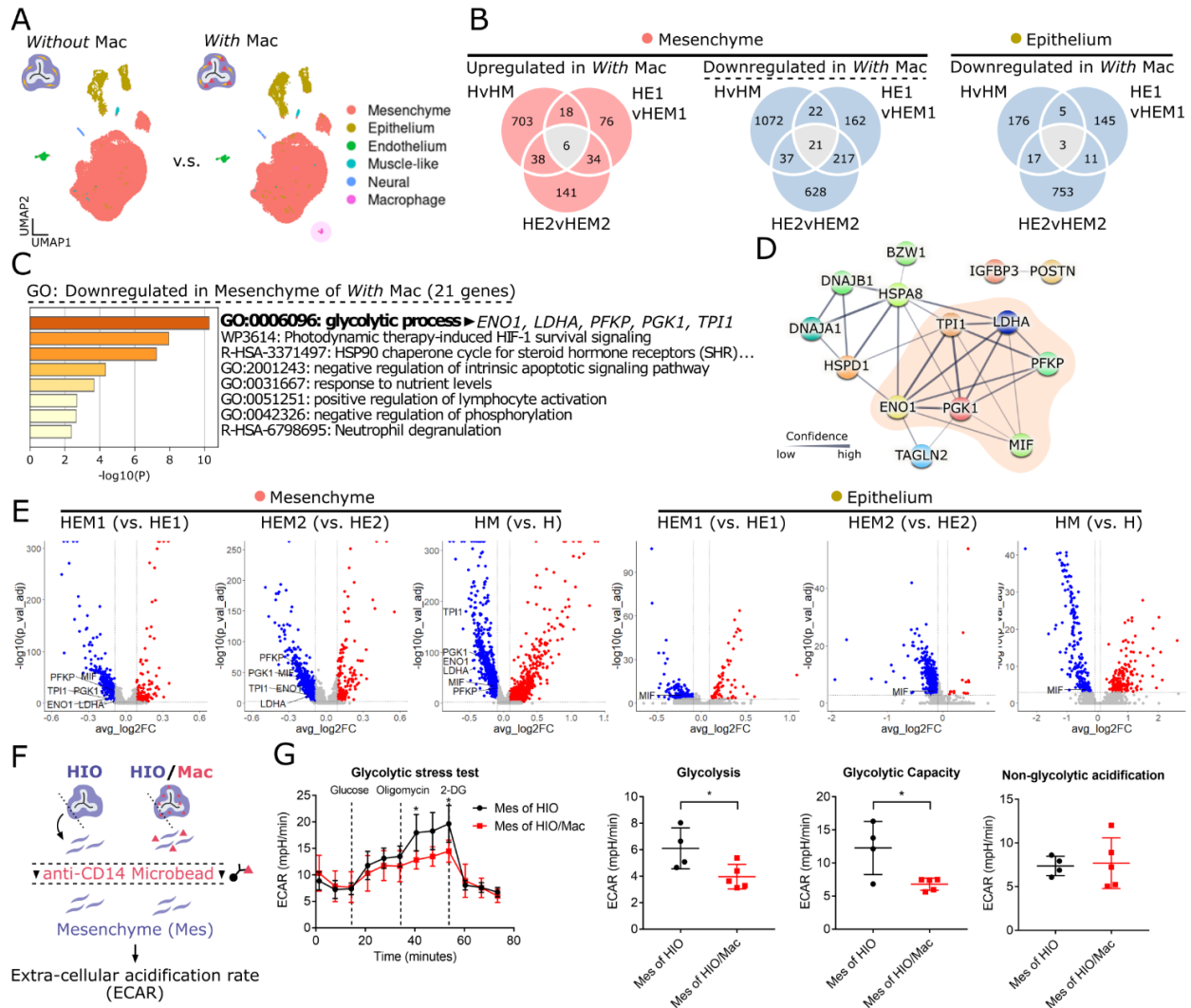


**Figure6. Macrophages attenuate mesenchymal cell glycolysis in developing intestinal organoids.**

(A) Representative UMAP plots from scRNAseq datasets of in vitro organoids without or with macrophages (Mac). Merged dataset of HIO/ENS's and HIO/ENS/Mac's.

(B) Venn diagram of the number of differentially expressed genes in organoids With macrophages against organoids Without macrophages between the three separate comparisons. Differentially expressed genes in common between the three were found in mesenchyme and epithelium. HvHM: HIO vs. HIO/Mac; HE1(2)vHEM1(2):

*HIO/ENS1(2) vs. HIO/ENS/Mac1(2). Each sample is a pool of 4-5 dissociated organoids. Threshold of discovery: adjusted p-value < 0.001, Log2fold change > 0.09, Wilcoxon rank sum test.*

*(C) Gene ontology analysis on the 21 genes downregulated in organoid mesenchymal cells by organoid macrophages from (B).*

*(D) Protein-Protein association map of the 21 genes from (B) using STRING. Only the genes with at least one association are displayed.*

*(E) Volcano plots annotated with genes involved in glycolytic process found with gene ontology (C) and protein-protein association map (D). Dotted lines: adjusted p-value < 0.001, Log2fold change > 0.09 & < -0.09, Wilcoxon rank sum test.*

*(F) Schematic of mesenchymal cell isolation from in vitro organoids for the glycolytic stress test.*

*(G) Extra-cellular acidification rate (ECAR) measurement in the glycolytic stress test. Oligomycin (ATP synthase inhibitor). 2-DG, 2-Deoxy-D-glucose (competitive inhibitor of glucose). Quantification of glycolysis, glycolytic capacity, and non-glycolytic acidification from the glycolytic stress test. See STAR methods for calculation. Result of one experiment. Mean & s.d (i-k).  $p < 0.0001$ , Two-way ANOVA;  $p = 0.0311$ ,  $p = 0.0289$ , post-hoc: Sidek-Bonferroni (i). Each data point represents a technical replicate well.  $p = 0.0360$  (j),  $p = 0.0199$  (k),  $p = 0.8452$  (l), student's t-test.*

## Oncostatin M (OSM) reduces glycolytic gene expression in mesenchymal cells

Activation of HIPPO pathway inhibits YAP protein from promoting its target gene expression. One of the cellular processes that HIPPO pathway regulates is glycolysis<sup>128,129</sup>. Furthermore, LIFR signaling activation has been shown to activate HIPPO pathway, inhibiting YAP target genes, such as glycolytic genes<sup>130</sup>. Organoid macrophages expressed OSM, a LIFR ligand, and mesenchymal cells expressed LIFR (Figure7A). We hypothesized that OSM produced by organoid macrophages down regulate glycolysis in mesenchymal cells. Mesenchymal cells were isolated from HIO and treated with OSM (Figure7B). Glycolytic gene expression of ENO1, PGK1, and TPI1 decreased in mesenchymal cells in response to OSM treatment, measured by qPCR. The results so far indicate OSM from macrophages can negatively regulate glycolysis in mesenchymal cells in the developing organoid.

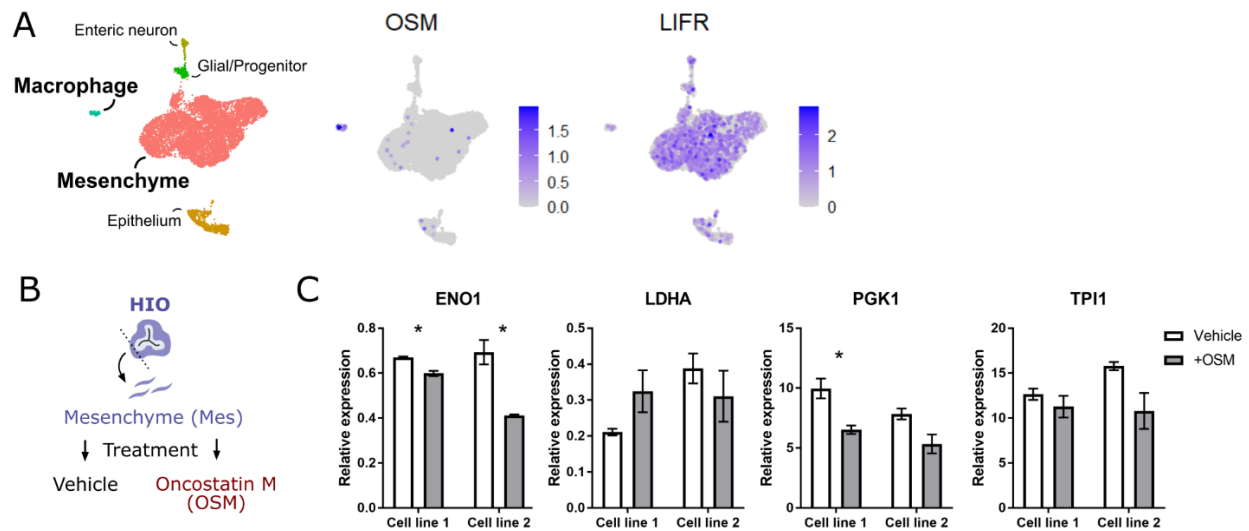


**Figure7.** Oncostatin M (OSM) reduces glycolytic gene expression in mesenchymal cells

(A) Expression of OSM and LIFR in the in vitro organoid.

(B) Schematic of mesenchymal cells isolation from in vitro organoids and treatment with

*either vehicle (0.1% BSA in PBS) or OSM (500ng/ml).*

*Glycolytic gene expressions in OSM treated mesenchymal cells by qPCR. Normalized to HPRT1 expression. ENO1:  $p=0.0138$ ,  $p=0.0182$ ; PGK1:  $p=0.0326$ ,  $p=0.0602$ ; LDHA:  $p=0.1135$ ,  $p=0.3160$ ; TPI1:  $p=0.2882$ ,  $p=0.0753$ .*



## **Methodology (Chapter 1)**

### **Experimental model and subject details**

#### **Cell lines and tissues**

The use of human pluripotent stem cells was approved by the ethical committee at the participating institution CHU-Sainte Justine, Montreal QC, Canada. The hiPSCs and their derivations were routinely tested for mycoplasma (LT07-118, Lonza) and tested negative.

Human fetal (17-21 weeks) tissue was obtained after written informed consent and was approved by the ethical committee of CHU Sainte-Justine, Montreal QC, Canada.

#### **Mice**

The animal procedures were approved by the animal committee of CHU Sainte-Justine, Montreal QC, Canada.

#### **Pluripotent stem cell culture**

Human induced pluripotent stem cells (hiPSC) were generated at CR-CHUSJ Stem Cell core or in-house. The hiPSC lines Sji3252C2 and SJ3013C2 were derived from human fibroblasts using Cytotune 1.0™ (Invitrogen) and were previously characterized<sup>131</sup>. EU03.C2, and EU148.C5 were derived from human PBMC with Cytotune™ 2.0 (A16517, Invitrogen). The hiPSC<sup>eGFP</sup> line (SEC61BGFP/AICS-0010) was acquired from Allen Institute for Cell Science<sup>132</sup>. The hiPSCs were cultured in hypoxic condition (5%CO<sub>2</sub>, 5%O<sub>2</sub>, 37°C incubator) until passage 15-20, otherwise all cells and derivatives were cultured in normoxic condition (5%CO<sub>2</sub>, 37°C incubator). They were cultured with mTeSR1 (85850, StemCell Technologies) with 1X penicillin-streptomycin (450-201-EL,

MultiCell) and hESC-qualified Matrigel (354277, Corning). Matrigel was coated onto Nunc Delta surface plates (14-832-11, Thermo Scientific) as per manufacturer recommendation. The cells were passaged as small clusters using 0.5mM ethylenediaminetetraacetic acid (EDTA) in phosphate buffered saline (PBS). The cells were cryopreserved with NutriFreez™D10 (05-713-1E, Biological Industries) as per manufacturer recommendation.

## **Method details**

### **Human intestinal organoid derivation**

Human intestinal organoids (HIO) were derived with the hiPSC-lines SJi3252C2 or SJ3013C2 as previously described with minor modifications<sup>73,75,133</sup>. Briefly, 85% confluent hiPSCs in a 6 well plate was passaged with EDTA and seeded 1/14-1/16 of a cell suspension per single well of 24 well plate. The cells were fed mTeSR1 daily for two days or until the confluency reached 80%. On the first day, the media was changed with endoderm differentiation media base (EDM-base): RPMI1640 (11875-093, Gibco), 1X pen-strep (15015067, Wisent), 1X nonessential amino acid (11140050, Gibco) with 100ng/ml Activin A (338AC010, R&D systems). On the second day, the cells were fed EDM-base supplemented with 100ng/ml Activin A and 0.2% FBS (HyClone™, Fisher Scientific). On the third day, the cells were fed the same as the second but with 2% FBS. At the end of the third day, the monolayer expressed definitive endoderm markers SOX17 and FOXA2 (FigureS6a). The fourth day, the confluent monolayer of cells was fed with mid-hindgut differentiation media (MHDM): EDM-base, 2% FBS, 500ng/ml FGF4 (235F4025CF, R&D systems), 3µM CHIR99021 (S1263, Selleckchem). The cells were fed MHDM daily for a total of 4 days. At the end of mid-hindgut differentiation, the free-

floating spheroids were collected and suspended in Matrigel (354234, Corning) supplemented with 1X B27<sup>TM</sup> supplement (17504044, Gibco) and 100ng/ml EGF (236EG200, R&D systems; AF-100-15, PeproTech). The Matrigel suspension were plated as a droplet with 15-20 spheroids per droplet on a plate (14-832-11 or 130184, Thermo Scientific) and polymerized at 37°C for 10 min. Note that some tissue culture plate types are not suitable for Matrigel droplet formation. The spheroids were fed intestinal basal media (IBM): Advanced DMEM-F12 (12634-010, Gibco), 1X B27 (17504044, Gibco), 1X Glutamax (35050061, Gibco), 1X pen-strep, 15mM HEPES (15630080, Gibco) supplemented with 100ng/ml EGF and 100ng/ml Noggin (6057NG025CF, R&D systems) for four days changing the medium every 48 hours. They were then fed IBM supplemented with 100ng/ml EGF (IBMe) every 48 hours. Two weeks after the spheroid collection, the organoids were passaged by manually separating from each other with sterile syringe needle and re-embedding in the Matrigel droplet as before. From this point onward, the organoids were fed IBMe and passaged every two weeks until the experiment. The organoids were positive for intestine-specific epithelial marker CDX2 (FigureS6a).

### **Vagal neural crest derivation**

Vagal neural crest cells (VNCC) were derived from the hiPSC-line SJ3013C2 as previously described with minor modifications<sup>75,103</sup>. Briefly, in a 6 well plate, small colonies of hiPSC were seeded at low density (1/80 of a confluent well of 6 well plate) and grown for 5 days. On the first day of differentiation, the colonies were lifted with 500U/ml collagenase IV (17104019, Gibco) in mTeSR1 for up to 1hour in the incubator or until the colonies detached completely with gentle taps to the plate. The colonies were washed

with 2ml of DMEM/F12 (319-075-CL, Wisent) three times. They were then suspended in neural induction media (NIM): 1:1 ratio of DMEM-F12 and Neurobasal media (21103049, Gibco), 0.5X B27, 0.5X N2, 5ug/ml insulin (I2643, Sigma), 20ng/ml basic-FGF (100-18B, PeproTech), 20ng/ml EGF, and 1X pen-strep with 5uM of Rock inhibitor Y27632 (S1049, Selleckchem) and transferred to non-tissue culture treated plate (08-772-51, Fisher scientific). The NIM was changed daily with decreasing Y27632 (Y27) concentration (Day 2: 2.5uM Y27, Day 3 and beyond: no Y27), for additional 5 to 6 days until the neurospheres had clear round borders. The neurospheres were then fed NIM with 2uM all-trans-retinoic acid (R2625, Sigma Aldrich) daily for two days. The neurospheres were transferred on to the fibronectin (PHE0023, Gibco) coated plate in NIM (w/o retinoic acid) and left undisturbed for 48hours. Fibronectin coated plates were prepared by incubating plastic tissue culture plates with 15ug/ml fibronectin in PBS without calcium or magnesium at 37°C overnight. Afterwards, the NIM was changed daily until neural crest cells migrated and spread out onto the plate (6-10days). Neurospheres were mechanically removed, and the migrated neural crest cells were lifted as single cells with a 5 minute incubation at 37°C with 1X TrypLE (A1217701, Gibco). Cells were washed by diluting with 9ml of room temperature DMEM/F12 and centrifuging at 300G for 4min. The supernatant was removed, and cells were resuspended in DMEM/F12 for co-culture with HIO or resuspended in NIM and plated back onto fibronectin coated plate and maintained until the experiment. The cells were positive for known vagal fate neural crest cell markers and gene expression (FigureS6B,C).

### **Macrophage derivation**

Macrophages were derived from EU03.C2 or EU148.C5 or AICS-0010 as previously described with modifications<sup>77</sup>. Briefly, embryoid bodies (EB) were formed as follows. The hiPSC were cultured to 85-90% confluency in a 6 well plate with mTeSR1 and Geltrex matrix (A1413301, Gibco) and divided into smaller segments by scratching the bottom of the well into around 100 squares with a 100ul tip. The segments were detached mechanically with a scraper and the cells clumps were transferred into 6 well ultra-low attachment plate (3471, Corning) with EB media: mTeSR1 supplemented with 50 ng/ml BMP4 (120-05ET, PeproTech), 50 ng/ml of VEGF (100-20A, PeproTech), 20ng/ml of SCF (130-093-991, Miltenyi Biotec) and 10uM Y-27632 (72304, Stem Cell Technologies) and cultured in a 37°C, 5%CO<sub>2</sub> incubator. Every two days, half of the EB media was replaced with fresh EB media without Y-27632 for a total of 7 days. The EBs were then transferred to a 6 well tissue plate (10-15 EBs/well) in Factory EB (f-EB) media consisting of X-VIVO15 (BE04-418F, Lonza) supplemented with 100 ng/ml of M-CSF (216-GMP-500, R&D), 25 ng/ml of IL-3 (PHC0031, Gibco), 1X Glutamax, 1X pen-strep and 0.055 mM β-mercaptoethanol (31350-010, Invitrogen). The f-EB media were replaced weekly. Macrophage precursors started to emerge in the supernatant after approximately 15-20 days, reaching the maturity after 30 to 45 days in f-EBs cultures, assessed by the cell surface markers expression (CD34<sup>neg or low</sup>, CD14<sup>high</sup>, CD45<sup>high</sup>) through flow cytometry (FigureS6D). The precursors were harvested every two weeks for experimentation. Harvested precursors were cultured in RPMI media (SH3009601, Hyclone) supplemented with 100ng/ml of M-CSF, 2mM L-glutamine, 10% FBS (080150, Wisent) and 1X pen-strep for 7 days, replacing the media every two days. Differentiated macrophages were assessed with flow cytometry for the expression of macrophage

markers (CD14<sup>high</sup>, CD206<sup>high</sup> CD163<sup>high</sup>, CD16<sup>high</sup> CD11b<sup>high</sup>, HLADR<sup>neg</sup>) (FigureS6E). Additionally, dendritic cell marker FLT3 expression in the macrophages were low to none (FigureS2B).

### **HIO combination with VNCC and macrophage**

Prior to the procedure, two-to-three-week HIOs (since spheroid collection), differentiated macrophages, and vagal neural crest cells were derived as required. Matrigel was supplemented with 1X B27 and 100ng/ml EGF. In a 5ml tube, 50K VNCC and/or 100K macrophages were added to maximum x15 HIOs. Optimal number of VNCC and macrophages may vary depending on the cell line. The mix was briefly pipetted up and down using a cold 1000ul pipette-tip where 1mm of the end of the tip was cut. The mix was then centrifuged at 300G for 3min. The HIOs and the cells were then gently resuspended and centrifuged again. Supernatant was removed as much as possible and 50ul of cold Matrigel was added. The tube was kept on a cold tube from this point on. Using a cut-pipette tip that is cold, HIO and cells were gently resuspended, and the total volume was gently pipetted as a droplet on a pre-warmed 6well plate. Up to four droplets were plated per well. The plate was gently transferred to the incubator and allowed to polymerize for 10min. The well was then filled with 2ml of IBMe supplemented with 20ng/ml MCSF (Thermofisher, PHC9501; PeproTech, 300-25). After 48hr, the medium was replaced with fresh IBMe. The medium was refreshed every 48hr. One week after the co-culture, the organoids were removed from the Matrigel with gentle titration and dissection with sterile syringe needles. They were then re-embedded in new Matrigel droplets. HIOs were maintained with IBMe on the same feeding interval as before for another week before experimentation unless specified otherwise.

## **Human dendritic cell**

Human dendritic cells used as positive control for FLT3 qPCR were derived from purified cord blood CD34+ progenitors as previously described<sup>134</sup>.

## **Immunocytochemistry**

Cells were grown on plastic coverslips (174969, Thermo Fisher). At room temperature, cells were washed once with PBS and fixed in 4% paraformaldehyde (PFA) for 10min. PFA was removed and washed three times with cold PBS 5 minutes each. Cells were then incubated in blocking buffer (0.5% Triton X-100 and 10% donkey serum in PBS) for 1hr. Blocking buffer was removed, and cells were incubated with primary antibody in blocking buffer at 4°C overnight. The next day, primary antibody buffer was removed, and cells were washed in cold PBS four times 4minutes each then incubated in secondary antibody in blocking buffer for 1hour at room temperature in the dark. The secondary antibody buffer was removed, and cells were washed in PBS four times 4minutes each. Cells were then stained with DAPI (D-21490, Invitrogen) and washed once with distilled water. The coverslip was mounted on 1.5 coverslips with aqueous mounting medium (S3023, Dako) as per manufacturer recommendation before imaging.

## **Immunofluorescence and histology**

*In vitro* organoids, E9.5, and E10.5 mouse embryos were fixed with 4% PFA for 3hours at 4°C. Fetal proximal intestine, grafted organoids (cut in half), E12.5, and E15.5 mouse embryos (heads removed) were fixed for 12-16 hours at 4°C. The samples were washed with PBS on ice for 1hour three times with rocking and incubated in 30% sucrose in PBS at 4°C until it sank to the bottom of the tube. It was then incubated with optimal cutting

temperature (OCT, FSC22, Surgipath) compound at 4°C for 30 min, frozen-embedded in fresh OCT, and stored at -80°C. The samples were cut 5-10µm thickness and mounted on a charged glass slide (12-550-15, Fisherbrand). The sections were dried at room temperature for minimum 30minutes before the staining procedure. The sections were washed with PBS for 5 minutes two times and incubated in 0.5% Triton X-100 in PBS for 20 minutes. They were then incubated in the blocking buffer (10% Donkey serum and 0.3% Triton-X100 in PBS) for 30 minutes and incubated with primary antibody overnight at 4°C in a humid chamber. The next day, the slides were washed three times for 5 minutes each in PBS and incubated with the secondary antibody buffer for 1hour at room temperature. The slides were washed four times for 5 minutes each in PBS. The sections were counterstained with DAPI (D-21490, Invitrogen) for 10 minutes and washed once with distilled water. The slides were mounted with aqueous mounting medium (S3023, DAKO) with 1.5 glass coverslip and cured overnight at room temperature. The samples were then imaged with widefield (DMI8, Leica) or confocal (TCS SP8, Leica) microscope. Colorimetric staining (H&E+S and TMS) were performed by CHU-Sainte Justine pathology laboratory.

### **Quantitative PCR**

RNA was isolated with a DNase treatment (74104, 79254, Qiagen; Z6111, Promega) and cDNA was synthesized (18090050, Invitrogen) with oligo-dT (18418012, Invitrogen). SyberGreen (34226600, Roche) was used to quantify gene expression with Roche LightCycler 96 or LightCycler 480. A total of 15ng of cDNA and 0.3uM of each primer pair was used for a 15ul reaction as per manufacturer instruction. The primer sequences were designed using NCBI Primer-BLAST. Relative expression refers to 2 to the power of

difference in Ct values of target and reference gene, used for normalization. Refer to table1 for the list of primer sequences.

### **Grafting of organoids to immunodeficient mice**

Two to three weeks after the macrophage co-culture, organoids with single epithelial structure were grafted under the kidney capsules of immunodeficient mice as previously described, but without the collagen encapsulation of the organoid prior to grafting<sup>74</sup>. The organoids were collected at corresponding time points.

### **E.Coli particles injection into the grafted organoid lumen**

Kidneys with the grafted HIO/Macs were surgically exposed again 10 weeks after the engraftment. With an insulin syringe, up to 50-200ul of fluid was removed from the lumen of the organoid and an equal volume of 4mg/ml of pH-sensitive E.Coli Bioparticle (P35361, Thermofisher) reconstituted in PBS was injected into the lumen. The grafted kidney was placed back in the mice with the same procedure for grafting the organoids. The organoids were collected 24 hours later, sectioned in half with a surgical scalpel, and fixed in 4%PFA for 3 hours. The tissue was processed and examined with the method as described in 'Immunofluorescence' but stained only with DAPI.

### **Live imaging of injured HIO/Mac**

HIO/Mac combined with hiPSC<sup>eGFP</sup>-derived macrophages were cultured in suspension in ultra low attachment plate (3471, Corning) with phenol-free IBMe for two days prior to injury. Advanced DMEM-F12 was replaced with high-glucose phenol-free DMEMF12 (D1145, SigmaAldrich) to make phenol-free IBMe. To injure the organoid, 20G blunt tip

needle attached to a 1ml syringe was used to puncture the organoid at the center. The plunger of the syringe was drawn slowly after insertion into the organoid in order to remove the punctured material. The injured organoid was then placed in a glass-bottom dish (0030 740.017, Eppendorf) with phenol-free IBMe and imaged at a 10min interval for 12-18hours with up to a 100um z-depth (TCS SP8 confocal or DMI8 widefield, Leica). The stage-top incubator was set at 5% CO<sub>2</sub> at 37°C (iNU GSI2, Tokaihit). From the maximal projection image, cells were tracked with ImageJ plugin: Manual Tracking. The region of the injury was determined in situ from the images and the center of that region was used for downstream analysis. For controls, an arbitrary point at the center of the image was set, blinded from tracking of the cells. Directness and chemotactic precision index (CPI) were calculated as previously described<sup>135</sup>.

### **Isometric Force Measurement**

At week 12 of engraftment, HIO/ENS and HIO/ENS/Mac were isolated from the mice into Krebs buffer (NaCl 117mM, KCl 4.7mM, MgCl hexahydrate 1.2mM, NaH<sub>2</sub>PO<sub>4</sub> 1.2mM, NaHCO<sub>3</sub> 25mM, CaCl<sub>2</sub> dihydrate 2.5mM, Glucose 11mM). Each whole organoid was then hooked at the opposite end with silk strings and transferred to organ bath chambers with 37°C Krebs buffer fed with 95% O<sub>2</sub> and 5%CO<sub>2</sub>. The samples were then connected to the isometric force transducer and equilibrated at 1g of tension for an hour before the acquisition (Biopac MP150; Acqknowledge, Biopac). Spontaneous contractions were measured for 20-40min. The last 20min segment of regular contractions were taken for analyses. Maximal force is the highest peak. Contraction and relaxation time are averages of measure from trough to peak and peak to trough, respectively. Frequency of contraction is the number of peaks.

## **Single cell RNA sequencing and analysis**

For the preparation of single cell suspension, all samples were cut into <1mm pieces using a scalpel and dissociated using 1000U/ml collagenase IV (17104019, Thermofisher) in 2X TrypLE (A1217701, Thermofisher) with 10mM Glucose for 100-120minutes at 37°C. The suspension was gently pipetted up and down every 10 minutes to facilitate the dissociation. Cells were then passed through a 70um filter and ten-fold diluted in cold 1%FBS in PBS. The cells were then centrifuged 500G 5min at 4°C. The pellet was resuspended in 1%FBS in PBS and viable cell numbers were quantified with trypan blue and hemocytometer. For grafted day 121 HIO/ENS/Mac, GFP<sup>+</sup> macrophages were enriched using fluorescence-activated cell sorting (FACS). The cDNA and the libraries were then generated using Chromium Next GEM v3.1 according to the manufacturer guideline (1000268, 10X Genomics; manual: CG000315 RevB) and sequenced at Génome Québec with Novaseq 6000 S4 (20027466, Illumina). Human fetal scRNAseq FASTQs were acquired from ArrayExpress: E-MTAB-8221, E-MTAB-9720<sup>106,118</sup>. For the comparison of human fetal and organoid datasets, both were processed with SoupX to negate the effect of ambient RNA, largely arising from the red blood cells<sup>136</sup>. Otherwise, FASTQs were processed with CellRanger and downstream analyses performed with R using Seurat and visualized with ggplot2<sup>137,138</sup>. When the sex of the samples could not be matched in differential gene expression, chromosome X and Y genes were omitted from further analyses and visualization. Gene ontology analyses were performed with Metascape and protein association analyses with STRING<sup>139,140</sup>.

## **Glycolytic Stress Test**

Mesenchyme of HIOs co-cultured with or without macrophages for 7 days were dissected and dissociated into single cells with the same method as described in 'Single cell RNA sequencing and analysis'. In order to remove the macrophages from the cell suspension, all samples were processed with magnetic cell sorting with CD14 Microbead (130-050-200, Miltenyi biotec), LS column (130-042-401), and MidiMACS Separator (130-042-302) according to the manufacturer recommendation. Sorted cell suspension were centrifuged 400G for 5min at 4°C. Cells were resuspended in 4°C IBM, counted using hemocytometer, and 50K cells per well in 180ul volume were distributed to the Seahorse 96well microplate (101085-004, Agilent) pre-coated with hESC-qualified Matrigel (354277, Corning) as per manufacturer instructions. The plate was then centrifuged 300G for 1min. The mesenchymal cells were incubated at 5%CO<sub>2</sub>, 37°C incubator for 1 hour for cell attachment. Subsequently, the culture media was replaced with 37°C assay media (DMEM 5030 media, 2mM glutamine) and equilibrated at 37°C non-CO<sub>2</sub> incubator for 1 hour prior to extracellular acidification rate (ECAR) measurements with the Seahorse XFe96 Flux Analyzer. Following reagents were prepared according to the manufacturer instruction to perform the glycolytic stress test: 10mM Glucose, 5µM Oligomycin (O4876, Sigma-Aldrich), 100mM 2-Deoxy-D-glucose (2-DG, sc-202010A, Santa Cruz).

### **Quantification and statistical analysis**

The number of biologically independent samples (e.g. organoids) or animals is indicated by "n", whereas each organoid single cell RNAseq dataset in this study is a pool of 4-5 dissociated organoids. "N.S." means not significant. All relevant figures are in mean and error bars are in standard deviation ("s.d."). In single cell transcriptomic comparison between fetal and organoid samples, the threshold of discovery (dotted line) were

log<sub>2</sub>fold change > 1, adjusted p-value < 0.001 where Wilcoxon rank sum test was used. For comparison of organoid size between two conditions, two-dimensional area of the image of organoid was quantified with Imagej and the weight of the organoid was measured by scale. Welch's t-test was used for statistical testing. For exponential regression of the size of the grafted organoids over time from two way ANOVA was used. For quantification of level of apoptosis in grafted organoids, the area of cleaved caspase 3 divided by the area of nuclei (DAPI) in confocal microscopy images of immunofluorescence. Welch's t-test was used for statistical testing. For combined size comparison of all 10-week grafted organoids, one way ANOVA was used and posthoc Tuckey. For single cell transcriptomic comparison between *in vitro* organoids with or without macrophages, threshold of discovery was set to adjusted p-value < 0.001, Log<sub>2</sub>fold change > 0.09 & < -0.09 where Wilcoxon rank sum test was used. For statistical analysis of ECAR time course Two-way ANOVA was used with post-hoc Sidek-Bonferroni. For glycolysis and glycolytic capacity in the glycolytic stress test, following formula was used: Glycolysis (maximum rate measurement before oligomycin measurement – last rate measurement before glucose injection), glycolytic capacity (maximum rate measurement after oligomycin measurement - last rate measurement before glucose injection), and non-glycolytic acidification (last rate measurement prior to glucose injection). Student's t-test was used for statistics and each data point represent a technical replicate well. Specific statistical details for each experiment can be found in the Figurelegends.

Statistical analyses were performed using GraphPad Prism v.7.04 and R statistical software.

## Chapter 2: Modelling Chronic Atrial and Intestinal Dysrhythmia in patient iPSC-derived human intestinal organoid and cells.

### Research findings (Chapter 2)

#### Patient enteric neurons have disorganized morphology and lack surrounding interstitial cells of cajal

We have previously reported mislocalization of enteric ganglia in the disrupted patient intestinal biopsies<sup>1</sup>. Further immunohistological assessment showed disrupted enteric neuron morphology within the ganglia and lack of interstitial cells of cajal (ICC) that normally surrounds the ganglia. Staining for ELAVL4, a neuronal marker, were more fragmented and diffuse in patient neurons indicating a disruption at a cellular level. Enteric ganglia between the two smooth muscle layers (myenteric) are surrounded by ICCs; however, these ICCs were either missing or sparse in patients (Figure1). In conclusion, CAID patients display abnormal enteric neuronal morphology and loss of ICC.

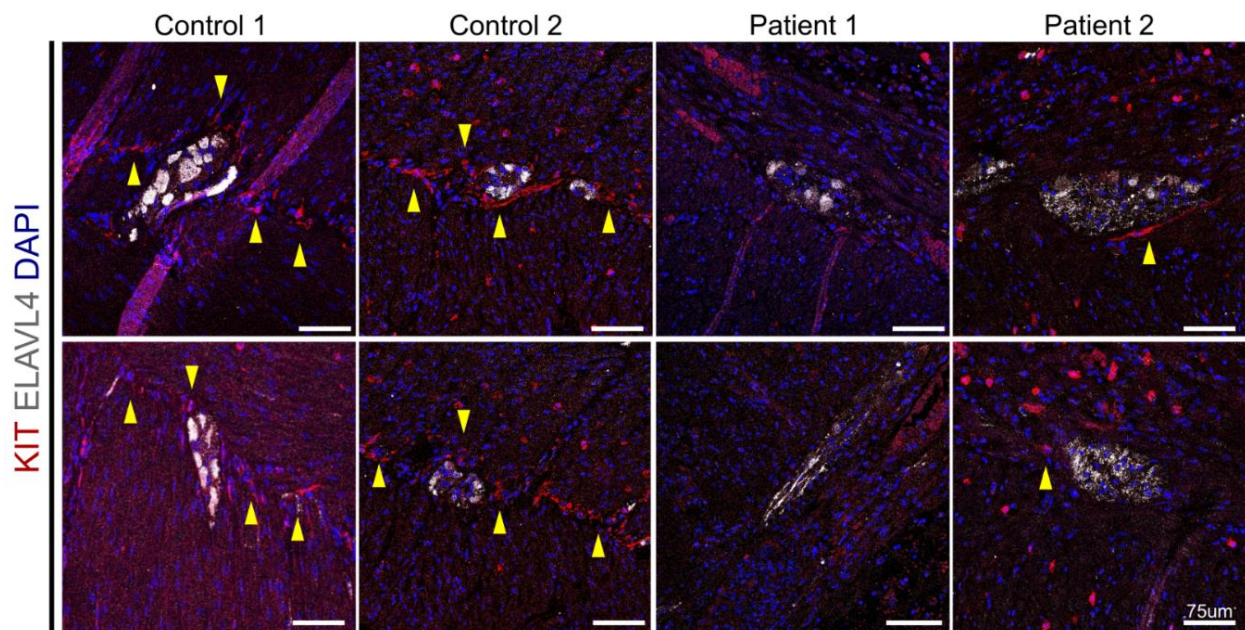


**Figure1. Patient enteric neurons have disorganized morphology and lack surrounding interstitial cells of cajal (ICC).**

*Immunofluorescence staining of patient and control intestinal biopsies. ICC (KIT), ELAVL4 (neuron), DAPI (nucleus). The images show enteric ganglia at the myenteric plexus of each sample. Yellow arrow heads point to ICCs surrounding the enteric ganglia. Two biological replicates per control and patient biopsies. Scale bar = 75 um.*

**Patient iPSC-derived organoids show erratic contractile pattern**

Derivation of human intestinal organoid with enteric nervous system were previously described<sup>75,103</sup>. Both HIO and vagal neural crest cells were derived from patient iPSCs and co-cultured to derive HIO/ENS (Figure2A). HIO/ENS were then grafted to immunodeficient mice for further maturation where organoids displayed spontaneous contractile activity. Isometric force measurement of the organoids showed migrating motor complex-like contractile pattern with repetition of active contractile phase (phase III-IV) and quiescent phase (phase I-II). Comparison of IFM recording showed more erratic contractile pattern in the patient organoids compared to the control, seemingly having more activity during quiescent phases (Figure2B). Standard deviation of contractions in phase I-II, or quiescent phase, were indeed higher in patient organoids (Figure3C). In conclusion, we observed more active quiescent phases in patient organoids without rest.

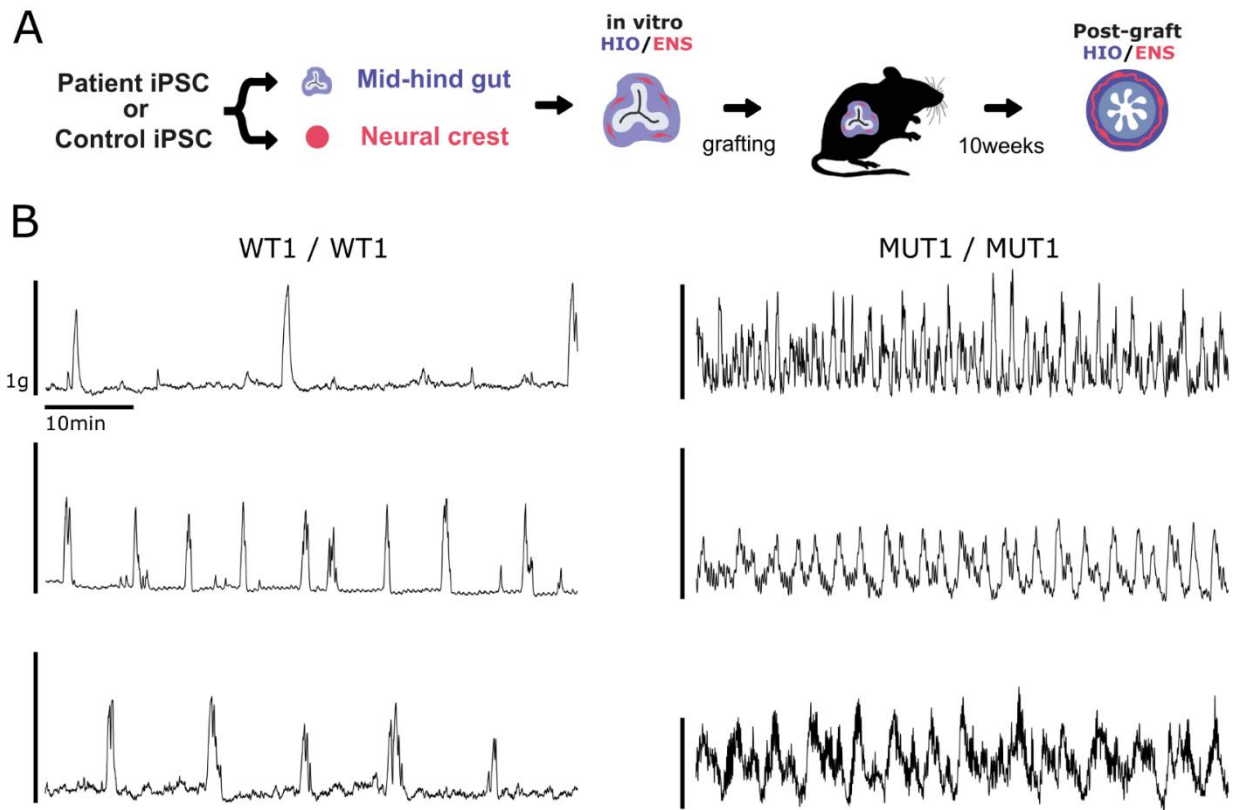


**Figure2. Patient iPSC-derived organoids show erratic contractile pattern**

A) Schematic of human intestinal organoid with enteric nervous system (HIO/ENS) derivation and engraftment in immunodeficient mice for maturation.

B) Representative isometric force measurement (IFM) tracings of 10-week grafted HIO/ENS. WT = control iPSC line, MUT = patient iPSC line. WT1 = SJ3252c2, MUT1 = SJ2551c2. See Methods. Each row represents an IFM tracing of a single organoid. WT1/WT1 n=4, MUT1/MUT1 n=10.

### **Organoids with patient iPSC-derived VNCCs have more erratic contractile pattern**

In order to test if the enteric nervous system were causing the erratic contractile patterns observed in patient organoids, we derived HIO and VNCC each from either control iPSC lines or patient iPSC lines to generate genotypically hybrid HIO/ENS. IFM of the hybrid organoids showed erratic contractile patterns in organoids where ENS (VNCC) were derived from patient iPSC lines. Intriguingly, organoids where HIO were from patient iPSC and ENS were from control iPSC showed normal contractile pattern comparable to all-control-line derived HIO/ENS (Figure3A-C). Upon histological assessment of the organoid tissue, however, many samples were missing neuronal cells. Lack of neuronal cells were not associated with the patient vs. control status of iPSC lines used (FigureS1). In conclusion, organoids with enteric neural progenitors derived from patient iPSC showed more erratic contractile pattern; however, if this phenotype is originating from enteric neuron remains unclear.

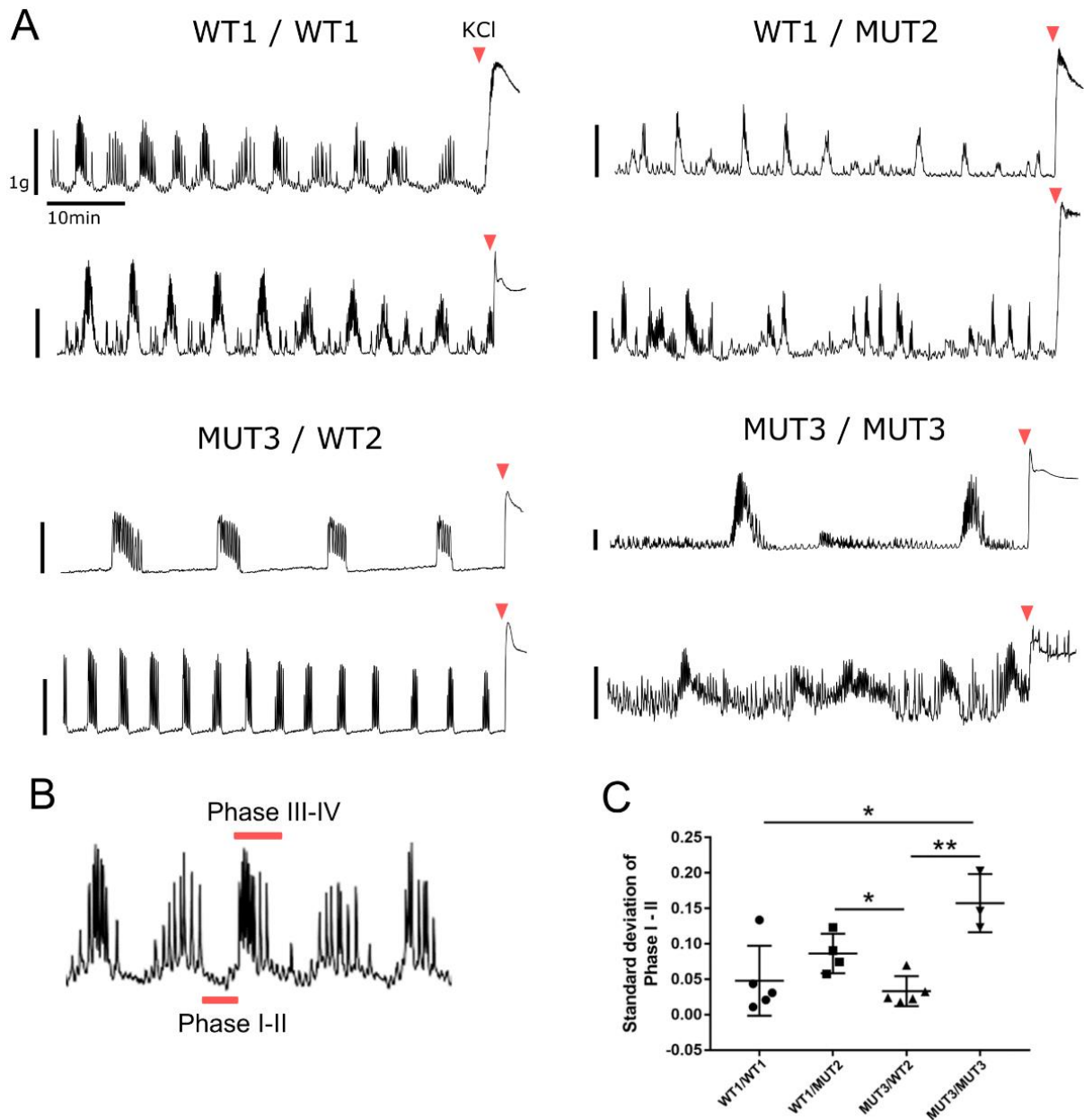


**Figure 3. Organoids with patient iPSC-derived VNCCs have more erratic contractile pattern**

A) Representative isometric force measurement (IFM) tracings of 10-week grafted HIO/ENS with mixed genotypic origin. WT = control iPSC line, MUT = patient iPSC line. WT1 = SJ3252c2, WT2 = WTC3, MUT2 = SJ2550c2, MUT3 = SJ2391c2. See

*Methods. Each row represents an IFM tracing of a single organoid. WT1/WT1: n=6, WT1/MUT2: n=4, MUT3/WT2: n=5, MUT3/MUT3: n=3.*

*B) Schematic indicating phase I-II and phase III-IV.*

*C) Quantification of standard deviation of force recorded during phase I-II of all samples. Results from two independent experiments. Note that phase I-II from MUT1/MUT1 (Figure1B) could not be distinguished thus not included here.*

### **Patient iPSC-derived VNCCs are normal in size, proliferation, and migration**

The patient vagal neural crest cells were contributing to the abnormal motility. Thus, we characterized characteristics of patient iPSC-derived VNCCs. SGO1 plays a role in cell division and cell cycle arrest can lead to increased cell size. Cell size or MKI67<sup>+</sup> proliferating cells, however, did not significantly differ from the control (Figure4A,B). Previous report shows RAD21, another protein in a cohesin complex, depletion in zebrafish causes lack of cardiac neural crest incorporation in the heart and mislocalization of melanocytes, which are neural crest derived. In order to test if migration capacity itself is affected in patient VNCCs, we performed scratch migration assay. Migratory/proliferative capacity of patient VNCC, however, were not different from the control (Figure4C). In conclusion, we did not observe changes in cell size, proliferation, or migratory capacity in patient iPSC-derived VNCCs.

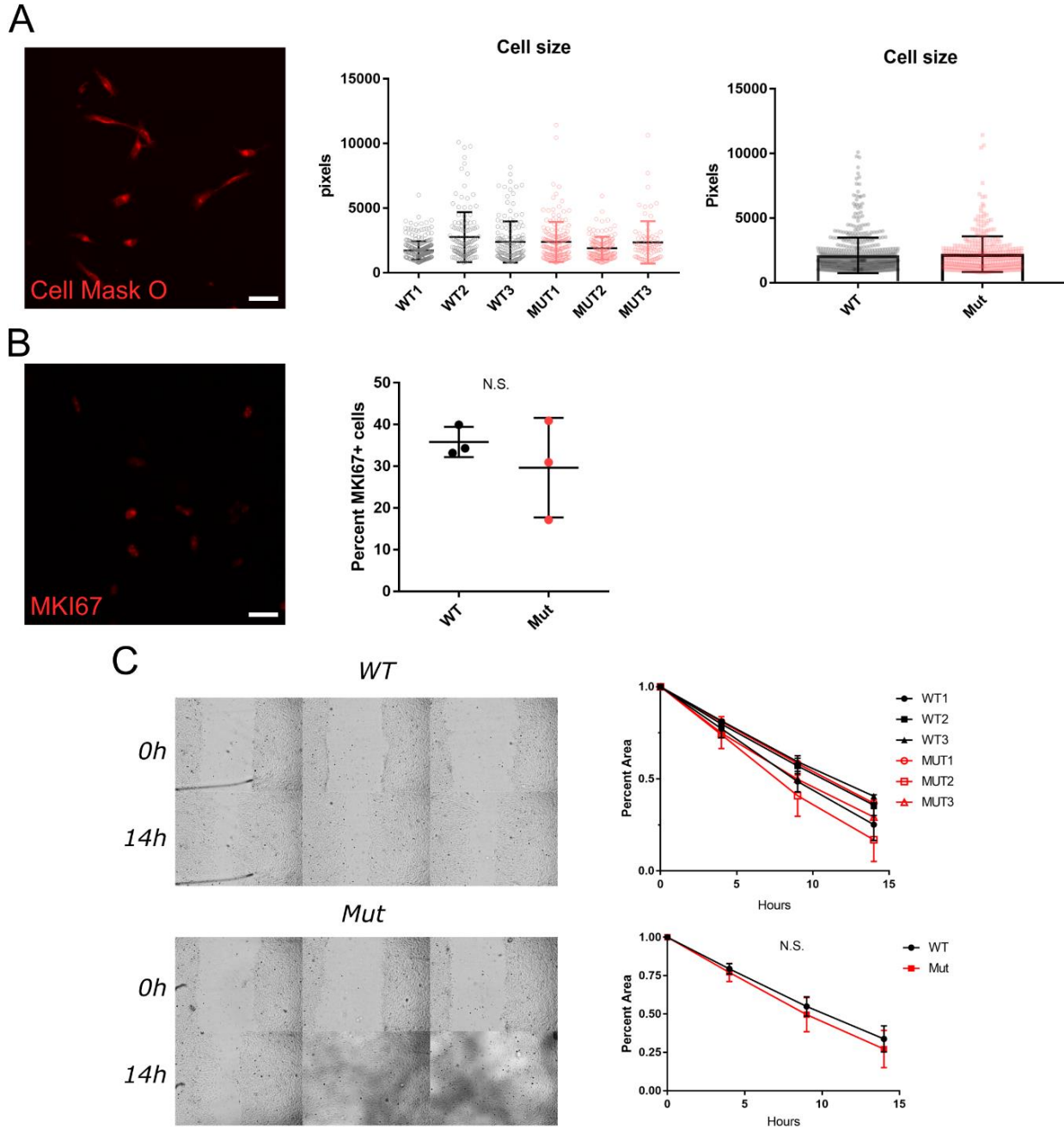


**Figure 4. Patient iPSC-derived VNCCs are normal in size, proliferation, and migration.**

A) Cell size quantification of VNCCs by staining the membrane staining agent Cell Mask O.

B) Quantification of percent proliferating VNCCs by ratio of MKI67-positive cells to the number of total cells (DAPI).

C) Scratch migration-proliferation assay of VNCCs.

WT1 = SJ3252c2, WT2 = WTC3, WT3 = SJ3013c2, MUT1 = SJ2551c2, MUT2 = SJ2550c2, MUT3 = SJ2391c2. Scale bar = 60um.

### **Patient iPSC-derived VNCCs overexpress *PLXNA3***

Cohesin protein *RAD21* knock out results in dysregulation of neuronal maturation gene expression<sup>87</sup>. In order to probe the effect of *SGO1* mutation in VNCCs in this context, we performed bulk RNA sequencing on patient and control VNCCs and iPSCs. In patient iPSCs, *IKBK*G was downregulated and *FZD2* upregulated. *IKBK*G mutations causes diseases of ectodermal lineage, such as incontinentia pigmenti and hypohidrotic ectodermal dysplasia<sup>141-143</sup>. *FZD2* is a member of *WNT* receptor proteins. *WNT* pathway is required for neural crest formation from ectoderm<sup>94</sup>. Mutations are associated with omodysplasia and Robinow syndrome<sup>144,145</sup>. Other differentially expressed genes included increased readthrough RNAs (*ABCF2-H2BK1*, and *DNAJC25-GNG10*) and decreased pseudo gene (*PCDHA14*) expression in patient iPSCs. In VNCCs, *PLXNA3* was upregulated (Figure5A,B). *PLXNA3* has been shown to be involved in ENS development in zebrafish and it's mutation causes Kallmann syndrome-like phenotype in mice. Kallmann syndrome is caused by underdevelopment of hypothalamic neurons<sup>96,97</sup>. In conclusion, patient iPSC had differential expression of ectoderm and neural crest-

related genes (*IKBKKG*, *FZD2*) and the differentiated VNCCs showed increase in gene expression involved in ENS development (*PLXNA3*).

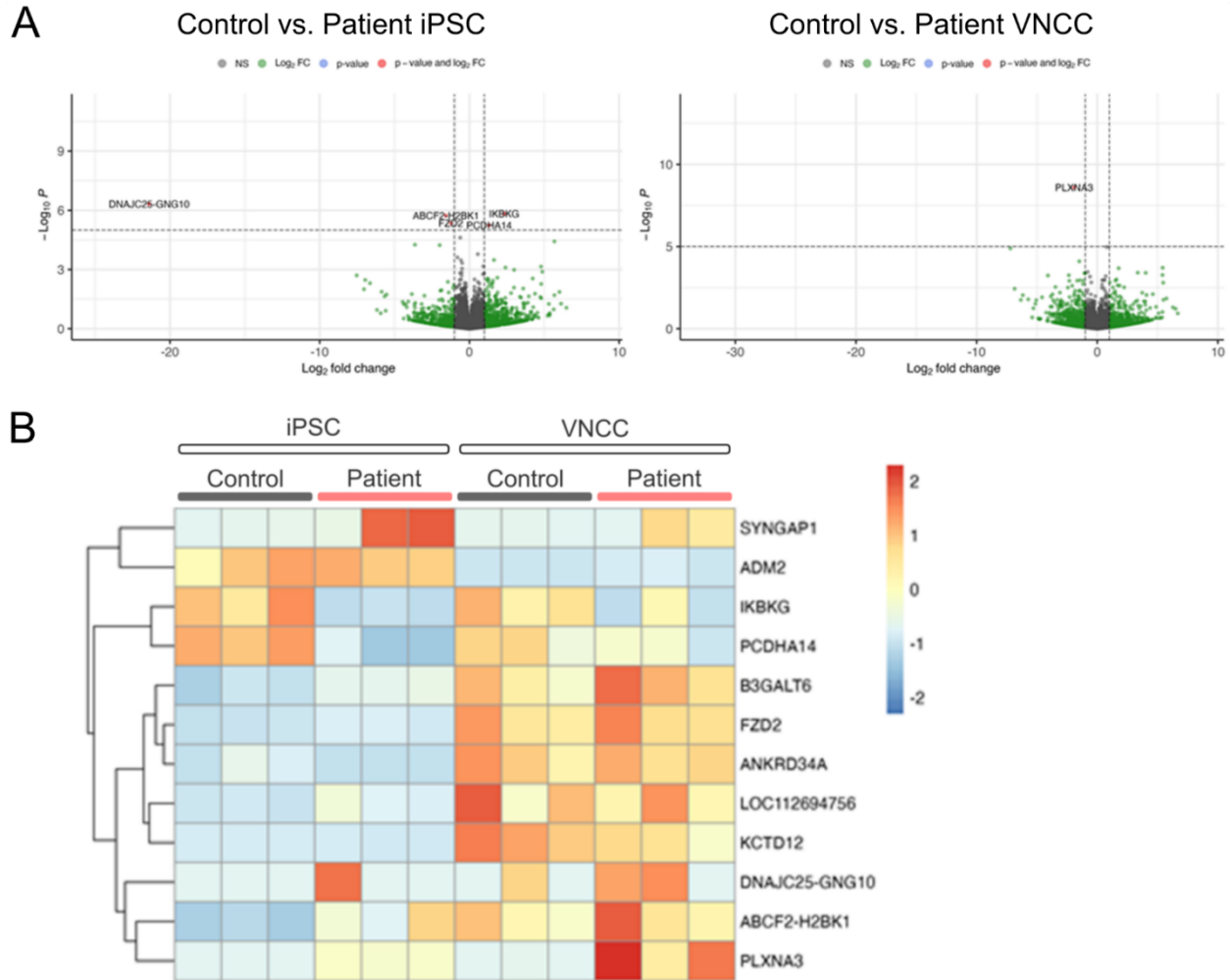


**Figure5. Patient iPSC-derived VNCCs overexpress PLXNA3.**

*Differential gene expression analysis of bulk RNA sequencing datasets of iPSCs and iPSC-derived VNCCs from control and patients.*

*A) Volcano plot of significantly expressed genes in control iPSC and VNCC compared to patient iPSC and VNCC. Log<sub>2</sub>Fold change threshold = 1, p-value threshold = 0.00001, adjusted p-value threshold = 0.01. control*

*B) Heat map of top genes differentially expressed. Scaled expression level.*

*Three biological replicate per condition, WT = control, MUT = patient. Cell lines: WT1 = SJ3252c2, WT2 = WTC3, WT3 = SJ3013c2, MUT1 = SJ2551c2, MUT2 = SJ2550c2, MUT3 = SJ2391c2.*

## **Methodology (Chapter 2)**

*Methodology described here are unique to Chapter 2. Other methodologies overlap with Chapter 1 and can be found in 'Methodology (Chapter 1)'.*

### **Isometric force measurement**

Acqknowledge (Biopac) software was used to transform the force tracing. Troughs were taken as Phase I-II and Peaks were taken as Phase III-IV. Standard deviation of the trough was then calculated using the Acqknowledge software.

### **Cell size, proliferation, and migration.**

Cell Mask O and MKI67 staining was performed as per manufacturer recommendation and as described in 'Chapter 1 Methodology: immunocytochemistry'. Quantification was performed using Fiji (ImageJ). For cell migration, wound induction was performed using an automated tool (Agilent BioTek Autoscratch) as per manufacturer recommendation. Time-lapse images were taken using Lionheart FX microscope (Agilent BioTek) in culture media (NIM).

### **Bulk RNA sequencing**

RNA was isolated with a DNase treatment (74104, 79254, Qiagen; Z6111, Promega) and cDNA was synthesized (18090050, Invitrogen) with oligo-dT (18418012, Invitrogen). The library preparation and sequencing were performed at Génome Québec with Novaseq 6000. The transcripts were quantified directly from the fastqs using Salmon v.1.4.0. Indexing was done using release 108 of GRCh37 (hg19) from Ensembl.

Org.Hs.eg.db in R was then used to generate a transcript-to-gene file. Tximport was used to load the quantification files and get both counts and abundance (TPM) values for each gene across each of the samples. Finally, differential gene expression analysis was performed using DEseq2. Wald test for calculating the p-values.

## **Comprehensive discussion**

### **Relevance: Chapter 1**

Here, we studied the effect of macrophages on human intestinal development by engineering and utilizing a pluripotent stem cell-derived intestinal tissue model with macrophages. We describe an efficient and reproducible means of deriving human intestinal organoid with macrophages (HIO/Mac) in which the macrophages localized to known micro-anatomical intestinal niches and acquired a similar transcriptional profile to fetal intestinal macrophages. Our approach improves complexity of HIOs and improves on a previously published approach by providing tissue architecture with physiologically relevant macrophage distribution, higher reproducibility, and developmental relevance<sup>76</sup>. Organoid macrophages acquired fetal intestinal macrophage-like transcriptional profile and displayed expected behaviors such as phagocytosis of luminal antigen and migration to wounds upon injury. Finally, we demonstrate that macrophages regulate the metabolism and organ growth of the developing intestinal organoid.

### **Derivation of human intestinal organoids with macrophages (HIO/Mac)**

Single cell RNA sequencing has become more prevalent and efforts to sequence human fetal samples increased the access to such highly informative datasets. However, samples captured at time points earlier than day 47 was not available, likely due to lower number of termination of pregnancies at on early time points. The gap in the dataset on early human developmental samples would have to be mediated by murine samples and organoid models as we have done here; however, ongoing effort in minimizing this gap would be immensely helpful in better understanding human development and developmental illnesses.

Though initial macrophage dispersion throughout the embryo from yolk-sac and fetal liver occurs via circulatory system, efficient migration of macrophages throughout the organoid tissue indicates that the vasculature is just an initial step in the migration. Embryonic macrophages are, unsurprisingly, likely capable of navigating throughout the embryonic tissue after the vascular delivery to establish and apply self-avoidance for proper distribution<sup>146</sup>. Further investigation on this matter may be fruitful in understanding fundamental nature of how intercellular organization works considering macrophages are tissue resident but are constantly replenished in many organs.

### **Cellular composition of the intestinal organoid resembles fetal intestine**

Though the method to incorporate macrophages into HIO described here was highly reproducible, we did find the ratio of macrophages within the HIO was smaller than that of fetal intestine, albeit intestine being 10 days older. We suspect that optimization to increase the number of macrophages incorporated will be useful but only to a certain degree since organoid macrophages are capable of proliferating locally. On this matter, what induces macrophage proliferation within the tissue in steady-state vs. inflammation?<sup>147</sup> Why is local production of intestinal macrophage in adult not the norm when local proliferation in the brain is the status quo? If it is the intestinal tissue environment that does not allow local production, then why is intestinal epithelial stem cell maintained locally? Further investigation is warranted.

Modularity of the HIO/Mac, as demonstrated by vagal neural crest cell or macrophage exclusion experiments here, is particularly useful when cellular composition is an experimental variable. Similar cell exclusion experiment should be useful to examine

specific effects of embryonic macrophages in tissue development, such as their role on vascular and lymphatic development<sup>44,49,50</sup>.

### **Macrophage recruitment and retention by the organoid**

We identified mesenchymal cells to be the major producer of CSF1 in the early developing intestine and the organoid. Previous study in E17.5 mice have identified endothelial and interstitial cells of Cajal (ICC) to have significant *Csf1* expression<sup>36</sup>. Our single cell analyses on human fetal intestine (day 47, 85, 127) and organoid (day 37) also observed expression of *CSF1* in both endothelial and ICC. However, the relative expression level, percentage of the cells expressing, and percentage within the intestine expressing was not comparable to mesenchymal cells. Thus, we conclude that mesenchymal cells are quantitatively the major source of CSF1 during early human intestinal development.

### **Enteric neurons do not affect resident macrophage establishment**

As shown previously in mouse and in our study, macrophages do not require enteric neurons to establish in the intestine. However, it is clear that enteric neuron-macrophage relation is functional and crucial for enteric neurons in adult. A recent report demonstrated that intestinal macrophages are required for enteric nervous system development in post-natal mice, similar to the microglia's (brain macrophage) post-natal effect on central nervous system development<sup>54,55,57</sup>. Why do we see more pronounced phenotype in post-natal development in both organs? It would be interesting to explore if nervous system development triggered at birth specifically requires interaction with macrophages.

### **Macrophages migrate to the wound site upon injury**

Macrophages are required for proper regeneration in adult<sup>20,21</sup>. Scar-less wound healing in the fetus can be an intriguing avenue to study mammalian wound healing. Further adaptation of the method described here should be useful to explore the mechanisms and limitations of wound healing and how macrophages react to fetal injury or infection. For example, utilizing a confocal scanning microscope to induce a spatially-specific laser injury would enable us to observe macrophage behavior in a more controlled manner.

### **Macrophages localize to intestinal micro-anatomical niches in xenograft-matured organoids**

Organoid macrophages established themselves at the crypt as intestinal macrophages would. Furthermore, we observed increased number of MKI67<sup>+</sup> in the crypt region of the epithelium in organoids with macrophages, similar to what was observed in the macrophage ablation study in adult mice<sup>41</sup>. At glance, this is at odds with the decreased size in organoids with iPSC-derived macrophages, since MKI67 is a marker of cell proliferation. We propose two potential explanations. Firstly, non-epithelial growth inhibition outweighs epithelial proliferation in affecting the overall size of the organoid. Previous report on the mechanism of vilification during the embryonic development show physical-spatial restriction by smooth muscle buckles the expanding epithelium and thus, at least partially, contributes to the epithelial folding or villi formation<sup>8</sup>. Thus, it is reasonable that epithelium expansion in the organoid is restricted within the mesenchymal and smooth muscle confine and does not or contributes little to the overall size of the organoid. Secondly, MKI67 is not necessarily marking the proliferation of cells but stemness of the epithelial cells. Previous reports indicate that MKI67 is required for

stemness of cancer cells but not proliferation<sup>148</sup>. Furthermore, MKI67 is expressed in a gradient throughout G1-M phase, rather than being a binary marker of cell cycle<sup>149</sup>. Thus, considering that duration of G1 phase varies in different cell types, it is worth considering if MKI67 is a direct indication of proliferation itself or an indication of stem cell state in the crypt. Previous studies in adult mice also show that macrophage ablation result in a decreased proportion of MKI67-positive crypt cells. In these ablations, however, they show a small decrease in the small intestine but also significant increase in the villi/crypt length of large intestine. These reports indicate that changes in MKI67-positive crypt cells does not necessarily correlate with epithelial length in this biological context<sup>41,46</sup>. Further investigation is required.

Organoid macrophage also localized with enteric ganglia. We also did not observe any contractile difference in grafted HIO/ENS with or without macrophages. Enteric neuronal pruning by macrophages which happens extensively after birth may indicate that the delayed functional association between ENS and macrophage is not recapitulated in this stage of the model, since grafted organoids still represents a fetal intestinal tissue<sup>57</sup>. Presence of NSG mouse macrophages in the organoids should also be taken into consideration in future studies.

### **Organoid macrophages acquire transcriptomic profile alike fetal intestinal macrophages**

Fetal cell atlas project previously noted that antigen-presenting macrophages were found mostly in the gastro-intestinal tract<sup>150</sup>. We found that intestinal macrophages acquire this antigen-presenting profile over time, indicating that this functional characteristic is induced by intestinal environment rather than deriving from the ontological origin of the

embryonic macrophages. Furthermore, acquisition of antigen-presenting profile of organoid macrophage suggests HIO/Mac replicates this intestinal environment in this regard. It is intriguing to note that the organoids were kept in aseptic conditions during both *in vitro* culture and engraftment. Thus, the induction of the antigen-presentation profile in organoid macrophages, also observed in fetal intestine, occurred in the absence of microbiota. This suggests that intestinal tissue itself can induce antigen-presentation profile of macrophages in the prenatal stage.

### **Macrophages regulate intestinal organoid growth**

Unexpectedly, we find that HIO/Mac are smaller than HIO, suggesting that macrophages have an anti-growth effect in the developing organ. Macrophages did not cause fibrosis nor was there accumulation of apoptotic cells that can cause the size difference. Our scRNAseq and metabolic analysis suggest that this is associated with the decrease in glycolysis and glycolytic capacity of the mesenchymal cells, limiting the overall organ growth. However, taken together with the increased number of proliferating cells in the epithelial crypt region in the HIO/Mac, our results suggest that macrophages' regulatory effect during the development should be approached in a niche-specific manner. We also observed pro-growth effect of ENS on HIOs, which were independent from anti-growth effect by macrophages. Pro-growth effect of ENS may be, at least in part, due to increased epithelial growth as recently observed in gastric organoids<sup>151</sup>. In short, we found evidences that suggest embryonic macrophages function as a negative regulator of glycolysis and growth during human intestinal development unlike pro-growth effect of tumor-associated macrophages in most cases<sup>152</sup>.

## **Macrophages attenuate mesenchymal cell glycolysis in developing intestinal organoids**

Macrophages positively regulated adipocyte thermogenesis and negatively regulate glucose uptake in response to insulin.<sup>16,17</sup> On the other hand, they were also shown to upregulate glycolysis in cancer cells and promote tumor growth<sup>64</sup>. Previous accounts of macrophage regulating peripheral cell's metabolism is not yet abundant, but they indicate that such regulation is highly context or niche-dependent and can be both stimulatory and inhibitory in nature. In intestinal organoids, macrophages seem to have an inhibitory regulation on glycolysis of mesenchymal cells. Function of this mechanism remains to be understood but we speculate that macrophages are mediating a negative impact of sustained hyperglycemia in mesenchymal cells, which negatively affect proliferative capacity and differentiation<sup>153</sup>. The organoid culture condition, like most cell culture, are in hyperglycemic range, thus triggering downregulation of glycolysis by macrophages. At large, this homeostatic mechanism may exist to regulate the metabolism of available glucose, which is crucial during embryonic development<sup>154–156</sup>.

## **Oncostatin M (OSM) reduces glycolytic gene expression in mesenchymal cells**

LIFR signaling, receptor of OSM, has been shown to activate HIPPO pathway, inhibiting YAP target genes, such as glycolytic genes<sup>130</sup>. We found that the OSM, which is expressed by macrophages, reduced glycolytic gene expression in mesenchymal cells. Not all genes we found in scRNAseq of HIO with or without macrophages; however, seem to be consistently downregulated, such as LDHA. Thus, we suspect there are other ligands or mechanisms that induces the full effect of glycolytic downregulation in mesenchymal cells that we observed in the scRNAseq experiment.

Furthermore, HIPPO pathway regulate ectopic organ growth, where over-activation of YAP results in overgrowth of an organ<sup>129</sup>. Considering the smaller organoid size in HIO with macrophages, organoid macrophages' effect on glycolysis and organ growth may both be a result of regulation of HIPPO pathway. Further investigation on the effect of signaling pathways, such as OSM, on HIPPO activation is warranted.

### **Limitations of the study**

We utilized derivation of macrophages that is MYB-independent and thus yolk sac-like in ontogeny<sup>78</sup>. From mice, we can deduce that yolk sac macrophages are the first to occupy the embryonic intestine, likely followed by fetal liver. It is still to be determined if functional differences are present among embryonic macrophages dependent on the ontogeny as tissue macrophages, such as yolk sac vs, fetal liver vs. aorta-gonad mesonephros. Depletion and repopulation experiment in mice lung suggests that functionality between the ontogenies is comparable<sup>157</sup>. However, if otherwise in the intestine, alternate macrophage derivation method would have to be utilized than what is described here to recapitulate the ontological differences.

### **Relevance: Chapter 2**

#### **Patient enteric neurons have disorganized morphology and lack surrounding interstitial cells of cajal (ICC)**

Enteric neuronal morphology was fragmented, and the myenteric ICCs were lacking in the patient intestinal biopsies. Intestinal occlusion (obstruction) model in mice have demonstrated that myenteric ICCs are lost around the occlusion site and restored upon the removal of artificial occlusion<sup>102</sup>. This indicates that lack of ICC is likely a secondary effect of the pseudo-obstruction. On the other hand, enteric neurons undergo hypertrophy

upon partial obstruction of the intestinal passageway in a similar model<sup>158</sup>. This indicates pseudo-obstruction itself is unlikely to cause small size or disrupted morphology seen here and in the previous report<sup>1</sup>. However, these histological findings alone are insufficient to assign neuropathological origin to the CAID's CIPO.

### **Patient iPSC-derived organoids show erratic contractile pattern**

Patient iPSC-derived HIO/ENS lacked quiescent phase in comparison to organoids derived from control iPSC lines. At a clinical level, manometry of myopathic origin usually manifests as low amplitude contractions whereas neuropathic origin presents as disorganized and uncoordinated patterns. CAID patient manometry show both myopathic and neuropathic pattern where it failed to respond to promotility agents. Such manometry, however, was taken when the signs and symptoms have manifested themselves noticeably. Thus, the erratic contractile pattern we observe in the patient organoids may represent the phenotype at beginning of the disease before secondary effects of the initial insult have taken place.

### **Organoids with patient iPSC-derived VNCCs have more erratic contractile pattern**

We showed that the erratic contractile pattern observed in the all-patient-line (MUT/MUT) organoids are caused by patient VNCCs. However, enteric neuronal cells were not found in some of the organoids to our surprise, and this lack of enteric neurons did not correlate with erratic contractile pattern. We currently do not have reasonable explanation for how the phenotype is reproducibly present in the presence or absence of expected cell type, enteric neurons. Nonetheless, the erratic contractile profile we have observed in two independent derivations seems to be linked with vagal neural crest cells. Intriguingly, mutation in *Rad21*, a cohesin complex protein, also causes CIPO and is expressed in

enteric neuronal cells<sup>88</sup>. Cohesin proteins are also directly associated with neural crest behavior and associated anatomical structures. *Rad21* morpholino knock down and *Rad21* knock out zebrafish showed a failure of cardiac neural crest cells to populate the heart and results in functional and morphological defects<sup>159</sup>. Neural crest cell-specific knock out of *Nipbl* also results in craniofacial defect, a structure made up of neural crest cells<sup>160</sup>. Together, the results indicate that cohesin complex proteins can have a direct association of neural crest behavior.

### **Patient iPSC-derived VNCCs are normal in size, proliferation, and migration**

VNCCs showed comparable cell size, number of proliferating cells, and migration capacity between the controls and patients. Thus, we conclude that the *SGO1* mutation in the patients does not necessarily affect the above parameters to give rise to the disease. Previous report shows *RAD21* knock out results in dysregulation of central nervous system neuronal maturation and homeostatic gene expression in post-mitotic neurons. Knock out also affected the maturation of the post-mitotic neurons<sup>87</sup>. Our original aim was to differentiate the vagal neural crest into enteric-like neurons; however, our differentiation attempts did not result in convincing enteric neurons<sup>161,162</sup>. Thus, we next proceeded to analyze the gene expression pattern of the vagal neural crest cells.

### **Patient iPSC-derived VNCCs overexpress *PLXNA3***

Intriguingly, all the differentially expressed genes we found in both iPSCs and VNCCs were associated with neural lineages. In detail, *IKBKG*, which causes diseases in ectodermal lineages when mutated, and *FZD2*, a *WNT* receptor required for neural crest formation<sup>94,143</sup>. Dysregulation of ectodermal-related genes in iPSCs suggest that the *SGO1* mutation can influence cell fate commitment. Furthermore, patient VNCCs also

expressed higher levels of *PLXNA3*, gene involved in neuronal guidance and enteric nervous system development<sup>95-97</sup>. The mechanism behind how *SGO1* affects a seemingly unrelated category of genes may be associated with cohesin complex's involvement in chromatin remodeling with *CTCF*. Additionally, knock down of *CTCF* results in repressive histone marks<sup>163</sup>. We have previously reported a higher global methylation in CAID's patient fibroblasts<sup>85</sup>. *RAD21* knockout causes gene expression changes and morphological changes associated with neuronal processes in CNS neurons. Furthermore, the knock out induces modification in chromatin loop length, which modifies expression of genes, in a neuron associated gene (*BDNF*)<sup>87</sup>. Notably, readthrough RNAs (*ABCF2-H2BK1*, and *DNAJC25-GNG10*) were detected at a higher level in patient iPSCs. Readthrough RNAs are combination of exons of two or more genes in a single transcript. Previous report suggests chromatin open state associates with occurrence of readthrough transcript<sup>164</sup>. Thus, increased occurrence in these annotated readthrough transcript may be an indication of alterations in chromatin structure in patient genome. *SGO1* mutation in CAID patients, thus may dysregulate cohesin's function in chromatin remodelling, resulting in aberration of neural-specific gene expression. Further investigation into the effect of *SGO1* mutation in chromatin remodelling of neural crest lineage and functional effect in differentiated enteric neurons are warranted.

### **Limitations of the study**

Some HIO/ENS lacked enteric neurons. The lack of neurons did not correlate whether the VNCCs were derived with control or patient iPSCs. Though the HIO/ENS lacked enteric neurons, the erratic contractile profile was still observable in organoids derived with patient-derived VNCCs in two independent derivations. Lack of the neurons were

mostly observed in MUT3-iPSC line organoids combined with other VNCCs; thus, there may be biological cause behind this phenomenon. Nonetheless, derivations with additional iPSC lines will be required for clarification.

For bulk-RNA sequencing experiment, though the identification of the differentially expressed genes were statistically significant, there were noticeable variations in some genes between different patients. Sequencing of additional patient iPSC lines and VNCCs is warranted for future studies.

## **Overview**

Organoid models are a powerful tool to mimic organismal development and add human biological context and validations found in other model organisms. Organoid models are however, not a complete replica of human organ or organ systems yet. Two main points remain to be improved in the human intestinal organoids and organoids in general. Firstly, as demonstrated in the findings, lack several cell types such as vascular cells, and lymphocytes. The interpretation of the results taken from the model must take into account the cell types present in the model. Additionally, in order to completely model a human being, one must take organ-to-organ interaction into account. This concept has arisen in multiple occasions and are currently referred to as 'human-on-a-chip'<sup>165</sup>. However, attempts so far are a micro-fluidic link between two-dimensional cultures. This similar approach can be applied with more complex models such as organoids. Furthermore, for such 'human-on-a-chip' to be more widely available, major organ-type complex organoids would have to be commercially available for individual labs and organizations to configure them as needed, as we currently do with cell lines. In summary, improvement in individual organoid derivation and method to distribute the organoids will enable such

technologies to fully reap its benefits. Secondly, organoids the literatures describe are still at a fetal stage, including the grafted human intestinal organoids. The development of the organoids may simply require more time in culture for complete development; however, the issue of proper vascularization of the organoid tissue has not been properly addressed. The aim to integrate vascularization and tissue maturation will also be crucial in use of the organoids as a replacement for organ transplantation in the future. Organs such as intestine and heart requires fully formed tissue architecture for proper function (e.g. tubular form) compared to pancreas or liver. Furthermore, such vascularized tissue will have to be reliably distributable to conFigureinto a human-on-a-chip organ-system model. Many discoveries and engineering efforts remain to achieve this full potential; however, the end result can drastically improve our capacity for drug discovery and screening. In closing, I demonstrated in this thesis the uses of pluripotent stem cell-derived tissue and cellular models for studying development and disease, and found versatility and complexity of the models to be promising.

## **Final conclusion and summary**

### **Relevance Chapter 1**

The objectives were met as follows:

- 1) Macrophage migration into intestine were recapitulated to engineer human intestinal organoids with resident macrophages (HIO/Mac).

- 2) These HIO/Mac were characterized with histology, single-cell transcriptomic, and functionally, which showed similarity between the HIO/Mac to the *in vivo* counterpart.
- 3) Organoids with or without macrophages were then compared with histology, single-cell transcriptomic, and functional assays which showed surprising effects of macrophages on metabolism and organ growth.

In conclusion, we engineered early intestinal tissue with macrophages from human pluripotent stem cells in order to model the effect the macrophages on intestinal development. Our results provide a novel insight into potential macrophage function in embryonic development where they regulate metabolism and tissue growth. In addition, due to the relative simplicity of the derivation method and reproducibility, we expect the model to facilitate the study of macrophage specifications and functions in development further.

### **Relevance: Chapter 2**

The objectives were met as follows:

- 1) Patient iPSC-derived human intestinal organoid with enteric nervous system (HIO/ENS) were derived and their motility was assessed with isometric force measurement.
- 2) The patient organoids displayed intestinal motility phenotype, showing lack of quiescent phase in their contractions. Thus, genetic hybrids of HIO and ENS from

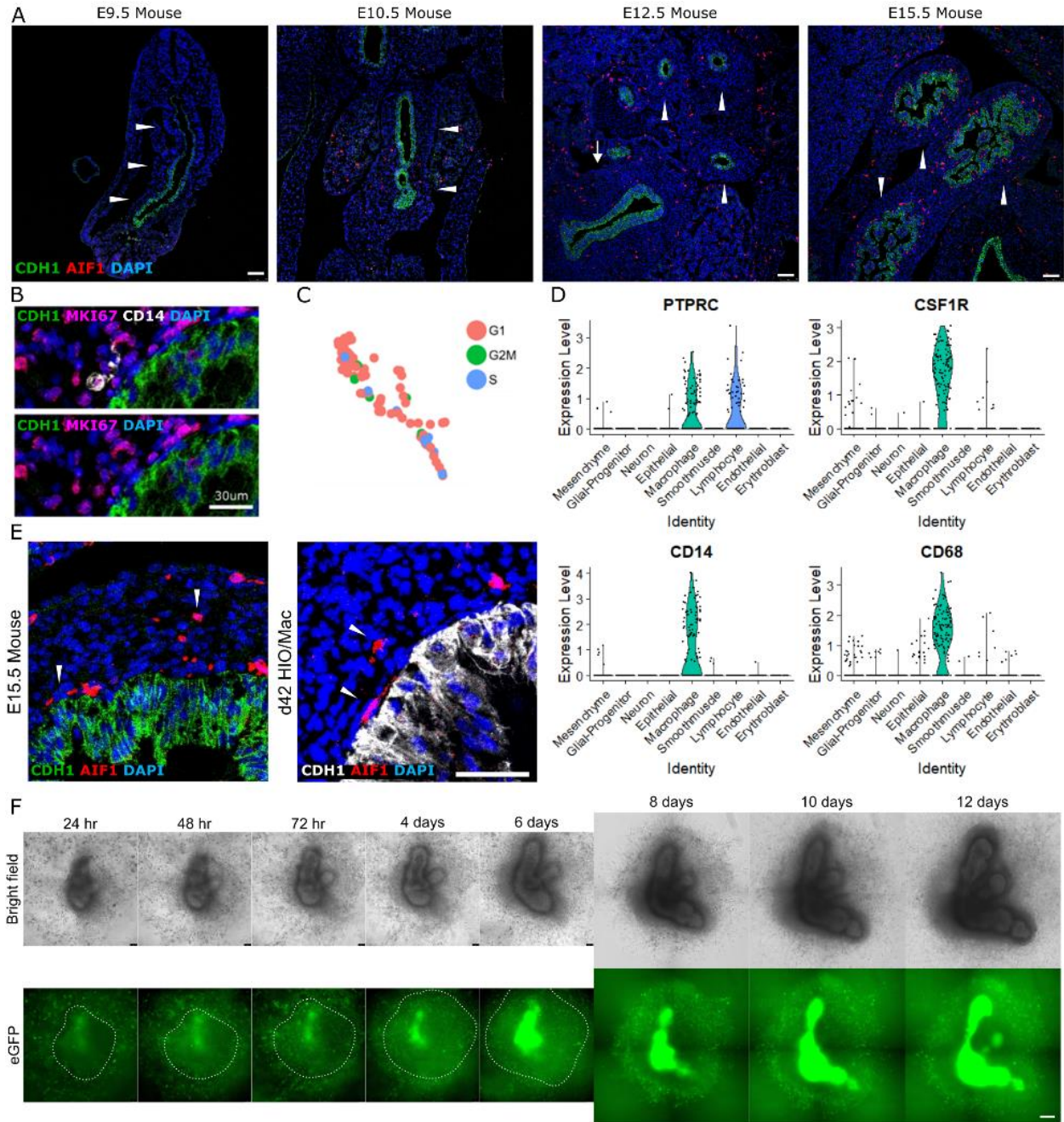
patient vs. control iPSC lines were derived. Similar erratic motility profile was observed when ENS (VNCC) were derived from patient iPSC lines.

- 3) Patient iPSC-derived neural crest cells were assessed against controls. RNA sequencing showed differential expression in neurodevelopmental genes.

We used patient iPSC-derived human intestinal organoids (HIO) and vagal neural crest cell (VNCC) and combined to engineer HIO with enteric nervous system (HIO/ENS) in order to study the pathomechanism of a heritable chronic intestinal pseudo-obstruction (CIPO). Isometric force measurement of the patient organoids showed erratic contractile pattern. Subsequent experiment with hybrid HIO/ENS, mixed derivation from patient or control iPSCs, indicated that VNCCs to be the driver of the erratic contractile pattern. Though we did not observe morphological or migratory disruption in patient VNCCs, RNA sequencing showed upregulation of *PLXNA3* expression, a gene involved in neuronal development. Additionally, patient iPSC also showed dysregulation in ectodermal-related genes *IKBKG* and *FZD2*. In conclusion, our patient-derived organoid and cellular model indicate neuropathological origin of intestinal dysfunction seen in CAID syndrome.

# Appendices

## Supplementary figures (Chapter 1)



**FigureS1. Macrophages in early embryonic mouse intestine, fetal intestine, and human intestinal organoid (HIO), related to Figure1 & 2 & 4.**

(A) Representative immunofluorescence images of mouse embryonic intestine for macrophages (AIF1), epithelium (CDH1), and nuclei (DAPI) at four time points of development. Arrowhead, mid-hindgut. Arrow, Foregut. E9.5, n=4, E10.5, n=6, E12.5, n=6, E15.5, n=6. Scale bar = 75 $\mu$ m.

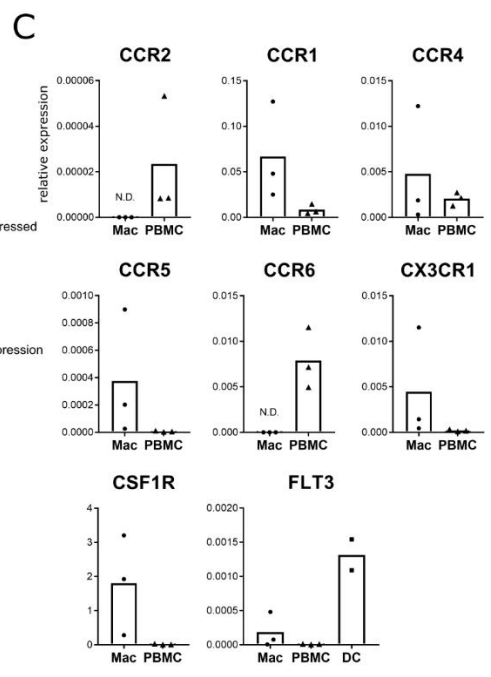
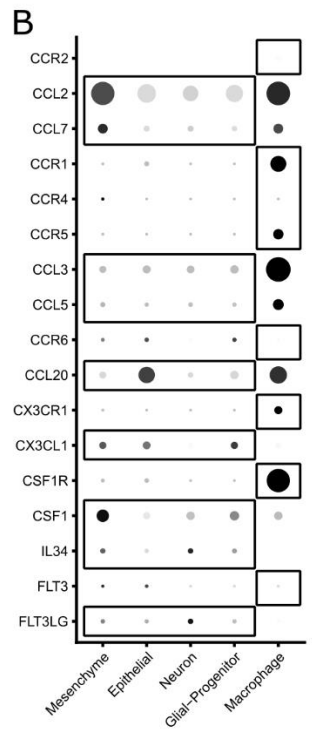
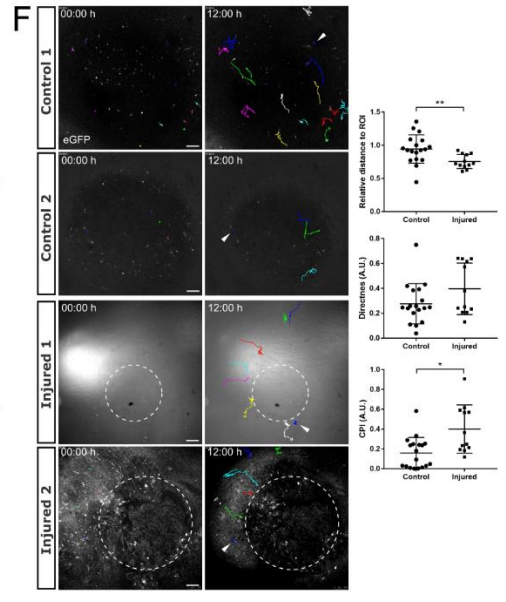
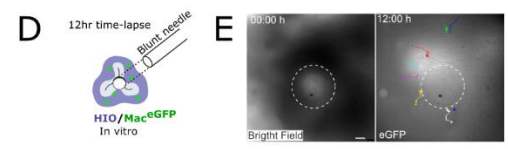
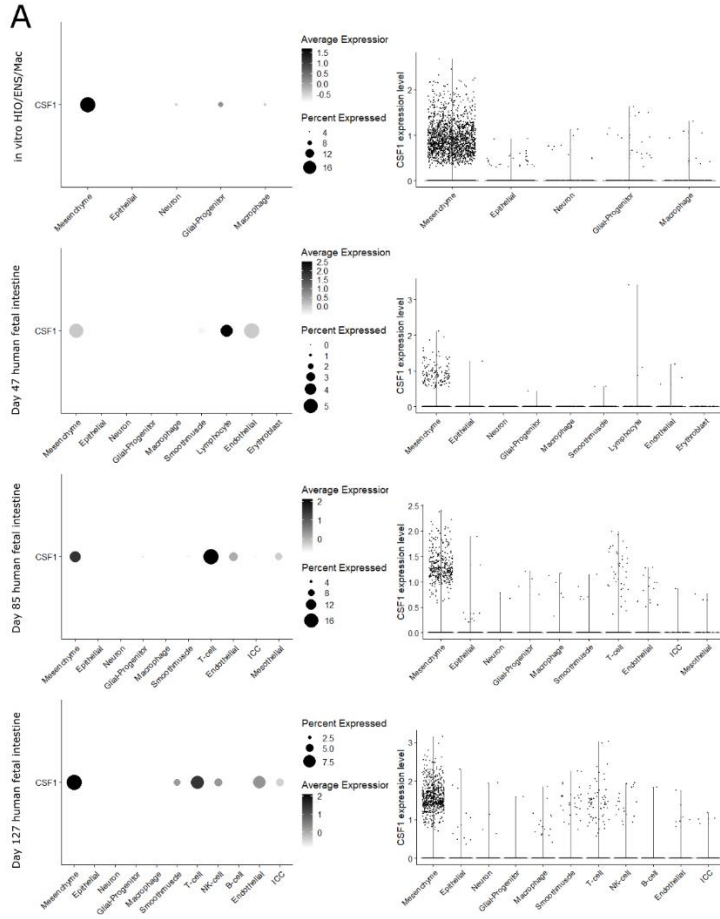
(B) Representative immunofluorescence image of day 42 HIO/Mac for epithelium (CDH1), proliferation (MKI67), macrophages (CD14), and nuclei (DAPI). Scale bar = 30 $\mu$ m

(C) Cell cycle status of macrophages in day 37 HIO/Mac from scRNAseq.

(D) Violin plot of gene markers used to identify the unsupervised cluster as macrophage in scRNAseq.

(E) Representative immunofluorescence images for macrophages (AIF1), epithelium (CDH1), and nuclei (DAPI) in E15.5 mouse intestine and day 42 HIO/Mac. Arrowhead, macrophages localized at adjacent to epithelium and within mesenchyme. Scale bar = 50 $\mu$ m

(F) Bright field and GFP fluorescence images of human intestinal organoid (HIO) and macrophage co-culture over the course of 12 days. Macrophages were derived from hiPSC<sup>eGFP</sup>. Scale bar = 150 $\mu$ m.



**FigureS2. Migration and retention of macrophages in the organoid, related to Figure1 & 2.**

**(A)** Dot plots and violin plots of *CSF1* expression in presumptively annotated unsupervised clusters of the day 37 organoid, day 47, day 85, day 127 fetal intestine datasets. Dot plots: Percent Expressed, percentage of cells within the cluster expressing the gene. Violin plot: Each dot represents a cell.

**(B)** Dot plot of ligand and receptor involved in macrophage recruitment in scRNAseq of HIO/ENS/Mac.

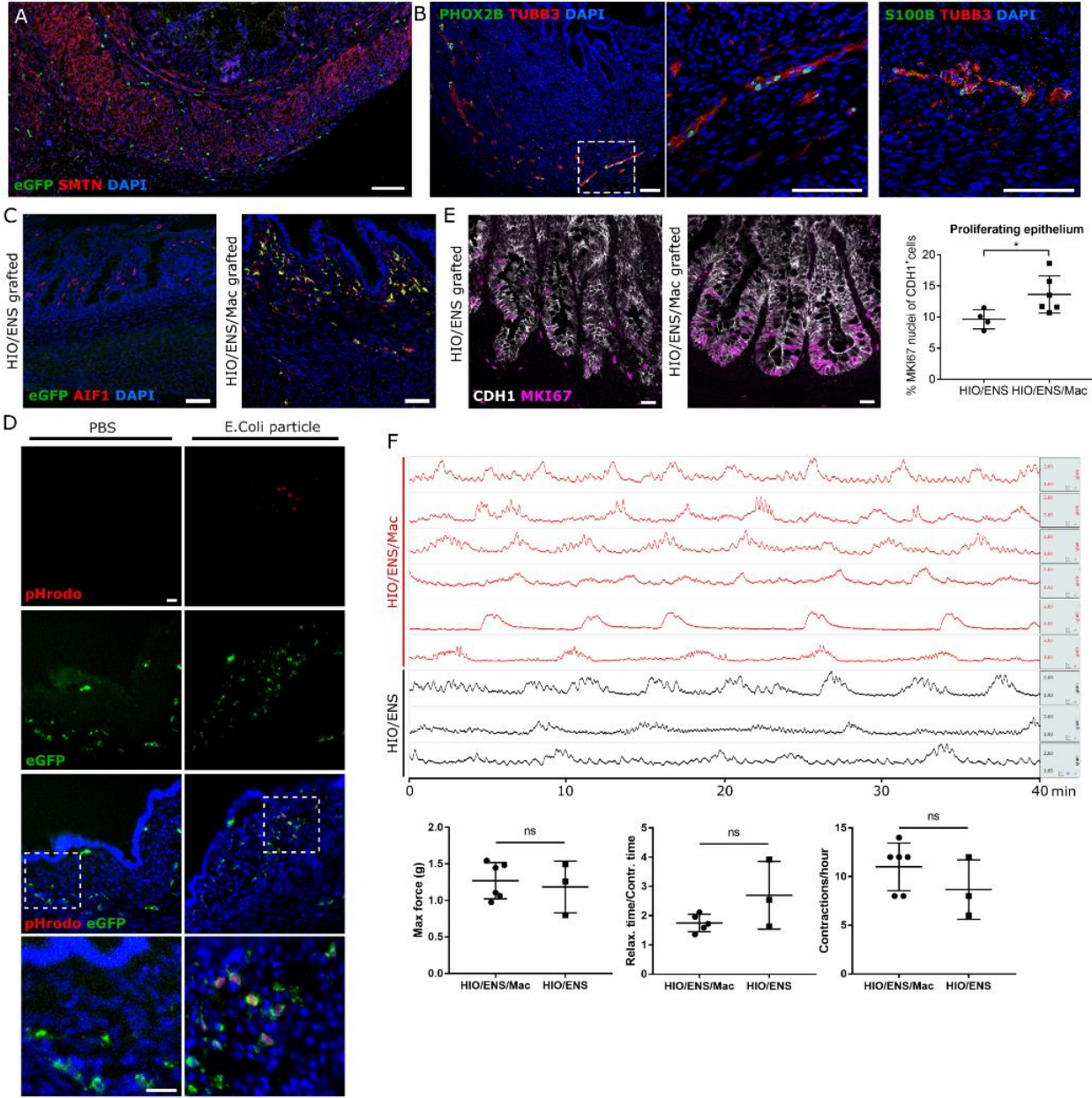
**(C)** qPCR of receptor genes for hiPSC-derived macrophages (Mac) prior to co-culture with HIO. Peripheral blood mononuclear cell (PBMC) and dendritic cell (DC) used as a reference previously shown to express the genes. Normalized to GAPDH expression. Mac, n = 3, PBMC, n = 3, DC, n = 2, biological replicates.

**(D)** Schematic of the *in vitro* organoid puncture injury.

**(E)** Demarcation of the injury as indicated by the bright field image and the corresponding hiPSC<sup>eGFP</sup>-derived macrophages (Mac<sup>eGFP</sup>) tracing.

**(F)** Representative GFP fluorescence images from the 12 hour time lapses of control and injured *in vitro* HIO/Mac<sup>eGFP</sup>. Colored lines and dots: tracing of the macrophage location over time. Dotted circle: region of the injury. Arrowhead: stationary points in the organoid to track the drifting of the entire sample. To the right: Quantification of relative distance of the macrophages, at 12 hours vs. 0 hour, from the center of the injury (Injured) or an arbitrary point within the image determined blinded (control). A measure of straightness of cell trajectories quantified as directness. Degree of directed migration

towards a region of interest quantified as chemotactic precision index (CPI). See Methods for calculation. Control, n = 2 organoids, n = 18 cells, Injury, n = 2 organoids, n = 12 cells, each data point represents a cell. Mean & s.d. (d-f). p = 0.0037, Welch's t-test (d). p = 0.2486 (e), p = 0.0116 (f), Wilcoxon rank sum test (Mann-Whitney). Scale bar=100 $\mu$ m.



**FigureS3. Characterization of grafted organoids, related to Figure3.**

(A) Representative immunofluorescence image of 10 week grafted HIO/ENS/Mac<sup>eGFP</sup> probed for macrophages (eGFP), smooth muscle (SMTN). Nuclei (DAPI). Scale bar=100 $\mu$ m.

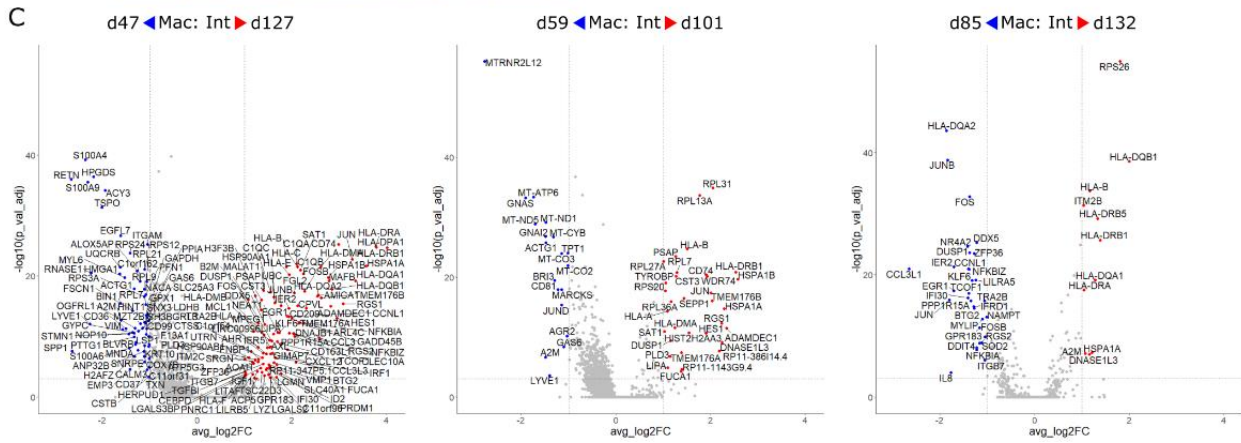
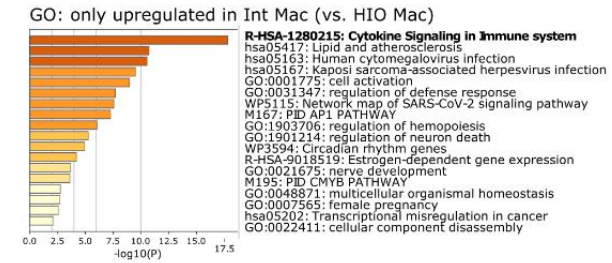
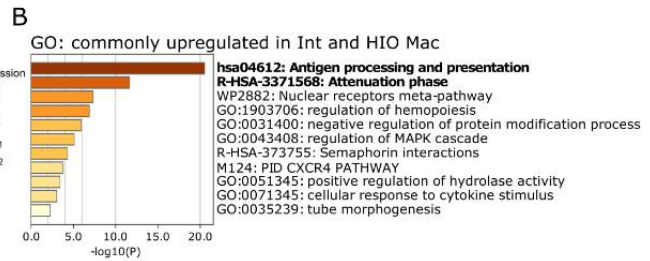
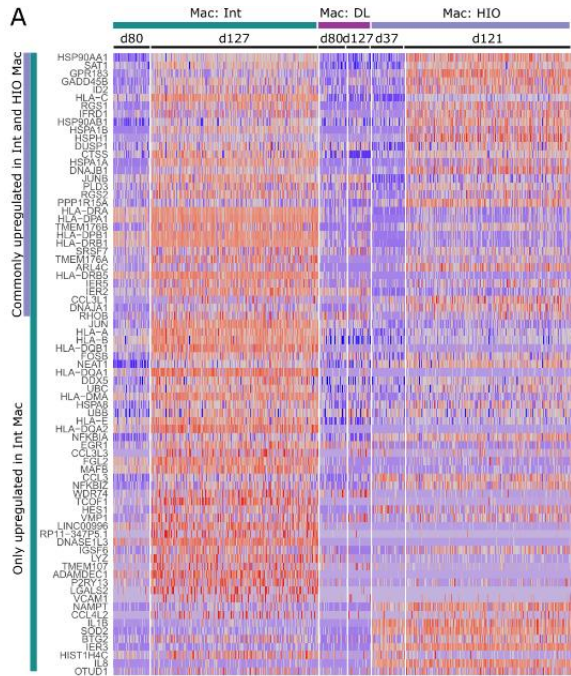
(B) Representative immunofluorescence image of enteric neurons (PHOX2B, TUBB3) and glial cells (S100B) in 10 week grafted HIO/ENS/Mac. Nuclei (DAPI). Scale bar=100 $\mu$ m.

(C) Representative immunofluorescence images of grafted organoids combined without (HIO/ENS) or with hiPSC<sup>eGFP</sup> derived macrophages (HIO/ENS/Mac<sup>eGFP</sup>). Probed for iPSC-derived macrophages (eGFP) and macrophages (AIF1). Scale bar=50 $\mu$ m.

(D) Tissue sections of grafted HIO/Mac<sup>eGFP</sup> injected with pHrodo-E.Coli particle conjugates or PBS (vehicle) into the lumen. Tissue sections counterstained with DAPI. Internalized E.Coli signals were only found in flat epithelial areas. n=3; PBS control, n=2 pHrodo-E.Coli particle. Scale bar=25 $\mu$ m.

(E) Immunofluorescence images of the crypt for proliferating (MKI67) epithelial cells (CDH1) and the quantification of MKI67-positive epithelial cells. HIO/ENS, n = 4, HIO/ENS/Mac, n = 6. p=0.0264. Welch's t-test. Mean & s.d. Scale bar=25 $\mu$ m.

(F) Isometric force measurements of grafted organoids with or without combined macrophages. Each row represents an individual grafted organoid sample. Quantification of maximal force recorded, ratio of time required for relaxation to contraction, and frequency of contraction. See Methods. HIO/ENS/Mac, n = 6, HIO/ENS, n = 3. p = 0.7303, p = 3252, p = 0.2904, Welch's t-test. Mean & s.d.

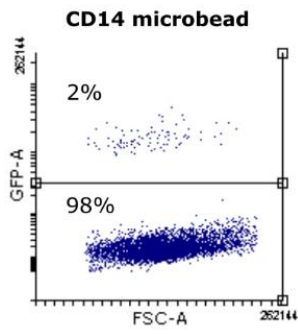
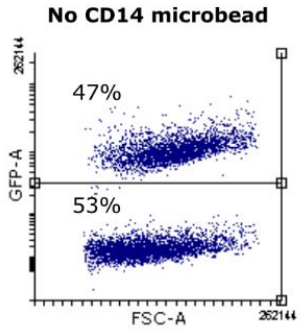
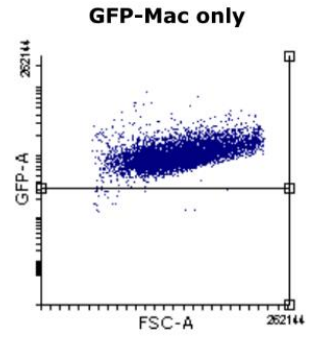
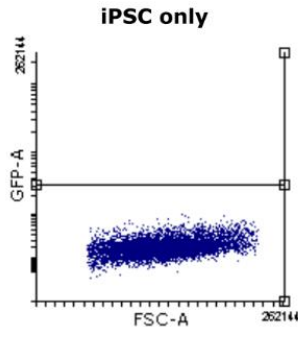
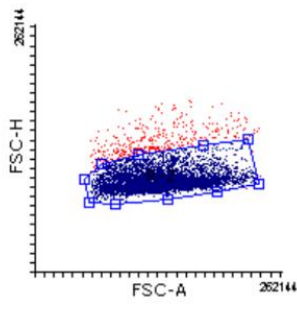
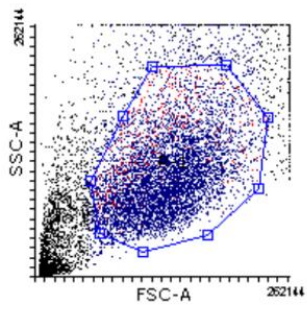


**FigureS4. scRNAseq analyses of fetal intestine and organoid macrophages, related to Figure4.**

(A) Heatmap of all 77 upregulated genes in fetal intestinal macrophages between day 127 and day 80.

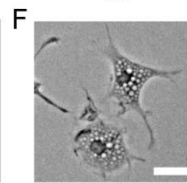
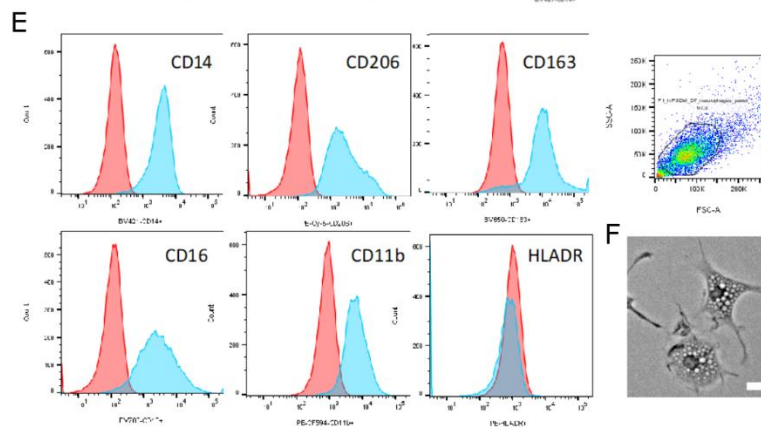
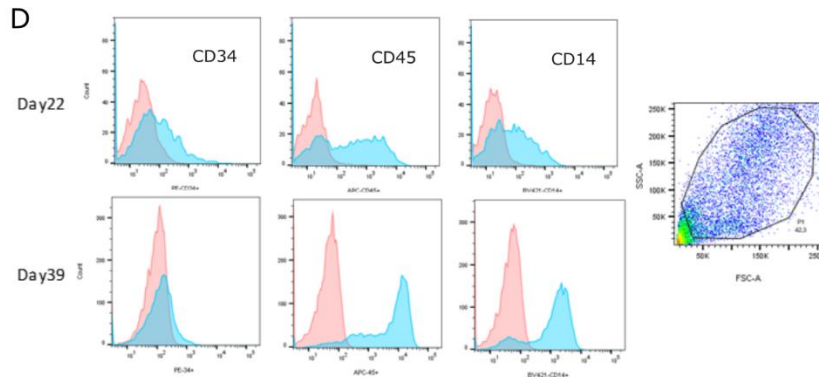
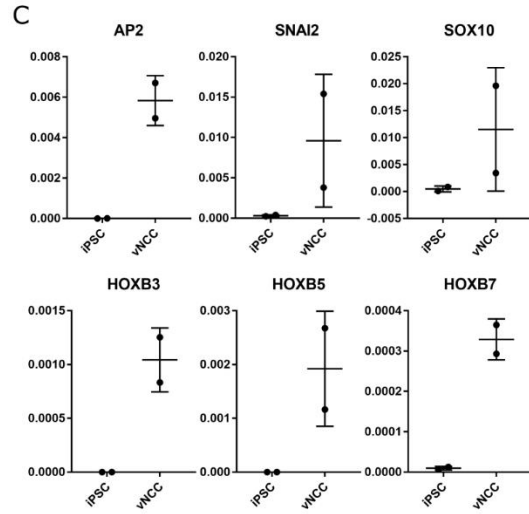
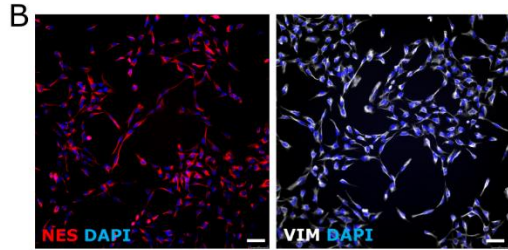
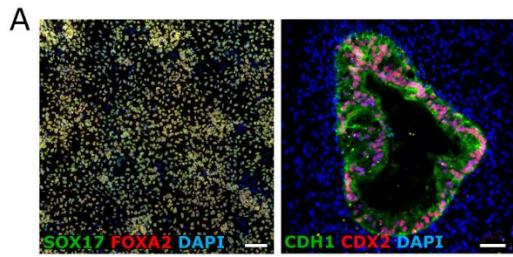
(B) Gene ontology annotations of differentially expressed genes from for commonly upregulated genes between fetal intestinal and organoid macrophages and upregulated only in fetal intestinal macrophages.

(C) Volcano plots of differentially expressed genes in fetal intestinal macrophages between day 127 vs. day 47, day 101 vs. day 59, day 132 vs. day 85. Threshold of discovery (dotted line),  $\log_2$ fold change > 1, adjusted p-value < 0.001, Wilcoxon rank sum test.



**FigureS5. Efficiency of macrophage removal using magnetic microbead, related to FigureMethods & Figure6.**

Efficiency of macrophage removal with microbead and ECAR baseline for the glycolytic stress. Left, gating for cytometry of 1:1 cell mix of hiPSC<sup>wt</sup> and hiPSC<sup>eGFP</sup>-derived macrophage. Right, percent GFP-positive cells with only hiPSC<sup>WT</sup> or only hiPSC<sup>eGFP</sup>-derived macrophage. Bottom, percent GFP-positive macrophages of the cell mix either without or with anti-CD14 microbead mediated macrophage removal.



**FigureS6. Characterization of hiPSC-derived human intestinal organoid, vagal neural crest, and macrophage, related to Methods.**

(A) Immunocytochemistry of markers for definitive endoderm (SOX17, FOXA2) and nucleus (DAPI) of endoderm monolayer during HIO derivation. Immunofluorescence of intestinal epithelial markers (CDH1, CDX2) in day 28 HIO. Scale bar=50 $\mu$ m.

(B) Immunocytochemistry for neural crest cell marker (NES, VIM) on the vagal neural crest cells. Scale bar=50 $\mu$ m.

(C) qPCR for genetic markers of neural crest (AP2, SNAI2, SOX10) and vagal fate (HOXB3, HOXB5, HOXB7) on the vagal neural crest cells. Normalized to GAPDH expression. hiPSC, n = 2, VNCC, n = 2. Biological replicates. Mean & s.d.

(D) Flow cytometry histograms showing staining (shaded blues) compared to the compensated unstained control (shaded red) for cell surface markers CD34, CD45 and CD14 on pre-macrophages released from adherent factory embryoid bodies (f-EB) harvested at day 22 and 39 since the beginning of the differentiation and the gating.

(E) Flow cytometry histograms showing cell surface markers CD14, CD206, CD163, CD16, CD11b and HLADR on macrophages differentiated from pre-macrophages and the gating.

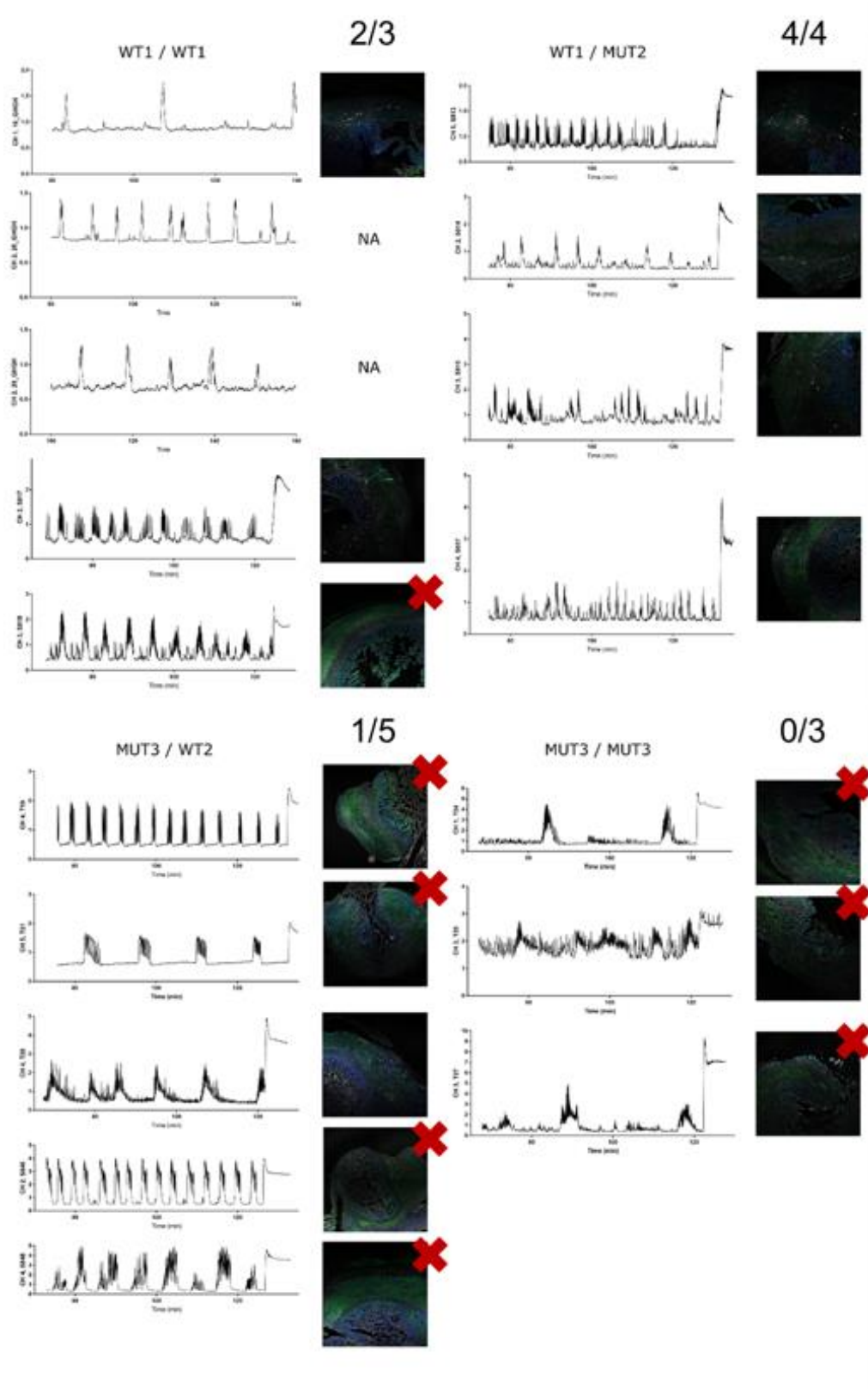
(F) Bright field image of the differentiated macrophages. Scale bar=25 $\mu$ m.

**Table S1. Oligonucleotides, related to Figure2, 7, and S6.**

<b>Species</b>	<b>Target gene</b>	<b>Direction</b>	<b>Primer sequence</b>
Human	<i>CCR2</i>	Forward	GGCATAGGGCAGTGAGAGTC
Human	<i>CCR2</i>	Reverse	TGTGAAAAGGCTTCTGAACTTCT
Human	<i>CCR1</i>	Forward	TCCCTTGGAACCAGAGAGAAG
Human	<i>CCR1</i>	Reverse	ACCAAGGAGTACAGAGGGGG
Human	<i>CCR4</i>	Forward	AAAGCAAGCTGCTTCTGGTTG
Human	<i>CCR4</i>	Reverse	CTCCCCAAATGCCTTGATGC
Human	<i>CCR5</i>	Forward	ATCCAGTGAGAAAAGCCCGT
Human	<i>CCR5</i>	Reverse	TTCCACCCGGGGAGAGTTT
Human	<i>CCR6</i>	Forward	AAGAGAGGGCCCACGTGTAT
Human	<i>CCR6</i>	Reverse	ATTGATTCCCGCTCATTGTG
Human	<i>CX3CR1</i>	Forward	TGGCCAAACACTGAGACCAA
Human	<i>CX3CR1</i>	Reverse	TGAAGGCCTCTAGTCGCTGT
Human	<i>CSF1R</i>	Forward	GTGGCTGTGAAGATGCTGAA
Human	<i>CSF1R</i>	Reverse	CCTTCCTTCGCAGAAAGTTG
Human	<i>FLT3</i>	Forward	CTCCAGGCGGCATCGC
Human	<i>FLT3</i>	Reverse	AAAACAACGAGCAGCGGCA
Human	<i>AP2</i>	Forward	ATGCTTTGGAAATTGACGGA
Human	<i>AP2</i>	Reverse	ATTGACCTACAGTGCCCAGC
Human	<i>SOX10</i>	Forward	AGCTCAGCAAGACGCTGG

Human	<i>SOX10</i>	Reverse	CTTTCTTGTGCTGCATACGG
Human	<i>SNAI2</i>	Forward	TGACCTGTCTGCAAATGCTC
Human	<i>SNAI2</i>	Reverse	CAGACCCTGGTTGCTTCAA
Human	<i>HOXB3</i>	Forward	CGTCATGAATGGGATCTGC
Human	<i>HOXB3</i>	Reverse	ATATTCACATCGAGCCCCAG
Human	<i>HOXB5</i>	Forward	GGAAGCTTCACATCAGCCAT
Human	<i>HOXB5</i>	Reverse	GGAACTCCTTTTCCAGCTCC
Human	<i>HOXB7</i>	Forward	AACTTCCGGATCTACCCCTG
Human	<i>HOXB7</i>	Reverse	CTTTCTCCAGCTCCAGGGTC
Human	<i>GAPDH</i>	Forward	GAAGGTGAAGGTCGGAGT
Human	<i>GAPDH</i>	Reverse	GAAGATGGTGATGGGATTC
Human	<i>ENO1</i>	Forward	TCTCTTCACCTCAAAGGTCTCT
Human	<i>ENO1</i>	Reverse	TGTGGGTTCTAAGGCTTACCC
Human	<i>TPI1</i>	Forward	GGAATCGGAGTAATCGCCTG
Human	<i>TPI1</i>	Reverse	GTAATTCCTGGGCCTGTTGG
Human	<i>LDHA</i>	Forward	CTGGCAAAGTGGATATCTTGAC
Human	<i>LDHA</i>	Reverse	ACTCCATACAGGCACACTGG
Human	<i>PGK1</i>	Forward	TTGACCGAATCACCGACCTC
Human	<i>PGK1</i>	Reverse	AGCAGCCTTAATCCTCTGGTT
Human	<i>HPRT1</i>	Forward	CCTGGCGTCGTGATTAGTGA
Human	<i>HPRT1</i>	Reverse	CGAGCAAGACGTTTCAGTCCT

Supplementary figures (Chapter 2)



**Supplementary Figure1. Some organoids lack enteric neurons and erratic contractile pattern does not correlate. Related to Figure2 and 3.**

Representative isometric force measurement (IFM) tracings of 10-week grafted HIO/ENS with mixed genotypic origin and corresponding immunofluorescence image for enteric neuronal markers (PHOX2B-Green, TUBB3-Red, ELAVL4-Gray). Ratio indicates number of samples with enteric neurons over the total number of samples. WT = control iPSC line, MUT = patient iPSC line. WT1 = SJ3252c2, WT2 = WTC3, MUT2 = SJ2550c2, MUT3 = SJ2391c2. See Methods. Each row represents an IFM tracing of a single organoid. WT1/WT1: n=6, WT1/MUT2: n=4, MUT3/WT2: n=5, MUT3/MUT3: n=3.

## Bibliography

1. Chetaille, P., Preuss, C., Burkhard, S., Côté, J.-M., Houde, C., Castilloux, J., Piché, J., Gosset, N., Leclerc, S., Wünnemann, F., et al. (2014). Mutations in SGOL1 cause a novel cohesinopathy affecting heart and gut rhythm. *Nat. Genet.* *46*, 1245–1249. 10.1038/ng.3113.
2. Mowat, A.M., and Agace, W.W. (2014). Regional specialization within the intestinal immune system. *Nat. Rev. Immunol.* 2014 1410 *14*, 667–685. 10.1038/nri3738.
3. Smythies, L.E., Sellers, M., Clements, R.H., Mosteller-Barnum, M., Meng, G., Benjamin, W.H., Orenstein, J.M., and Smith, P.D. (2005). Human intestinal macrophages display profound inflammatory anergy despite avid phagocytic and bacteriocidal activity. *J. Clin. Invest.* *115*, 66–75. 10.1172/JCI200519229.
4. Spencer, N.J., and Hu, H. (2020). Enteric nervous system: sensory transduction, neural circuits and gastrointestinal motility. *Nat. Rev. Gastroenterol. Hepatol.*, 1–14. 10.1038/s41575-020-0271-2.
5. Rao, M., and Gershon, M.D. (2018). Enteric nervous system development: what could possibly go wrong? *Nat. Rev. Neurosci.* 2018 199 *19*, 552–565. 10.1038/s41583-018-0041-0.
6. Zorn, A.M., and Wells, J.M. (2009). Vertebrate Endoderm Development and Organ Formation. *Annu. Rev. Cell Dev. Biol.* *25*, 221. 10.1146/ANNUREV.CELLBIO.042308.113344.
7. Spence, J.R., Lauf, R., and Shroyer, N.F. (2011). Vertebrate intestinal endoderm

- development. *Dev. Dyn.* 240, 501–520. 10.1002/dvdy.22540.
8. Shyer, A.E., Tallinen, T., Nerurkar, N.L., Wei, Z., Gil, E.S., Kaplan, D.L., Tabin, C.J., and Mahadevan, † L Villification: How the Gut Gets Its Villi.
  9. Gomez Perdiguero, E., Klapproth, K., Schulz, C., Busch, K., Azzoni, E., Crozet, L., Garner, H., Trouillet, C., de Bruijn, M.F., Geissmann, F., et al. (2015). Tissue-resident macrophages originate from yolk-sac-derived erythro-myeloid progenitors. *Nature* 518, 547–551. 10.1038/nature13989.
  10. Hoeffel, G., and Ginhoux, F. (2018). Fetal monocytes and the origins of tissue-resident macrophages. *Cell. Immunol.* 330, 5–15. 10.1016/j.cellimm.2018.01.001.
  11. Davies, L.C., Jenkins, S.J., Allen, J.E., and Taylor, P.R. (2013). Tissue-resident macrophages. *Nat. Immunol.* 14, 986–995. 10.1038/ni.2705.
  12. Hulsmans, M., Clauss, S., Xiao, L., Aguirre, A.D., King, K.R., Hanley, A., Hucker, W.J., Wülfers, E.M., Seemann, G., Courties, G., et al. (2017). Macrophages Facilitate Electrical Conduction in the Heart. *Cell* 169, 510-522.e20. 10.1016/j.cell.2017.03.050.
  13. Hulsmans, M., Sager, H.B., Roh, J.D., Valero-Muñoz, M., Houstis, N.E., Iwamoto, Y., Sun, Y., Wilson, R.M., Wojtkiewicz, G., Tricot, B., et al. (2018). Cardiac macrophages promote diastolic dysfunction. *J. Exp. Med.*, jem.20171274. 10.1084/jem.20171274.
  14. Takahashi, N., Udagawa, N., Tanaka, S., Murakami, H., Owan, I., Tamura, T., and Suda, T. (1994). Postmitotic Osteoclast Precursors Are Mononuclear Cells

- Which Express Macrophage-Associated Phenotypes. *Dev. Biol.* **163**, 212–221.  
10.1006/DBIO.1994.1137.
15. Wu, Y., and Hirschi, K.K. (2021). Tissue-Resident Macrophage Development and Function. *Front. Cell Dev. Biol.* **8**, 617879. 10.3389/FCELL.2020.617879/BIBTEX.
  16. Odegaard, J.I., Ricardo-Gonzalez, R.R., Goforth, M.H., Morel, C.R., Subramanian, V., Mukundan, L., Red Eagle, A., Vats, D., Brombacher, F., Ferrante, A.W., et al. (2007). Macrophage-specific PPARgamma controls alternative activation and improves insulin resistance. *Nature* **447**, 1116–1120.  
10.1038/nature05894.
  17. Nguyen, K.D., Qiu, Y., Cui, X., Goh, Y.P.S., Mwangi, J., David, T., Mukundan, L., Brombacher, F., Locksley, R.M., and Chawla, A. (2011). Alternatively activated macrophages produce catecholamines to sustain adaptive thermogenesis. *Nature* **480**, 104–108. 10.1038/nature10653.
  18. Lee, C.Z.W., and Ginhoux, F. (2022). Biology of resident tissue macrophages. *Development* **149**. 10.1242/dev.200270.
  19. Krzyszczyk, P., Schloss, R., Palmer, A., and Berthiaume, F. (2018). The Role of Macrophages in Acute and Chronic Wound Healing and Interventions to Promote Pro-wound Healing Phenotypes. *Front. Physiol.* **9**, 1–22.  
10.3389/fphys.2018.00419.
  20. Godwin, J.W., Pinto, A.R., and Rosenthal, N.A. (2013). Macrophages are required for adult salamander limb regeneration. *Proc. Natl. Acad. Sci.* **110**, 9415–9420.  
10.1073/pnas.1300290110.

21. Wynn, T.A., and Vannella, K.M. (2016). Macrophages in Tissue Repair, Regeneration, and Fibrosis. *Immunity* 44, 450–462.  
10.1016/j.immuni.2016.02.015.
22. Hopkinson-Woolley, J., Hughes, D., Gordon, S., and Martin, P. (1994). Macrophage recruitment during limb development and wound healing in the embryonic and foetal mouse. *J. Cell Sci.* 107, 1159–1167.  
10.1242/jcs.107.5.1159.
23. Bain, C.C., Bravo-Blas, A., Scott, C.L., Perdiguero, E.G., Geissmann, F., Henri, S., Malissen, B., Osborne, L.C., Artis, D., and Mowat, A.M. (2014). Constant replenishment from circulating monocytes maintains the macrophage pool in the intestine of adult mice. *Nat. Immunol.* 15, 929–937. 10.1038/ni.2967.
24. Szymczak, W.A., and George S. Deepe, J. (2009). The CCL7-CCL2-CCR2 Axis Regulates IL-4 Production in Lungs and Fungal Immunity. *J. Immunol.* 183, 1964.  
10.4049/JIMMUNOL.0901316.
25. Kim, J.Y., Kim, J., Huang, M., Kosonen, R., and Lee, J.E. (2022). CCR4 and CCR5 Involvement in Monocyte-Derived Macrophage Migration in Neuroinflammation. *Front. Immunol.* 13. 10.3389/FIMMU.2022.876033.
26. Furuichi, K., Gao, J.-L., Horuk, R., Wada, T., Kaneko, S., and Murphy, P.M. (2008). Chemokine Receptor CCR1 Regulates Inflammatory Cell Infiltration after Renal Ischemia-Reperfusion Injury. *J. Immunol.* 181, 8670.  
10.4049/JIMMUNOL.181.12.8670.
27. Mass, E., Ballesteros, I., Farlik, M., Halbritter, F., Günther, P., Crozet, L., Jacome-

- Galarza, C.E., Händler, K., Klughammer, J., Kobayashi, Y., et al. (2016). Specification of tissue-resident macrophages during organogenesis. *Science* (80-). *353*, aaf4238–aaf4238. 10.1126/science.aaf4238.
28. McDermott, D.H., Fong, A.M., Yang, Q., Sechler, J.M., Cupples, L.A., Merrell, M.N., Wilson, P.W.F., D’Agostino, R.B., O’Donnell, C.J., Patel, D.D., et al. (2003). Chemokine receptor mutant CX3CR1-M280 has impaired adhesive function and correlates with protection from cardiovascular disease in humans. *J. Clin. Invest.* *111*, 1241–1250. 10.1172/JCI16790.
29. Combadière, C., Potteaux, S., Gao, J.L., Esposito, B., Casanova, S., Lee, E.J., Debré, P., Tedgui, A., Murphy, P.M., and Mallat, Z. (2003). Decreased atherosclerotic lesion formation in CX3CR1/apolipoprotein E double knockout mice. *Circulation* *107*, 1009–1016. 10.1161/01.CIR.0000057548.68243.42.
30. Rojo, R., Raper, A., Ozdemir, D.D., Lefevre, L., Grabert, K., Wollscheid-Lengeling, E., Bradford, B., Caruso, M., Gazova, I., Sánchez, A., et al. (2019). Deletion of a *Csf1r* enhancer selectively impacts CSF1R expression and development of tissue macrophage populations. *Nat. Commun.* *10*. 10.1038/s41467-019-11053-8.
31. Keshvari, S., Caruso, M., Teakle, N., Batoon, L., Sehgal, A., Patkar, O.L., Ferrari-Cestari, M., Snell, C.E., Chen, C., Stevenson, A., et al. (2021). CSF1R-dependent macrophages control postnatal somatic growth and organ maturation. *PLOS Genet.* *17*, e1009605. 10.1371/journal.pgen.1009605.
32. Pierce, J.H., Di Marco, E., Cox, G.W., Lombardi, D., Ruggiero, M., Varesio, L.,

- Wang, L.M., Choudhury, G.G., Sakaguchi, A.Y., and Di Fiore, P.P. (1990). Macrophage-colony-stimulating factor (CSF-1) induces proliferation, chemotaxis, and reversible monocytic differentiation in myeloid progenitor cells transfected with the human c-fms/CSF-1 receptor cDNA. *Proc. Natl. Acad. Sci.* *87*, 5613–5617. [10.1073/pnas.87.15.5613](https://doi.org/10.1073/pnas.87.15.5613).
33. Uhlén, M., Fagerberg, L., Hallström, B.M., Lindskog, C., Oksvold, P., Mardinoglu, A., Sivertsson, Å., Kampf, C., Sjöstedt, E., Asplund, A., et al. (2015). Tissue-based map of the human proteome. *Science* (80-. ). *347*. [10.1126/SCIENCE.1260419/SUPPL\\_FILE/1260419\\_UHLEN.SM.PDF](https://doi.org/10.1126/SCIENCE.1260419/SUPPL_FILE/1260419_UHLEN.SM.PDF).
34. Munro, D.A., Wineberg, Y., Tarnick, J., Vink, C.S., Li, Z., Pridans, C., Dzierzak, E., Kalisky, T., Hohenstein, P., and Davies, J.A. (2019). Macrophages restrict the nephrogenic field and promote endothelial connections during kidney development. *Elife* *8*, 1–27. [10.7554/eLife.43271](https://doi.org/10.7554/eLife.43271).
35. De Schepper, S., Verheijden, S., Aguilera-Lizarraga, J., Viola, M.F., Boesmans, W., Stakenborg, N., Voytyuk, I., Smidt, I., Boeckx, B., Dierckx de Casterlé, I., et al. (2018). Self-Maintaining Gut Macrophages Are Essential for Intestinal Homeostasis. *Cell*, 1–16. [10.1016/j.cell.2018.07.048](https://doi.org/10.1016/j.cell.2018.07.048).
36. Avetisyan, M., Rood, J.E., Huerta Lopez, S., Sengupta, R., Wright-Jin, E., Dougherty, J.D., Behrens, E.M., and Heuckeroth, R.O. (2018). Muscularis macrophage development in the absence of an enteric nervous system. *Proc. Natl. Acad. Sci.* *115*, 4696–4701. [10.1073/pnas.1802490115](https://doi.org/10.1073/pnas.1802490115).
37. Niess, J.H., Brand, S., Gu, X., Landsman, L., Jung, S., McCormick, B.A., Vyas,

- J.M., Boes, M., Ploegh, H.L., Fox, J.G., et al. (2005). CX3CR1-Mediated Dendritic Cell Access to the Intestinal Lumen and Bacterial Clearance. *Science* (80-. ). *307*, 254–258. 10.1126/science.1102901.
38. Wang, J., Gusti, V., Saraswati, A., and Lo, D.D. (2011). Convergent and Divergent Development among M Cell Lineages in Mouse Mucosal Epithelium. *J. Immunol.* *187*, 5277–5285. 10.4049/jimmunol.1102077.
39. Lelouard, H., Fallet, M., de Bovis, B., Méresse, S., and Gorvel, J. (2012). Peyer's Patch Dendritic Cells Sample Antigens by Extending Dendrites Through M Cell-Specific Transcellular Pores. *Gastroenterology* *142*, 592-601.e3. 10.1053/j.gastro.2011.11.039.
40. Cosín-Roger, J., Ortiz-Masiá, D., Calatayud, S., Hernández, C., Esplugues, J. V., and Barrachina, M.D. (2016). The activation of Wnt signaling by a STAT6-dependent macrophage phenotype promotes mucosal repair in murine IBD. *Mucosal Immunol.* *9*, 986–998. 10.1038/mi.2015.123.
41. Sehgal, A., Donaldson, D.S., Pridans, C., Sauter, K.A., Hume, D.A., and Mabbott, N.A. (2018). The role of CSF1R-dependent macrophages in control of the intestinal stem-cell niche. *Nat. Commun.* *9*, 1272. 10.1038/s41467-018-03638-6.
42. Pull, S.L., Doherty, J.M., Mills, J.C., Gordon, J.I., and Stappenbeck, T.S. (2005). Activated macrophages are an adaptive element of the colonic epithelial progenitor niche necessary for regenerative responses to injury. *Proc. Natl. Acad. Sci.* *102*, 99–104. 10.1073/pnas.0405979102.
43. Gabanyi, I., Muller, P.A., Feighery, L., Oliveira, T.Y., Costa-Pinto, F.A., and

- Mucida, D. (2016). Neuro-immune Interactions Drive Tissue Programming in Intestinal Macrophages. *Cell* 164, 378–391. 10.1016/j.cell.2015.12.023.
44. Muller, P.A., Koscsó, B., Rajani, G.M., Stevanovic, K., Berres, M.-L., Hashimoto, D., Mortha, A., Leboeuf, M., Li, X.-M., Mucida, D., et al. (2014). Crosstalk between muscularis macrophages and enteric neurons regulates gastrointestinal motility. *Cell* 158, 300–313. 10.1016/j.cell.2014.04.050.
45. Luo, J., Qian, A., Oetjen, L.K., Yu, W., Yang, P., Feng, J., Xie, Z., Liu, S., Yin, S., Dryn, D., et al. (2018). TRPV4 Channel Signaling in Macrophages Promotes Gastrointestinal Motility via Direct Effects on Smooth Muscle Cells. *Immunity* 49, 107-119.e4. 10.1016/j.immuni.2018.04.021.
46. Sauter, K.A., Pridans, C., Sehgal, A., Tsai, Y.T., Bradford, B.M., Raza, S., Moffat, L., Gow, D.J., Beard, P.M., Mabbott, N.A., et al. (2014). Pleiotropic effects of extended blockade of CSF1R signaling in adult mice. *J. Leukoc. Biol.* 96, 265–274. 10.1189/jlb.2A0114-006R.
47. Rae, F., Woods, K., Sasmono, T., Campanale, N., Taylor, D., Ovchinnikov, D.A., Grimmond, S.M., Hume, D.A., Ricardo, S.D., and Little, M.H. (2007). Characterisation and trophic functions of murine embryonic macrophages based upon the use of a Csf1r-EGFP transgene reporter. *Dev. Biol.* 308, 232–246. 10.1016/j.ydbio.2007.05.027.
48. Alikhan, M.A., Jones, C. V., Williams, T.M., Beckhouse, A.G., Fletcher, A.L., Kett, M.M., Sakkal, S., Samuel, C.S., Ramsay, R.G., Deane, J.A., et al. (2011). Colony-stimulating factor-1 promotes kidney growth and repair via alteration of

- macrophage responses. *Am. J. Pathol.* *179*, 1243–1256.  
10.1016/J.AJPATH.2011.05.037.
49. Leid, J., Carrelha, J., Boukarabila, H., Epelman, S., Jacobsen, S.E.W., and Lavine, K.J. (2016). Primitive Embryonic Macrophages are Required for Coronary Development and Maturation. *Circ. Res.* *118*, 1498–1511.  
10.1161/CIRCRESAHA.115.308270.
50. Cahill, T.J., Sun, X., Ravaud, C., Villa del Campo, C., Klaourakis, K., Lupu, I.-E., Lord, A.M., Browne, C., Jacobsen, S.E.W., Greaves, D.R., et al. (2021). Tissue-resident macrophages regulate lymphatic vessel growth and patterning in the developing heart. *Development* *148*. 10.1242/dev.194563.
51. Van Nguyen, A., and Pollard, J.W. (2002). Colony Stimulating Factor-1 Is Required to Recruit Macrophages into the Mammary Gland to Facilitate Mammary Ductal Outgrowth. *Dev. Biol.* *247*, 11–25. 10.1006/dbio.2002.0669.
52. Diez-Roux, G., Argilla, M., Makarenkova, H., Ko, K., and Lang, R.A. (1999). Macrophages kill capillary cells in G1 phase of the cell cycle during programmed vascular regression. *Development* *126*, 2141–2147. 10.1242/dev.126.10.2141.
53. Dawson, C.A., Pal, B., Vaillant, F., Gandolfo, L.C., Liu, Z., Bleriot, C., Ginhoux, F., Smyth, G.K., Lindeman, G.J., Mueller, S.N., et al. (2020). Tissue-resident ductal macrophages survey the mammary epithelium and facilitate tissue remodelling. *Nat. Cell Biol.* *22*, 546–558. 10.1038/s41556-020-0505-0.
54. Erblich, B., Zhu, L., Etgen, A.M., Dobrenis, K., and Pollard, J.W. (2011). Absence of Colony Stimulation Factor-1 Receptor Results in Loss of Microglia, Disrupted

- Brain Development and Olfactory Deficits. *PLoS One* 6, e26317.  
10.1371/journal.pone.0026317.
55. Paolicelli, R.C., Bolasco, G., Pagani, F., Maggi, L., Scianni, M., Panzanelli, P., Giustetto, M., Ferreira, T.A., Guiducci, E., Dumas, L., et al. (2011). Synaptic pruning by microglia is necessary for normal brain development. *Science* (80-. ). 333, 1456–1458. 10.1126/science.1202529.
  56. Michel, K., Kuch, B., Dengler, S., Demir, I.E., Zeller, F., and Schemann, M. (2022). How big is the little brain in the gut? Neuronal numbers in the enteric nervous system of mice, Guinea pig, and human. *Neurogastroenterol. Motil.* 34. 10.1111/nmo.14440.
  57. Viola, M.F., Chavero-Pierres, M., Modave, E., Delfini, M., Stakenborg, N., Estévez, M.C., Fabre, N., Appeltans, I., Martens, T., Vandereyken, K., et al. (2023). Dedicated macrophages organize and maintain the enteric nervous system. *Nat.* 2023 10, 1–9. 10.1038/s41586-023-06200-7.
  58. Patsouris, D., Li, P.-P., Thapar, D., Chapman, J., Olefsky, J.M., and Neels, J.G. (2008). Ablation of CD11c-Positive Cells Normalizes Insulin Sensitivity in Obese Insulin Resistant Animals. *Cell Metab.* 8, 301–309. 10.1016/j.cmet.2008.08.015.
  59. Dey, G., Radhakrishnan, A., Syed, N., Thomas, J.K., Nadig, A., Srikumar, K., Mathur, P.P., Pandey, A., Lin, S.-K., Raju, R., et al. (2013). Signaling network of Oncostatin M pathway. *J. Cell Commun. Signal.* 7, 103–108. 10.1007/s12079-012-0186-y.
  60. Komori, T., Tanaka, M., Senba, E., Miyajima, A., and Morikawa, Y. (2013). Lack

- of oncostatin M receptor  $\beta$  leads to adipose tissue inflammation and insulin resistance by switching macrophage phenotype. *J. Biol. Chem.* **288**, 21861–21875. 10.1074/JBC.M113.461905.
61. Komori, T., Tanaka, M., Senba, E., Miyajima, A., and Morikawa, Y. (2014). Deficiency of oncostatin M receptor  $\beta$  (OSMR $\beta$ ) exacerbates high-fat diet-induced obesity and related metabolic disorders in mice. *J. Biol. Chem.* **289**, 13821–13837. 10.1074/JBC.M113.542399.
62. Elks, C.M., Zha, P., Grant, R.W., Hang, H., Bailey, J.L., Burk, D.H., McNulty, M.A., Mynatt, R.L., and Stephens, J.M. (2016). Loss of Oncostatin M Signaling in Adipocytes Induces Insulin Resistance and Adipose Tissue Inflammation in Vivo. *J. Biol. Chem.* **291**, 17066–17076. 10.1074/JBC.M116.739110.
63. Piquer-Garcia, I., Campderros, L., Taxeràs, S.D., Gavaldà-Navarro, A., Pardo, R., Vila, M., Pellitero, S., Martínez, E., Tarascó, J., Moreno, P., et al. (2020). A Role for Oncostatin M in the Impairment of Glucose Homeostasis in Obesity. *J. Clin. Endocrinol. Metab.* **105**, e337–e348. 10.1210/clinem/dgz090.
64. Zhang, Y., Yu, G., Chu, H., Wang, X., Xiong, L., Cai, G., Liu, R., Gao, H., Tao, B., Li, W., et al. (2018). Macrophage-Associated PGK1 Phosphorylation Promotes Aerobic Glycolysis and Tumorigenesis. *Mol. Cell* **71**, 201-215.e7. 10.1016/j.molcel.2018.06.023.
65. Jung, S., Aliberti, J., Graemmel, P., Sunshine, M.J., Kreutzberg, G.W., Sher, A., and Littman, D.R. (2000). Analysis of fractalkine receptor CX(3)CR1 function by targeted deletion and green fluorescent protein reporter gene insertion. *Mol. Cell.*

- Biol. 20, 4106–4114. 10.1128/MCB.20.11.4106-4114.2000.
66. Burnett, S.H., Kershen, E.J., Zhang, J., Zeng, L., Straley, S.C., Kaplan, A.M., and Cohen, D.A. (2004). Conditional macrophage ablation in transgenic mice expressing a Fas-based suicide gene. *J. Leukoc. Biol.* 75, 612–623. 10.1189/JLB.0903442.
  67. Saito, M., Iwawaki, T., Taya, C., Yonekawa, H., Noda, M., Inui, Y., Mekada, E., Kimata, Y., Tsuru, A., and Kohno, K. (2001). Diphtheria toxin receptor–mediated conditional and targeted cell ablation in transgenic mice. *Nat. Biotechnol.* 2001 19, 746–750. 10.1038/90795.
  68. Hua, L., Shi, J., Shultz, L.D., and Ren, G. (2018). Genetic Models of Macrophage Depletion. In *Methods in Molecular Biology* (Humana Press Inc.), pp. 243–258. 10.1007/978-1-4939-7837-3\_22.
  69. Mendoza-Coronel, E., and Castañón-Arreola, M. (2016). Comparative evaluation of in vitro human macrophage models for mycobacterial infection study. *Pathog. Dis.* 74. 10.1093/FEMSPD/FTW052.
  70. Sato, T., Vries, R.G., Snippert, H.J., Van De Wetering, M., Barker, N., Stange, D.E., Van Es, J.H., Abo, A., Kujala, P., Peters, P.J., et al. (2009). Single Lgr5 stem cells build crypt-villus structures in vitro without a mesenchymal niche. *Nature.* 10.1038/nature07935.
  71. Takahashi, Y., Sato, S., Kurashima, Y., Yamamoto, T., Kurokawa, S., Yuki, Y., Takemura, N., Uematsu, S., Lai, C.Y., Otsu, M., et al. (2018). A Refined Culture System for Human Induced Pluripotent Stem Cell-Derived Intestinal Epithelial

- Organoids. *Stem cell reports* 10, 314–328. 10.1016/J.STEMCR.2017.11.004.
72. Spence, J.R., Mayhew, C.N., Rankin, S.A., Kuhar, M.F., Vallance, J.E., Tolle, K., Hoskins, E.E., Kalinichenko, V. V., Wells, S.I., Zorn, A.M., et al. (2011). Directed differentiation of human pluripotent stem cells into intestinal tissue in vitro. *Nature* 470, 105–109. 10.1038/nature09691.
73. McCracken, K.W., Howell, J.C., Wells, J.M., and Spence, J.R. (2011). Generating human intestinal tissue from pluripotent stem cells in vitro. *Nat. Protoc.* 6, 1920–1928. 10.1038/nprot.2011.410.
74. Watson, C.L., Mahe, M.M., Múnera, J., Howell, J.C., Sundaram, N., Poling, H.M., Schweitzer, J.I., Vallance, J.E., Mayhew, C.N., Sun, Y., et al. (2014). An in vivo model of human small intestine using pluripotent stem cells. *Nat. Med.* 20, 1310–1314. 10.1038/nm.3737.
75. Workman, M.J., Mahe, M.M., Trisno, S., Poling, H.M., Watson, C.L., Sundaram, N., Chang, C.-F., Schiesser, J., Aubert, P., Stanley, E.G., et al. (2016). Engineered human pluripotent-stem-cell-derived intestinal tissues with a functional enteric nervous system. *Nat. Med.* 10.1038/nm.4233.
76. Tsuruta, S., Kawasaki, T., Machida, M., Iwatsuki, K., Inaba, A., Shibata, S., Shindo, T., Nakabayashi, K., Hakamada, K., Umezawa, A., et al. (2022). Development of Human Gut Organoids With Resident Tissue Macrophages as a Model of Intestinal Immune Responses. *Cell. Mol. Gastroenterol. Hepatol.* 14, 726-729.e5. 10.1016/j.jcmgh.2022.06.006.
77. Wilgenburg, B. van, Browne, C., Vowles, J., and Cowley, S.A. (2013). Efficient,

- Long Term Production of Monocyte-Derived Macrophages from Human Pluripotent Stem Cells under Partly-Defined and Fully-Defined Conditions. *PLoS One* 8, e71098. 10.1371/journal.pone.0071098.
78. Buchrieser, J., James, W., and Moore, M.D. (2017). Human Induced Pluripotent Stem Cell-Derived Macrophages Share Ontogeny with MYB-Independent Tissue-Resident Macrophages. *Stem Cell Reports* 8, 334–345. 10.1016/j.stemcr.2016.12.020.
79. Di Nardo, G., Di Lorenzo, C., Lauro, A., Stanghellini, V., Thapar, N., Karunaratne, T.B., Volta, U., and De Giorgio, R. (2017). Chronic intestinal pseudo-obstruction in children and adults: diagnosis and therapeutic options. *Neurogastroenterol. Motil.* 29, e12945. 10.1111/nmo.12945.
80. Matera, I., Rusmini, M., Guo, Y., Lerone, M., Li, J., Zhang, J., Di Duca, M., Nozza, P., Mosconi, M., Prato, A.P., et al. (2016). Variants of the ACTG2 gene correlate with degree of severity and presence of megacystis in chronic intestinal pseudo-obstruction. *Eur. J. Hum. Genet.* 2016 248 24, 1211–1215. 10.1038/ejhg.2015.275.
81. Pingault, V., Zerad, L., Bertani-Torres, W., and Bondurand, N. (2022). SOX10: 20 years of phenotypic plurality and current understanding of its developmental function. *J. Med. Genet.* 59, 105–114. 10.1136/JMEDGENET-2021-108105.
82. Mohr, L., Buheitel, J., Schöckel, L., Karalus, D., Mayer, B., and Stemmann, O. (2015). An Alternatively Spliced Bifunctional Localization Signal Reprograms Human Shugoshin 1 to Protect Centrosomal Instead of Centromeric Cohesin. *Cell*

- Rep. 12, 2156–2168. 10.1016/j.celrep.2015.08.045.
83. Salic, A., Waters, J.C., and Mitchison, T.J. (2004). Vertebrate shugoshin links sister centromere cohesion and kinetochore microtubule stability in mitosis. *Cell* 118, 567–578. 10.1016/j.cell.2004.08.016.
84. Wang, X., Yang, Y., Duan, Q., Jiang, N., Huang, Y., Darzynkiewicz, Z., and Dai, W. (2008). sSgo1, a major splice variant of Sgo1, functions in centriole cohesion where it is regulated by Plk1. *Dev. Cell* 14, 331–341. 10.1016/j.devcel.2007.12.007.
85. Piché, J., Gosset, N., Legault, L.-M., Pacis, A., Oneglia, A., Caron, M., Chetaille, P., Barreiro, L., Liu, D., Qi, X., et al. (2019). Molecular Signature of CAID Syndrome: Noncanonical Roles of SGO1 in Regulation of TGF- $\beta$  Signaling and Epigenomics. *Cell. Mol. Gastroenterol. Hepatol.* 7, 411–431. 10.1016/j.jcmgh.2018.10.011.
86. Hansen, A.S., Pustova, I., Cattoglio, C., Tjian, R., and Darzacq, X. (2017). CTCF and cohesin regulate chromatin loop stability with distinct dynamics. *Elife* 6. 10.7554/ELIFE.25776.001.
87. Calderon, L., Weiss, F.D., Beagan, J.A., Oliveira, M.S., Georgieva, R., Wang, Y.F., Carroll, T., Dharmalingam, G., Gong, W., Tossell, K., et al. (2022). Cohesin-dependence of neuronal gene expression relates to chromatin loop length. *Elife* 11, 76539. 10.7554/eLife.76539.
88. Bonora, E., Bianco, F., Cordeddu, L., Bamshad, M., Francescatto, L., Dowless, D., Stanghellini, V., Cogliandro, R.F., Lindberg, G., Mungan, Z., et al. (2015).

- Mutations in RAD21 Disrupt Regulation of APOB in Patients With Chronic Intestinal Pseudo-Obstruction. *Gastroenterology* 148, 771-782.e11. 10.1053/j.gastro.2014.12.034.
89. Bianco, F., Eisenman, S.T., Colmenares Aguilar, M.G., Bonora, E., Clavenzani, P., Linden, D.R., De Giorgio, R., Farrugia, G., and Gibbons, S.J. (2018). Expression of RAD21 immunoreactivity in myenteric neurons of the human and mouse small intestine. *Neurogastroenterol. Motil.* 30, e13429. 10.1111/nmo.13429.
90. Deardorff, M.A., Wilde, J.J., Albrecht, M., Dickinson, E., Tennstedt, S., Braunholz, D., Mönnich, M., Yan, Y., Xu, W., Gil-Rodríguez, M.C., et al. (2012). RAD21 mutations cause a human cohesinopathy. *Am. J. Hum. Genet.* 10.1016/j.ajhg.2012.04.019.
91. Song, A.T., Galli, A., Leclerc, S., Nattel, S., Mandato, C., and Andelfinger, G. (2017). Characterization of Sgo1 expression in developing and adult mouse. *Gene Expr. Patterns* 25–26, 36–45. 10.1016/j.gep.2017.04.004.
92. R. B. Anderson, D. F. Newgreen, and HM Young Neural Crest and the Development of the Enteric Nervous System. *Madame Curie Biosci. Database.* <https://www.ncbi.nlm.nih.gov/books/NBK6273/>.
93. Furness, J.B. (2012). The enteric nervous system and neurogastroenterology. *Nat. Rev. Gastroenterol. Hepatol.* 9, 286–294. 10.1038/nrgastro.2012.32.
94. García-Castro, M.I., Marcelle, C., and Bronner-Fraser, M. (2002). Ectodermal Wnt function as a neural crest inducer. *Science* 297, 848–851.

10.1126/SCIENCE.1070824.

95. Roy-Carson, S., Natukunda, K., Chou, H. chao, Pal, N., Farris, C., Schneider, S.Q., and Kuhlman, J.A. (2017). Defining the transcriptomic landscape of the developing enteric nervous system and its cellular environment. *BMC Genomics* 18. 10.1186/S12864-017-3653-2.
96. Oleari, R., Caramello, A., Campinoti, S., Lettieri, A., Ioannou, E., Paganoni, A., Fantin, A., Cariboni, A., and Ruhrberg, C. (2019). PLXNA1 and PLXNA3 cooperate to pattern the nasal axons that guide gonadotropin-releasing hormone neurons. *Dev.* 146. 10.1242/DEV.176461/223144.
97. Kotan, L.D., Ternier, G., Cakir, A.D., Emeksiz, H.C., Turan, I., Delpouve, G., Kardelen, A.D., Ozcabi, B., Isik, E., Mengen, E., et al. (2021). Loss-of-function variants in SEMA3F and PLXNA3 encoding semaphorin-3F and its receptor plexin-A3 respectively cause idiopathic hypogonadotropic hypogonadism. *Genet. Med.* 23, 1008–1016. 10.1038/S41436-020-01087-5.
98. Savidge, T.C., Newman, P., Pothoulakis, C., Ruhl, A., Neunlist, M., Bourreille, A., Hurst, R., and Sofroniew, M. V. (2007). Enteric Glia Regulate Intestinal Barrier Function and Inflammation Via Release of S-Nitrosoglutathione. *Gastroenterology* 132, 1344–1358. 10.1053/j.gastro.2007.01.051.
99. Kirchgessner, A.L., Tamir, H., and Gershon, M.D. (1992). Identification and stimulation by serotonin of intrinsic sensory neurons of the submucosal plexus of the guinea pig gut: activity-induced expression of Fos immunoreactivity. *J. Neurosci.* 12, 235–248. 10.1523/JNEUROSCI.12-01-00235.1992.

100. Kunze, W.A.A., Furness, J.B., Bertrand, P.P., and Bornstein, J.C. (1998). Intracellular recording from myenteric neurons of the guinea-pig ileum that respond to stretch. *J. Physiol.* 506 ( Pt 3), 827–842. 10.1111/J.1469-7793.1998.827BV.X.
101. Sanders, K.M., Ward, S.M., and Koh, S.D. (2014). Interstitial Cells: Regulators of Smooth Muscle Function. *Physiol. Rev.* 94, 859–907. 10.1152/physrev.00037.2013.
102. Chang, I., Glasgow, N.J., Takayama, I., Horiguchi, K., Sanders, K.M., and Ward, S.M. (2001). Loss of interstitial cells of Cajal and development of electrical dysfunction in murine small bowel obstruction. *J. Physiol.* 536, 555–568. 10.1111/j.1469-7793.2001.0555c.xd.
103. Bajpai, R., Chen, D.A., Rada-Iglesias, A., Zhang, J., Xiong, Y., Helms, J., Chang, C.-P., Zhao, Y., Swigut, T., and Wysocka, J. (2010). CHD7 cooperates with PBAF to control multipotent neural crest formation. *Nature* 463, 958–962. 10.1038/nature08733.
104. Stremmel, C., Schuchert, R., Wagner, F., Thaler, R., Weinberger, T., Pick, R., Mass, E., Ishikawa-Ankerhold, H.C., Margraf, A., Hutter, S., et al. (2018). Yolk sac macrophage progenitors traffic to the embryo during defined stages of development. *Nat. Commun.* 9. 10.1038/s41467-017-02492-2.
105. Kaufmann, M. (1994). *The Atlas of Mouse Development Revised*. (Elsevier Ltd).
106. Holloway, E.M., Czerwinski, M., Tsai, Y.-H., Wu, J.H., Wu, A., Childs, C.J., Walton, K.D., Sweet, C.W., Yu, Q., Glass, I., et al. (2021). Mapping Development

- of the Human Intestinal Niche at Single-Cell Resolution. *Cell Stem Cell* 28, 568-580.e4. 10.1016/j.stem.2020.11.008.
107. Holloway, E.M., Wu, J.H., Czerwinski, M., Sweet, C.W., Wu, A., Tsai, Y.H., Huang, S., Stoddard, A.E., Capeling, M.M., Glass, I., et al. (2020). Differentiation of Human Intestinal Organoids with Endogenous Vascular Endothelial Cells. *Dev. Cell* 54, 516-528.e7. 10.1016/j.devcel.2020.07.023.
108. Menke, J., Rabacal, W.A., Byrne, K.T., Iwata, Y., Schwartz, M.M., Stanley, E.R., Schwarting, A., and Kelley, V.R. (2009). Circulating CSF-1 Promotes Monocyte and Macrophage Phenotypes that Enhance Lupus Nephritis. *J. Am. Soc. Nephrol.* 20, 2581–2592. 10.1681/ASN.2009050499.
109. Jones, C. V, and Ricardo, S.D. (2013). Macrophages and CSF-1. *Organogenesis* 9, 249–260. 10.4161/org.25676.
110. Saha, S., Aranda, E., Hayakawa, Y., Bhanja, P., Atay, S., Brodin, N.P., Li, J., Asfaha, S., Liu, L., Tailor, Y., et al. (2016). Macrophage-derived extracellular vesicle-packaged WNTs rescue intestinal stem cells and enhance survival after radiation injury. *Nat. Commun.* 7, 13096. 10.1038/ncomms13096.
111. Beck, F., Eler, T., Russell, A., and James, R. (1995). Expression of Cdx-2 in the mouse embryo and placenta: Possible role in patterning of the extra-embryonic membranes. *Dev. Dyn.* 204, 219–227. 10.1002/aja.1002040302.
112. Serreze, D. V., Gaedeke, J.W., and Leiter, E.H. (1993). Hematopoietic stem-cell defects underlying abnormal macrophage development and maturation in NOD/Lt mice: defective regulation of cytokine receptors and protein kinase C. *Proc. Natl.*

- Acad. Sci. 90, 9625–9629. 10.1073/pnas.90.20.9625.
113. Serreze, D. V, Gaskins, H.R., and Leiter, E.H. (1993). Defects in the differentiation and function of antigen presenting cells in NOD/Lt mice. *J. Immunol.* 150, 2534–2543.
  114. Shultz, L.D., Schweitzer, P.A., Christianson, S.W., Gott, B., Schweitzer, I.B., Tennent, B., McKenna, S., Mobraaten, L., Rajan, T. V, and Greiner, D.L. (1995). Multiple defects in innate and adaptive immunologic function in NOD/LtSz-scid mice. *J. Immunol.* 154, 180–191.
  115. SHIBATA, ASANO, NOGUCHI, NAITO, OGURA, and DOI (1998). Peritoneal macrophages play an important role in eliminating human cells from severe combined immunodeficient mice transplanted with human peripheral blood lymphocytes. *Immunology* 93, 524–532. 10.1046/j.1365-2567.1998.00458.x.
  116. Hu, Z., Van Rooijen, N., and Yang, Y.-G. (2011). Macrophages prevent human red blood cell reconstitution in immunodeficient mice. *Blood* 118, 5938–5946. 10.1182/blood-2010-11-321414.
  117. Takata, K., Kozaki, T., Lee, C.Z.W., Thion, M.S., Otsuka, M., Lim, S., Utami, K.H., Fidan, K., Park, D.S., Malleret, B., et al. (2017). Induced-Pluripotent-Stem-Cell-Derived Primitive Macrophages Provide a Platform for Modeling Tissue-Resident Macrophage Differentiation and Function. *Immunity* 47, 183-198.e6. 10.1016/j.immuni.2017.06.017.
  118. Miller, A.J., Yu, Q., Czerwinski, M., Tsai, Y.-H., Conway, R.F., Wu, A., Holloway, E.M., Walker, T., Glass, I.A., Treutlein, B., et al. (2020). In Vitro and In Vivo

- Development of the Human Airway at Single-Cell Resolution. *Dev. Cell* 53, 117-128.e6. 10.1016/j.devcel.2020.01.033.
119. Triantafilou, K., Triantafilou, M., and Dedrick, R.L. (2001). A CD14-independent LPS receptor cluster. *Nat. Immunol.* 2, 338–345. 10.1038/86342.
120. Binder, R.J., and Srivastava, P.K. (2005). Peptides chaperoned by heat-shock proteins are a necessary and sufficient source of antigen in the cross-priming of CD8+ T cells. *Nat. Immunol.* 6, 593–599. 10.1038/ni1201.
121. Srivastava, P. (2002). Roles of heat-shock proteins in innate and adaptive immunity. *Nat. Rev. Immunol.* 2, 185–194. 10.1038/nri749.
122. Cai, Y., Winn, M.E., Zehmer, J.K., Gillette, W.K., Lubkowski, J.T., Pilon, A.L., and Kimura, S. (2014). Preclinical evaluation of human secretoglobin 3A2 in mouse models of lung development and fibrosis. *Am. J. Physiol. Cell. Mol. Physiol.* 306, L10–L22. 10.1152/ajplung.00037.2013.
123. Dirami, G., Massaro, G.D., Clerch, L.B., Ryan, U.S., Reczek, P.R., and Massaro, D. (2004). Lung retinol storing cells synthesize and secrete retinoic acid, an inducer of alveolus formation. *Am. J. Physiol. Cell. Mol. Physiol.* 286, L249–L256. 10.1152/ajplung.00140.2003.
124. Krasny, L., Bland, P., Kogata, N., Wai, P., Howard, B.A., Natrajan, R.C., and Huang, P.H. (2018). SWATH mass spectrometry as a tool for quantitative profiling of the matrisome. *J. Proteomics* 189, 11–22. 10.1016/j.jprot.2018.02.026.
125. Brock, S.E., Rendon, B.E., Yaddanapudi, K., and Mitchell, R.A. (2012). Negative

- Regulation of AMP-activated Protein Kinase (AMPK) Activity by Macrophage Migration Inhibitory Factor (MIF) Family Members in Non-small Cell Lung Carcinomas. *J. Biol. Chem.* 287, 37917–37925. 10.1074/jbc.M112.378299.
126. Miller, E.J., Li, J., Leng, L., McDonald, C., Atsumi, T., Bucala, R., and Young, L.H. (2008). Macrophage migration inhibitory factor stimulates AMP-activated protein kinase in the ischaemic heart. *Nature* 451, 578–582. 10.1038/nature06504.
127. Maaser, C., Eckmann, L., Paesold, G., Kim, H.S., and Kagnoff, M.F. (2002). Ubiquitous production of macrophage migration inhibitory factor by human gastric and intestinal epithelium. *Gastroenterology* 122, 667–680. 10.1053/gast.2002.31891.
128. Wang, W., Xiao, Z.D., Li, X., Aziz, K.E., Gan, B., Johnson, R.L., and Chen, J. (2015). AMPK modulates Hippo pathway activity to regulate energy homeostasis. *Nat. Cell Biol.* 2014 174 17, 490–499. 10.1038/NCB3113.
129. Kowalczyk, W., Romanelli, L., Atkins, M., Hillen, H., Bravo González-Blas, C., Jacobs, J., Xie, J., Soheily, S., Verboven, E., Moya, I.M., et al. (2022). Hippo signaling instructs ectopic but not normal organ growth. *Science* (80-. ). 378. 10.1126/science.abg3679.
130. Chen, D., Sun, Y., Wei, Y., Zhang, P., Rezaeian, A.H., Teruya-Feldstein, J., Gupta, S., Liang, H., Lin, H.-K., Hung, M.-C., et al. (2012). LIFR is a breast cancer metastasis suppressor upstream of the Hippo-YAP pathway and a prognostic marker. *Nat. Med.* 18, 1511–1517. 10.1038/nm.2940.
131. Liu, D., Song, A.T., Qi, X., van Vliet, P.P., Xiao, J., Xiong, F., Andelfinger, G., and

- Nattel, S. (2021). Cohesin-protein Shugoshin-1 controls cardiac automaticity via HCN4 pacemaker channel. *Nat. Commun.* 12. 10.1038/s41467-021-22737-5.
132. Roberts, B., Haupt, A., Tucker, A., Grancharova, T., Arakaki, J., Fuqua, M.A., Nelson, A., Hookway, C., Ludmann, S.A., Mueller, I.A., et al. (2017). Systematic gene tagging using CRISPR/Cas9 in human stem cells to illuminate cell organization. *Mol. Biol. Cell* 28, 2854–2874. 10.1091/mbc.e17-03-0209.
133. Múnera, J.O., Sundaram, N., Rankin, S.A., Hill, D., Watson, C., Mahe, M., Vallance, J.E., Shroyer, N.F., Sinagoga, K.L., Zarzoso-Lacoste, A., et al. (2017). Differentiation of Human Pluripotent Stem Cells into Colonic Organoids via Transient Activation of BMP Signaling. *Cell Stem Cell* 21, 51-64.e6. 10.1016/j.stem.2017.05.020.
134. Díaz-Rodríguez, Y., Cordeiro, P., Belounis, A., Herblot, S., and Duval, M. (2017). In vitro differentiated plasmacytoid dendritic cells as a tool to induce anti-leukemia activity of natural killer cells. *Cancer Immunol. Immunother.* 66, 1307–1320. 10.1007/s00262-017-2022-y.
135. Rink, I., Rink, J., Helmer, D., Sachs, D., and Schmitz, K. (2015). A Haptotaxis Assay for Leukocytes Based on Surface-Bound Chemokine Gradients. *J. Immunol.* 194, 5549–5558. 10.4049/jimmunol.1500148.
136. Young, M.D., and Behjati, S. (2020). SoupX removes ambient RNA contamination from droplet-based single-cell RNA sequencing data. *Gigascience* 9. 10.1093/gigascience/giaa151.
137. Hao, Y., Hao, S., Andersen-Nissen, E., Mauck, W.M., Zheng, S., Butler, A., Lee,

- M.J., Wilk, A.J., Darby, C., Zager, M., et al. (2021). Integrated analysis of multimodal single-cell data. *Cell* 184, 3573-3587.e29. 10.1016/j.cell.2021.04.048.
138. Wickham, H. (2016). *ggplot2: Elegant Graphics for Data Analysis*.
139. Zhou, Y., Zhou, B., Pache, L., Chang, M., Khodabakhshi, A.H., Tanaseichuk, O., Benner, C., and Chanda, S.K. (2019). Metascape provides a biologist-oriented resource for the analysis of systems-level datasets. *Nat. Commun.* 10, 1523. 10.1038/s41467-019-09234-6.
140. Szklarczyk, D., Gable, A.L., Nastou, K.C., Lyon, D., Kirsch, R., Pyysalo, S., Doncheva, N.T., Legeay, M., Fang, T., Bork, P., et al. (2021). The STRING database in 2021: customizable protein–protein networks, and functional characterization of user-uploaded gene/measurement sets. *Nucleic Acids Res.* 49, D605–D612. 10.1093/nar/gkaa1074.
141. Berlin, A.L., Paller, A.S., and Chan, L.S. (2002). Incontinentia pigmenti: A review and update on the molecular basis of pathophysiology. *J. Am. Acad. Dermatol.* 47, 169–190. 10.1067/MJD.2002.125949.
142. Smahl, A., Courtols, G., Vabres, P., Yamaoka, S., Heuertz, S., Munnich, A., Israël, A., Helss, N.S., Klauck, S.M., Kloschls, P., et al. (2000). Genomic rearrangement in NEMO impairs NF-kappaB activation and is a cause of incontinentia pigmenti. The International Incontinentia Pigmenti (IP) Consortium. *Nature* 405, 466–472. 10.1038/35013114.
143. Döffinger, R., Smahi, A., Bessia, C., Geissmann, F., Feinberg, J., Durandy, A., Bodemer, C., Kenwrick, S., Dupuis-Girod, S., Blanche, S., et al. (2001). X-linked

- anhidrotic ectodermal dysplasia with immunodeficiency is caused by impaired NF-kappaB signaling. *Nat. Genet.* 27, 277–285. 10.1038/85837.
144. Saal, H.M., Prows, C.A., Guerreiro, I., Donlin, M., Knudson, L., Sund, K.L., Chang, C.F., Brugmann, S.A., and Stottmann, R.W. (2015). A mutation in FRIZZLED2 impairs Wnt signaling and causes autosomal dominant omodysplasia. *Hum. Mol. Genet.* 24, 3399–3409. 10.1093/HMG/DDV088.
145. White, J.J., Mazzeu, J.F., Coban-Akdemir, Z., Bayram, Y., Bahrambeigi, V., Hoischen, A., van Bon, B.W.M., Gezdirici, A., Gulec, E.Y., Ramond, F., et al. (2018). WNT Signaling Perturbations Underlie the Genetic Heterogeneity of Robinow Syndrome. *Am. J. Hum. Genet.* 102, 27–43. 10.1016/J.AJHG.2017.10.002.
146. Lawrence Zipursky, S., and Grueber, W.B. (2013). The Molecular Basis of Self-Avoidance. <https://doi.org/10.1146/annurev-neuro-062111-150414> 36, 547–568. 10.1146/ANNUREV-NEURO-062111-150414.
147. Jenkins, S.J., Knipper, J.A., and Zaiss, D.M.W. (2020). Local proliferation of monocytes. *J. Leukoc. Biol.* 107, 547–549. 10.1002/JLB.1CE0220-534RR.
148. Mrouj, K., Andrés-Sánchez, N., Dubra, G., Singh, P., Sobacki, M., Chahar, D., Al Ghoul, E., Aznar, A.B., Prieto, S., Pirot, N., et al. (2021). Ki-67 regulates global gene expression and promotes sequential stages of carcinogenesis. *Proc. Natl. Acad. Sci.* 118, 1–12. 10.1073/pnas.2026507118.
149. Miller, I., Min, M., Yang, C., Tian, C., Gookin, S., Carter, D., and Spencer, S.L. (2018). Ki67 is a Graded Rather than a Binary Marker of Proliferation versus

- Quiescence. *Cell Rep.* 24, 1105. 10.1016/J.CELREP.2018.06.110.
150. Cao, J., O'Day, D.R., Pliner, H.A., Kingsley, P.D., Deng, M., Daza, R.M., Zager, M.A., Aldinger, K.A., Blecher-Gonen, R., Zhang, F., et al. (2020). A human cell atlas of fetal gene expression. *Science* (80-. ). 370. 10.1126/science.aba7721.
151. Eicher, A.K., Kechele, D.O., Sundaram, N., Berns, H.M., Poling, H.M., Haines, L.E., Sanchez, J.G., Kishimoto, K., Krishnamurthy, M., Han, L., et al. (2021). Functional human gastrointestinal organoids can be engineered from three primary germ layers derived separately from pluripotent stem cells. *Cell Stem Cell.* 10.1016/j.stem.2021.10.010.
152. Vitale, I., Manic, G., Coussens, L.M., Kroemer, G., and Galluzzi, L. (2019). Macrophages and Metabolism in the Tumor Microenvironment. *Cell Metab.* 30, 36–50. 10.1016/j.cmet.2019.06.001.
153. Yin, M., Zhang, Y., Yu, H., and Li, X. (2021). Role of Hyperglycemia in the Senescence of Mesenchymal Stem Cells. *Front. Cell Dev. Biol.* 9. 10.3389/FCELL.2021.665412.
154. Titalii-Torres, K.F., and Morris, A.C. (2022). Embryonic hyperglycemia perturbs the development of specific retinal cell types, including photoreceptors. *J. Cell Sci.* 135. 10.1242/jcs.259187.
155. Scott-Drechsel, D.E., Rugonyi, S., Marks, D.L., Thornburg, K.L., and Hinds, M.T. (2013). Hyperglycemia Slows Embryonic Growth and Suppresses Cell Cycle via Cyclin D1 and p21. *Diabetes* 62, 234–242. 10.2337/db12-0161.

156. Fraser, R.B., Waite, S.L., Wood, K.A., and Martin, K.L. (2007). Impact of hyperglycemia on early embryo development and embryopathy: in vitro experiments using a mouse model. *Hum. Reprod.* 22, 3059–3068. 10.1093/HUMREP/DEM318.
157. van de Laar, L., Saelens, W., De Prijck, S., Martens, L., Scott, C.L., Van Isterdael, G., Hoffmann, E., Beyaert, R., Saeys, Y., Lambrecht, B.N., et al. (2016). Yolk Sac Macrophages, Fetal Liver, and Adult Monocytes Can Colonize an Empty Niche and Develop into Functional Tissue-Resident Macrophages. *Immunity* 44, 755–768. 10.1016/j.immuni.2016.02.017.
158. Ekblad, E., Sjuve, R., Arner, A., and Sundler, F. (1998). Enteric neuronal plasticity and a reduced number of interstitial cells of Cajal in hypertrophic rat ileum. *Gut* 42, 836–844. 10.1136/gut.42.6.836.
159. Schuster, K., Leeke, B., Meier, M., Wang, Y., Newman, T., Burgess, S., and Horsfield, J.A. (2015). A neural crest origin for cohesinopathy heart defects. *Hum. Mol. Genet.* 24, ddv402. 10.1093/hmg/ddv402.
160. Smith, T.G., Laval, S., Chen, F., Rock, M.J., Strachan, T., and Peters, H. (2014). Neural crest cell-specific inactivation of *Nipbl* or *Mau2* during mouse development results in a late onset of craniofacial defects. *Genesis* 52, 687–694. 10.1002/DVG.22780.
161. Fattahi, F., Steinbeck, J.A., Kriks, S., Tchieu, J., Zimmer, B., Kishinevsky, S., Zeltner, N., Mica, Y., El-Nachef, W., Zhao, H., et al. (2016). Deriving human ENS lineages for cell therapy and drug discovery in Hirschsprung disease. *Nature* 531,

- 105–109. 10.1038/nature16951.
162. Barber, K., Studer, L., and Fattahi, F. (2019). Derivation of enteric neuron lineages from human pluripotent stem cells. *Nat. Protoc.* *14*, 1261–1279. 10.1038/s41596-019-0141-y.
163. Hou, C., Dale, R., and Dean, A. (2010). Cell type specificity of chromatin organization mediated by CTCF and cohesin. *Proc. Natl. Acad. Sci. U. S. A.* *107*, 3651–3656. 10.1073/PNAS.0912087107.
164. Vilborg, A., Sabath, N., Wiesel, Y., Nathans, J., Levy-Adam, F., Yario, T.A., Steitz, J.A., and Shalgi, R. (2017). Comparative analysis reveals genomic features of stress-induced transcriptional readthrough. *Proc. Natl. Acad. Sci. U. S. A.* *114*, E8362–E8371. 10.1073/PNAS.1711120114/SUPPL\_FILE/PNAS.1711120114.SD02.XLSX.
165. Ingber, D.E. (2022). Human organs-on-chips for disease modelling, drug development and personalized medicine. *Nat. Rev. Genet.* *23*, 467–491. 10.1038/s41576-022-00466-9.